

# $\Delta M_{d,s}$ , $B_{d,s}^0 \rightarrow \mu^+ \mu^-$ and $B \rightarrow X_s \gamma$ in Supersymmetry at Large $\tan \beta$

Andrzej J. Buras<sup>1</sup>, Piotr H. Chankowski<sup>2</sup>,  
 Janusz Rosiek<sup>1,2</sup> and Łucja Ślavianowska<sup>2</sup>

<sup>1</sup> Physik Department, Technische Universität München,  
 D-85748 Garching, Germany

<sup>2</sup> Institute of Theoretical Physics, Warsaw University  
 Hoża 69, 00-681 Warsaw, Poland

## Abstract

We present an effective Lagrangian formalism for the calculation of flavour changing neutral and charged scalar currents in weak decays including  $SU(2) \times U(1)$  symmetry breaking effects and the effects of the electroweak couplings  $g_1$  and  $g_2$ . We apply this formalism to the MSSM with large  $\tan \beta$  with the CKM matrix as the only source of flavour violation, heavy supersymmetric particles and light Higgs bosons. We give analytic formulae for the neutral and charged Higgs boson couplings to quarks including large  $\tan \beta$  resummed corrections in the  $SU(2) \times U(1)$  limit and demonstrate that these formulae can only be used for a semi-quantitative analysis. In particular they overestimate the effects of large  $\tan \beta$  resummed corrections. We give also improved analytic formulae that reproduce the numerical results of the full approach within 5–10%. We present for the first time the predictions for the branching ratios  $B_{s,d}^0 \rightarrow \mu^+ \mu^-$  and the  $B_{d,s}^0 - \bar{B}_{d,s}^0$  mass differences  $\Delta M_{d,s}$  that include simultaneously the resummed large  $\tan \beta$  corrections,  $SU(2) \times U(1)$  breaking effects and the effects of the electroweak couplings. We perform an anatomy of the correlation between the *increase* of the rates of the decays  $B_{s,d}^0 \rightarrow \mu^+ \mu^-$  and the *suppression* of  $\Delta M_s$ , that for large  $\tan \beta$  are caused by the enhanced flavour changing neutral Higgs couplings to down quarks. We take into account the constraint from  $B \rightarrow X_s \gamma$  clarifying some points in the calculation of the large  $\tan \beta$  enhanced corrections to this decay.

# 1 Introduction

Supersymmetric theories are among the leading and most thoroughly investigated candidates for extensions of the Standard Model (SM). Even if supersymmetric particles are so heavy that they can be produced only in very high energy collisions to be studied at Tevatron, LHC and NLC, their virtual effects can be investigated also in low energy processes like particle-antiparticle mixing, CP violation and rare decays of hadrons and leptons. A number of laboratories in Europe, USA and Japan will contribute to this enterprise in an important manner in this decade.

Over the last fifteen years a vast number of papers discussing supersymmetric effects in such low energy processes has been published [1, 2, 3]. While  $K^0$ - $\bar{K}^0$  mixing,  $B_d^0$ - $\bar{B}_d^0$  mixing, CP violation in  $K \rightarrow \pi\pi$  decays and in particular the radiative decay  $\bar{B} \rightarrow X_s\gamma$  played the leading role in these analyses so far, in view of forthcoming experiments an even more important role will be played in the future by the rare decays  $\bar{B} \rightarrow X_s e^+ e^-$ ,  $B_{s,d}^0 \rightarrow \mu^+ \mu^-$  and  $K \rightarrow \pi\nu\bar{\nu}$ , the  $B_s^0$ - $\bar{B}_s^0$  mixing and various CP violating transitions and asymmetries.

In the version of the supersymmetric theory, in which the Cabibbo-Kobayashi-Maskawa (CKM) matrix remains the only source of flavour and CP violation in the quark sector and  $\tan\beta$  (the ratio of the two vacuum expectation values  $v_u/v_d$ ) is between<sup>1</sup> 2 and 10, the presence of supersymmetry does not drastically change the SM predictions for processes in question. While effects even as high as 30% could still be possible in  $\Delta F = 2$  transitions, generally smaller effects are predicted in rare K- and B-meson decays. Moreover, for supersymmetric particles heavier than  $\sim 500$  GeV their effects become unmeasurably small. Most recent analysis of this scenario has been presented in [4], where further references to a rich literature can be found. We will call this scenario minimal flavour violation (MFV) at low  $\tan\beta$ , deferring the precise definition of our scenario to section 3.

Much larger effects are still possible in supersymmetric models with new flavour violating interactions originating from the misalignment of quark and squark mass matrices [5, 1, 6, 7, 8]. However, such models contain many free parameters and their predictive power is small. The same is also true for models with broken R-parity.

In this paper we investigate another very interesting scenario, namely MFV in SUSY with large  $\tan\beta$ . It is theoretically appealing (e.g. it is consistent with the approximate unification of top and bottom Yukawa couplings at high energies predicted by some  $SO(10)$  models) and as predictive as MFV SUSY with low  $\tan\beta$  (the number of free parameters is the same in both cases). In this scenario very large deviations from the SM predictions in

---

<sup>1</sup>For top squarks below 1 TeV  $\tan\beta \lesssim 2$  is most likely excluded by the unsuccessful Higgs boson search at LEP.

certain low energy processes are possible even for heavy supersymmetric particles but the calculations are more technically involved due to the need for resummation of large  $\tan\beta$  enhanced contributions. One of the aims of the present work is to formulate a general framework allowing to handle these complications.

First discussions of large  $\tan\beta$  scenarios in multi-Higgs models and supergravity models can be found in [9] and [10], respectively. The importance of supersymmetric large  $\tan\beta$  effects in processes involving charged Higgs particles  $H^\pm$  and flavour conserving processes involving neutral scalars has been also known for some time [11, 12, 13, 14, 15]. They originate in the  $\tan\beta$  enhanced modifications of the standard relations between the original Lagrangian down-quark mass parameters  $m_d, m_s, m_b$  (which determine the relevant Yukawa couplings) and the running (“measured”) quark masses  $\overline{m}_d, \overline{m}_s, \overline{m}_b$ . For example, in the case of the  $b$ -quark one has

$$m_b = \frac{\overline{m}_b}{1 + \epsilon_b \tan\beta}. \quad (1.1)$$

The correction  $\epsilon_b$  results from supersymmetric QCD and electroweak one-loop corrections. As  $|\epsilon_b|$  can be of order 0.01, substantial enhancements or suppressions (depending on the sign of  $\epsilon_b$ ) of the Yukawa coupling are possible for  $\tan\beta = \mathcal{O}(50)$ . It has also been demonstrated [17] that expressing  $m_b$  through  $\overline{m}_b$  by means of eq. (1.1) in the tree level couplings  $\bar{t}H^+b, \bar{t}\chi^+b$  and in the flavour conserving neutral Higgs couplings resums for large values of  $\tan\beta$  dominant supersymmetric corrections to all orders of perturbation theory. Such a resummation is necessary for obtaining reliable predictions for measurable quantities [14, 16].

Even more important for phenomenology is the fact that for large values of  $\tan\beta$  flavour changing neutral currents in the down-quark sector mediated by Higgs scalars can be significantly enhanced. In the SM such currents are also induced at one loop by  $tW^\pm$  penguin-like diagrams with  $Z^0$  replaced by the neutral Higgs boson but contribute negligibly to the rare processes. In supersymmetry with large  $\tan\beta$  neutral Higgs boson penguin-like diagrams with charginos and stop-quarks in the loop can be more important than the standard  $Z^0$  penguins thanks to  $\tan\beta$  enhancement of the down-quark Yukawa couplings. They have been first considered in [18] in connection with the  $B \rightarrow X_s l^+ l^-$  decay and in [19] and subsequently found to *increase* by orders of magnitude the branching ratios of the rare decays  $B_{s,d}^0 \rightarrow \mu^+ \mu^-$  [20, 6, 21, 22] and to *decrease* significantly the  $B_s^0$ - $\bar{B}_s^0$  mass difference  $\Delta M_s$  [23] relative to the expectations based on the SM.

Two additional related aspects of large supersymmetric corrections in the down-quark sector are the following. Elements of the physical CKM matrix, to be called  $V_{JI}^{\text{eff}}$  in what follows, differ from  $V_{JI}$  present in the original Lagrangian by calculable flavour dependent

corrections  $f_{JI}$  [24, 19, 20]:

$$V_{JI} = V_{JI}^{\text{eff}} f_{JI} \quad (1.2)$$

( $J, I$  denote flavour indices).  $f_{JI}$  can substantially deviate from unity for large  $\tan\beta$  and can in principle affect all processes in which the CKM matrix is relevant.

Finally, as has been shown in [25] in the context of the analysis of  $\bar{B} \rightarrow X_s \gamma$  decay, there are additional large  $\tan\beta$  enhanced corrections in the charged Higgs couplings, that in ref. [25] have been parametrized by  $\epsilon'_b$  and  $\epsilon'_t$ .

It is desirable to calculate all the four effects, that is:

- 1) Large  $\tan\beta$  effects related to (1.1),
- 2) Enhanced neutral scalar-penguin diagrams,
- 3) Large  $\tan\beta$  effects related to (1.2),
- 4) Enhanced corrections to charged Higgs vertex diagrams

in a self-consistent framework and to include them in a phenomenological analysis correlating predictions for  $\bar{B} \rightarrow X_s \gamma$ ,  $B_{s,d}^0 \rightarrow \mu^+ \mu^-$  rates and for  $B_{s,d}^0 - \bar{B}_{s,d}^0$  mass differences  $\Delta M_{s,d}$ . It is also important to formulate general rules allowing to include large  $\tan\beta$  effects that can be used in other processes not considered in our paper.

Several steps towards this goal have been already made. In refs. [17, 25, 26] large  $\tan\beta$  effects related to 1) and 4) have been discussed in the context of the  $\bar{B} \rightarrow X_s \gamma$  decay and recipes for including them in the charged Higgs ( $H^\pm$ ) and charged Goldstone boson ( $G^\pm$ ) vertices have been formulated for specific quark flavours. In another elegant analysis [27] the effects 1)-3) in the case of  $B_{s,d}^0 \rightarrow \mu^+ \mu^-$  decays and  $B_{s,d}^0 - \bar{B}_{s,d}^0$  mixing have been calculated in the  $SU(2) \times U(1)$  symmetry limit, neglecting the electroweak couplings  $g_2$  and  $g_1$  in comparison with  $\alpha_s$ ,  $y_t$  and  $y_b$ . These authors confirmed sizeable enhancements of  $BR(B_{s,d}^0 \rightarrow \mu^+ \mu^-)$  and the suppression of  $B_s^0 - \bar{B}_s^0$  mixing pointed out previously in refs. [20, 6, 21, 22] and [23], respectively.

During the final stages of completion of our paper a model independent analysis of rare processes in theories with the CKM matrix as the unique source of flavour and CP violation has been presented in [28]. While those authors also investigated large  $\tan\beta$  effects in  $BR(B_{s,d}^0 \rightarrow \mu^+ \mu^-)$ ,  $\Delta M_s$  and  $\bar{B} \rightarrow X_s \gamma$ , their analysis was performed in the same  $SU(2) \times U(1)$  symmetry limit assuming the dominance of  $\alpha_s$ ,  $y_t$  and  $y_b$ .

In the present paper we go beyond these analyses by

- Calculating all the four effects in an effective Lagrangian approach that goes beyond the  $SU(2) \times U(1)$  symmetry limit considered in [27, 28] and includes the effects of the electroweak gauge couplings.

- Calculating all the four effects in the  $SU(2) \times U(1)$  symmetry limit with vanishing electroweak gauge couplings thereby confirming and, in certain cases, correcting and generalizing the analytical rules for the inclusion of large  $\tan\beta$  effects presented in refs. [25, 26]. Our results agree with those of [27, 28] if the factors denoted here by  $\epsilon_0$ ,  $\epsilon_Y$ ,  $\epsilon'_0$  and  $\epsilon'_Y$  are assumed to be flavour independent.
- Analysing numerically the validity of the above approximation and giving simple recipes which improve it significantly.
- Including all these effects in an analysis of the branching ratios  $BR(B_{d,s}^0 \rightarrow \mu^+\mu^-)$ ,  $B_s^0$ - $\bar{B}_s^0$  mass difference  $\Delta M_s$  and of correlations between them taking into account the constraint from  $\bar{B} \rightarrow X_s\gamma$ .

To our knowledge no complete analysis of all these topics has been presented in the literature so far. While the recent analysis in [28] considered many of these issues and went beyond supersymmetry, it was performed in the  $SU(2) \times U(1)$  symmetry limit with  $g_1 = g_2 = 0$ , the approximation the accuracy of which we want to investigate here. In particular it is interesting to see how big effects can still be expected in  $B_{d,s}^0 \rightarrow \mu^+\mu^-$  given the constraints on the magnitude of the scalar flavour changing neutral currents stemming from the  $B_s^0$ - $\bar{B}_s^0$  mixing [23]. This should also allow to assess the claim made on the basis of approximate formulae by the authors of ref. [27] that the effects found previously in [6, 22] and [23] can be decreased by a factor as large as 5 when the large  $\tan\beta$  effects described by (1.1) and (1.2) are properly taken into account.

In a recent letter [29] we have presented some of the formulae resulting from our analysis and in particular we have analyzed the correlation between the increase of the rates of the decays  $B_{s,d}^0 \rightarrow \mu^+\mu^-$  and the suppression of  $\Delta M_s$ . In this paper we present the details of our formalism, derive all results and extend the phenomenological analysis.

Our paper is organized as follows. In section 2 we present general formalism for calculating the Higgs flavour changing and flavour diagonal vertices based on the effective Lagrangian approach valid beyond the  $SU(2) \times U(1)$  symmetry limit. In section 3 we relate our approach to the one of [27, 28] and present explicit expressions for flavour violating neutral scalar ( $S^0$ ) and charged scalar ( $H^\pm, G^\pm$ ) couplings in the  $SU(2) \times U(1)$  symmetry limit. Subsequently we generalize these expressions to allow for flavour dependence in the parameters  $\epsilon_0$ ,  $\epsilon_Y$ ,  $\epsilon'_0$  and  $\epsilon'_Y$ . We compare our formulae with those present in the literature in section 4. In section 5 we assess numerically the importance of the corrections calculated in sections 2 and 3. We also investigate the effects of  $SU(2) \times U(1)$  breaking and of the effects of non-vanishing electroweak couplings comparing our results with those present in the literature. This includes in particular the parameters  $\epsilon$  and  $\epsilon'$  of refs. [25, 26].

Finally using the flavour dependent formulation of section 3 we find analytic formulae for various couplings that within 5 – 10% reproduce the numerical results of the full approach presented in section 2. In section 6 we collect the basic formulae for  $\Delta M_{d,s}$ ,  $BR(B_{d,s}^0 \rightarrow \mu^+ \mu^-)$  and  $BR(\bar{B} \rightarrow X_s \gamma)$  in supersymmetry at large  $\tan \beta$ . Section 7 is devoted to the numerical analysis of these quantities and the investigation of possible correlations mentioned above. We conclude in section 8.

## 2 General formalism

### 2.1 Effective Lagrangian

The most efficient way of handling heavy particle effects in low energy processes involving quarks, is the effective Lagrangian technique. Let us assume that a sector of heavy fields in a theory (e.g. sfermions, gluinos, charginos and neutralinos in the MSSM) can be integrated out without violating gauge invariance. We consider processes occurring at energies low enough so that the amplitudes cannot have imaginary parts related by unitarity to particles belonging to the heavy sector. Renormalized in the  $\overline{\text{MS}}$  scheme with some renormalization scale  $Q$ , virtual effects of the decoupled particles ( $Q$  should be chosen to be of the order of their masses) corresponding to self-energy diagrams in Fig. 1 can be summarized by the effective kinetic and mass terms of light fermions:

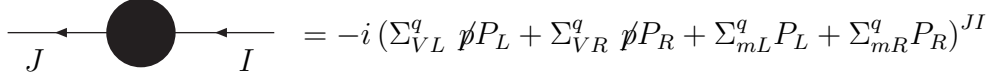
$$\begin{aligned} \mathcal{L}_{\text{eff}}^{\text{kin}} = & \overline{(d_J)_L} \left(1 - \Sigma_{VL}^d(0)\right)^{JI} i \not{\partial} (d_I)_L + \overline{(d_J)_R} \left(1 - \Sigma_{VR}^d(0)\right)^{JI} i \not{\partial} (d_I)_R \\ & - \overline{(d_J)_R} \left(m_d + \Sigma_{mL}^d(0)\right)^{JI} (d_I)_L - \overline{(d_J)_L} \left(m_d + \Sigma_{mR}^d(0)\right)^{JI} (d_I)_R \end{aligned} \quad (2.1)$$

plus similar terms for the up-type quarks and leptons. Here  $I, J$  are flavour indices with  $d_1 \equiv d$ ,  $d_2 \equiv s$ ,  $d_3 \equiv b$ . Analogous notation will be used for the up-type quarks. Exact expressions for quark self-energies are listed in the Appendix A.2.

In order to make the formulae more compact we denote (in some of them) the diagonal quark mass matrices simply by  $m_d \equiv \text{diag}(m_{d_1}, m_{d_2}, m_{d_3}) \equiv \text{diag}(m_d, m_s, m_b)$ ,  $m_u \equiv \text{diag}(m_{u_1}, m_{u_2}, m_{u_3}) \equiv \text{diag}(m_u, m_c, m_t)$ . Hermiticity of the effective Lagrangian ensures that  $(\Sigma_{VL}^q)^\dagger = \Sigma_{VL}^q$ ,  $(\Sigma_{VR}^q)^\dagger = \Sigma_{VR}^q$  and  $(\Sigma_{mL}^q)^\dagger = \Sigma_{mR}^q$ .

Similarly, virtual effects of the decoupled particles corresponding to fermion-gauge boson vertices of the type shown schematically in Fig. 2 can be summarised as

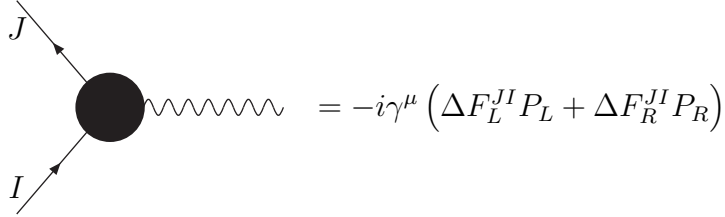
$$\begin{aligned} \mathcal{L}_{\text{eff}}^{\text{int}} = & -\overline{(d_J)_L} \gamma^\mu \left(F_L^{Zd} + \Delta F_L^{Zd}\right)^{JI} (d_I)_L Z_\mu^0 - \overline{(d_J)_R} \gamma^\mu \left(F_R^{Zd} + \Delta F_R^{Zd}\right)^{JI} (d_I)_R Z_\mu^0 \\ & - \overline{(u_J)_L} \gamma^\mu \left(F_L^{Zu} + \Delta F_L^{Zu}\right)^{JI} (u_I)_L Z_\mu^0 - \overline{(u_J)_R} \gamma^\mu \left(F_R^{Zu} + \Delta F_R^{Zu}\right)^{JI} (u_I)_R Z_\mu^0 \\ & - \overline{(u_J)_L} \gamma^\mu \left(F_L^W + \Delta F_L^W\right)^{JI} (d_I)_L W_\mu^+ - \overline{(u_J)_R} \gamma^\mu \left(F_R^W + \Delta F_R^W\right)^{JI} (d_I)_R W_\mu^+ + \text{H.c.} \end{aligned} \quad (2.2)$$



$$\text{Diagram} = -i(\Sigma_{VL}^q \not{p} P_L + \Sigma_{VR}^q \not{p} P_R + \Sigma_{mL}^q P_L + \Sigma_{mR}^q P_R)^{JI}$$

Figure 1: One-loop threshold corrections to fermion propagators.  $P_L \equiv \frac{1-\gamma^5}{2}$ ,  $P_R \equiv \frac{1+\gamma^5}{2}$  and  $q \equiv d$  or  $u$ .

where  $(F_L^{Zq})^{JI} \propto \delta^{JI}$ ,  $(F_L^W)^{JI} = (g/\sqrt{2})V_{JI}$  and, of course,  $F_R^W = 0$ .



$$\text{Diagram} = -i\gamma^\mu (\Delta F_L^{JI} P_L + \Delta F_R^{JI} P_R)$$

Figure 2: One-loop threshold corrections to fermion-gauge boson vertices.

Finally, other virtual effects of the decoupled heavy particles can be represented in the effective Lagrangian by various effective vertices which are operators of dimension higher than four (non-renormalizable operators) such as four-fermion operators or dimension 5 (chromo)magnetic operators etc.

## 2.2 Diagonalization

The next step is to rescale the quark fields so to render their kinetic terms canonical:

$$(d_I)_L \rightarrow \left(1 + \frac{1}{2}\Sigma_{VL}^d\right)^{IJ} (d_J)_L, \quad (d_I)_R \rightarrow \left(1 + \frac{1}{2}\Sigma_{VR}^d\right)^{IJ} (d_J)_R, \quad (2.3)$$

and the same for the up-type quarks. After this operation the quark mass terms become

$$\mathcal{L}_{\text{mass}} = -\overline{(d_J)_R} (m_d + \Delta m_d)^{JI} (d_I)_L - \overline{(d_J)_L} (m_d + \Delta m_d^\dagger)^{JI} (d_I)_R \quad (2.4)$$

where

$$\Delta m_d \equiv \Sigma_{mL}^d(0) + \frac{1}{2}\Sigma_{VR}^d(0)m_d + \frac{1}{2}m_d\Sigma_{VL}^d(0). \quad (2.5)$$

Similar expressions are obtained for the up-type quarks.

The mass terms (2.4) can be diagonalized by two independent rotations:

$$d_L \rightarrow \mathbf{D}_L d_L, \quad d_R \rightarrow \mathbf{D}_R d_R \quad (2.6)$$

so that

$$\left[ \mathbf{D}_R^\dagger (m_d + \Delta m_d) \mathbf{D}_L \right]^{JI} = \bar{m}_{d_J} \delta^{JI} \quad (2.7)$$

with  $\bar{m}_{d_J}$  denoting the corrected mass eigenvalues. To one-loop accuracy the transformations (2.6) read:

$$d_L \rightarrow (\mathbf{1} + \Delta \mathbf{D}_L) d_L, \quad d_R \rightarrow (\mathbf{1} + \Delta \mathbf{D}_R) d_R. \quad (2.8)$$

The unitarity of  $\mathbf{D}_{L(R)}$  requires that (up to higher order terms)  $\Delta \mathbf{D}_{L(R)}^\dagger = -\Delta \mathbf{D}_{L(R)}$  and  $\Delta \mathbf{D}_{L(R)}^{II} = 0$ . In this approximation the corrected mass eigenvalues are given by<sup>2</sup>

$$\bar{m}_{d_J} = m_{d_J} (1 + \kappa_{d_J}). \quad (2.9)$$

where

$$\kappa_{d_J} \equiv \frac{\Sigma_{mL}^{dJJ}(0)}{m_{d_J}} + \frac{1}{2} \Sigma_{VR}^{dJJ}(0) + \frac{1}{2} \Sigma_{VL}^{dJJ}(0) \equiv \frac{(\Delta m_d)^{JJ}}{m_{d_J}}. \quad (2.10)$$

Formula (2.9) generalizes (1.1) to arbitrary down-quark flavours.

In order to find the matrices  $\Delta \mathbf{D}_{L(R)}$  we follow ref. [27] and decompose  $\Delta m_d$  explicitly into its diagonal and off-diagonal parts

$$(\Delta m_d)^{JI} = m_{d_J} \kappa_{d_J} \delta^{JI} + (\Delta' m_d)^{JI} \quad (2.11)$$

where by definition  $(\Delta' m_d)^{JI} = (\Delta m_d)^{JI}$  for  $J \neq I$  and  $(\Delta' m_d)^{JJ} = 0$ .

The condition determining the  $\Delta \mathbf{D}_{L(R)}$  takes now the form

$$\left( \Delta \mathbf{D}_R^\dagger \bar{m}_d + \bar{m}_d \Delta \mathbf{D}_L + \Delta' m_d \right)^{JI} = 0 \quad (2.12)$$

for  $J \neq I$ . Note that following ref. [27] we multiply by  $\Delta \mathbf{D}_{L,R}$  also the  $\tan \beta$  enhanced diagonal correction to the down-type quark masses, i.e. include terms which are formally of higher order. The non-zero entries of  $\Delta \mathbf{D}_{L(R)}^\dagger$  are then

$$\Delta \mathbf{D}_L^{JI} = -\frac{\bar{m}_{d_J} \Delta m_d^{JI} + (\Delta m_d^\dagger)^{JI} \bar{m}_{d_I}}{\bar{m}_{d_J}^2 - \bar{m}_{d_I}^2} \quad J \neq I \quad (2.13)$$

---

<sup>2</sup>If the diagonal entries of the matrices  $\Sigma_{mL}^d$ ,  $\Sigma_{mR}^d$  are complex, the rotations (2.8) have to be supplemented by additional chiral rotations of the quark fields in order to get real and positive quark masses.



$$\Delta \mathbf{D}_R^{JI} = -\frac{\bar{m}_{d_J}(\Delta m_d^\dagger)^{JI} + \Delta m_d^{JI} \bar{m}_{d_I}}{\bar{m}_{d_J}^2 - \bar{m}_{d_I}^2} \quad J \neq I. \quad (2.14)$$

Using the hierarchy of quark masses:  $m_{d_3} \gg m_{d_2} \gg m_{d_1}$  ( $\bar{m}_{d_3} \gg \bar{m}_{d_2} \gg \bar{m}_{d_1}$ ) and the fact that  $\Delta m_d^{JI} \propto m_{d_J}$ ,  $(\Delta m_d^\dagger)^{JI} \propto m_{d_I}$  (see section 3 for explicit expressions) we find for  $J > I$

$$\begin{aligned} \Delta \mathbf{D}_L^{JI} &= -\frac{1}{\bar{m}_{d_J}} \Delta m_d^{JI} + \mathcal{O}\left(\frac{\bar{m}_{d_I}^2}{\bar{m}_{d_J}^2}\right), \\ \Delta \mathbf{D}_R^{JI} &= -\frac{1}{\bar{m}_{d_J}} (\Delta m_d^\dagger)^{JI} - \frac{\bar{m}_{d_I}}{\bar{m}_{d_J}^2} \Delta m_d^{JI} \sim \mathcal{O}\left(\frac{\bar{m}_{d_I}}{\bar{m}_{d_J}}\right) \end{aligned} \quad (2.15)$$

and for  $J < I$

$$\begin{aligned} \Delta \mathbf{D}_L^{JI} &= \frac{1}{\bar{m}_{d_I}} (\Delta m_d^\dagger)^{JI} + \mathcal{O}\left(\frac{\bar{m}_{d_J}^2}{\bar{m}_{d_I}^2}\right), \\ \Delta \mathbf{D}_R^{JI} &= \frac{1}{\bar{m}_{d_I}} \Delta m_d^{JI} + \frac{\bar{m}_{d_J}}{\bar{m}_{d_I}^2} (\Delta m_d^\dagger)^{JI} \sim \mathcal{O}\left(\frac{\bar{m}_{d_J}}{\bar{m}_{d_I}}\right) \end{aligned} \quad (2.16)$$

Note that  $\Delta \mathbf{D}_L$  is  $\mathcal{O}(1)$  with respect to the masses but  $\Delta \mathbf{D}_R$  is always suppressed. This suppression can be occasionally removed by a large mass multiplying  $\Delta \mathbf{D}_R$ .

The same formulae (with appropriate replacements  $d \rightarrow u$ ,  $\mathbf{D} \rightarrow \mathbf{U}$ ) hold also for the up-type quarks. In particular we have

$$\left[ \mathbf{U}_R^\dagger (m_u + \Delta m_u) \mathbf{U}_L \right]^{JI} = \bar{m}_{u_J} \delta^{JI} \quad (2.17)$$

with  $\bar{m}_{u_J}$  denoting the corrected mass eigenvalues. However the correction  $\Delta m_u$  is not enhanced for large  $\tan \beta$  (see the discussion following (3.16)) in contrast to  $\Delta m_d$  that is enhanced in this limit. Consequently one can set  $\bar{m}_{u_J} \approx m_{u_J}$  and the condition analogous to (2.12) reads

$$\left( \Delta \mathbf{U}_R^\dagger m_u + m_u \Delta \mathbf{U}_L + \Delta' m_u \right)^{JI} = 0 \quad (2.18)$$

for  $J \neq I$ . The explicit expressions for  $\Delta \mathbf{U}_{L(R)}^{JI}$  are then obtained directly from (2.13)-(2.16) by making appropriate replacements ( $\bar{m}_{d_J} \rightarrow m_{u_J}$ , etc).

Obviously, these are the masses  $\bar{m}_{d_J}$ , and  $\bar{m}_{u_J} \approx m_{u_J}$  that have to be identified with the running mass parameters of the low energy effective theory valid for scales  $\sim M_Z$ . Parameters  $\bar{m}_{d_J}$ ,  $\bar{m}_{u_J}$  are therefore directly related through the known QCD renormalization group running to the low energy quark mass parameters.

## 2.3 Effective CKM matrix

Rotations (2.8) have the effect of renormalizing the CKM matrix. After the operations (2.3) and (2.8) the  $W$ -boson vertices become

$$\mathcal{L}_{\text{eff}}^W = -\overline{(u_J)_L} \gamma^\mu \left( \tilde{F}_L^W + \Delta \hat{F}_L^W \right)^{JI} (d_I)_L W_\mu^+ - \overline{(u_J)_R} \gamma^\mu \left( \Delta \hat{F}_R^W \right)^{JI} (d_I)_R W_\mu^+ + \text{H.c.} \quad (2.19)$$

with

$$\Delta \hat{F}_L^W \equiv \Delta F_L^W + \frac{1}{2} \Sigma_{VL}^u F_L^W + \frac{1}{2} F_L^W \Sigma_{VL}^d, \quad \Delta \hat{F}_R^W \equiv \Delta F_R^W \quad (2.20)$$

and

$$(\tilde{F}_L^W)^{JI} = \frac{g_2}{\sqrt{2}} V_{JI}^{\text{eff}} \equiv \frac{g_2}{\sqrt{2}} \left( \mathbf{U}_L^\dagger V \mathbf{D}_L \right)^{JI} \approx \frac{g_2}{\sqrt{2}} \left( V + \mathbf{\Delta} \mathbf{U}_L^\dagger V + V \mathbf{\Delta} \mathbf{D}_L \right)^{JI}. \quad (2.21)$$

Since the corrections  $\Delta \hat{F}_{L,R}^W$  are negligible (for example, for all  $JI$  the gluino exchange computed in [33] gives  $\Delta \hat{F}_L^W / \tilde{F}_L^W \lesssim 3 \times 10^{-3}$ ), it is the matrix  $V_{JI}^{\text{eff}}$  that has to be identified with the CKM matrix whose elements are determined from the low energy processes. The matrix  $V_{JI}$  is the CKM matrix of the MSSM which for a given spectrum of sparticles is related in a calculable way to the measured matrix  $V_{JI}^{\text{eff}}$ . Thus, the formula (2.21) is the realization of the relation (1.2). The correct procedure in phenomenological applications is then to calculate first all relevant quantities in terms of  $V_{JI}$  and subsequently express the latter in terms of  $V_{JI}^{\text{eff}}$  that should be determined from the measured branching ratios.

It is known [24, 20], that for large  $\tan \beta$  the ratios of the elements  $V_{3I}^{\text{eff}} / V_{3I} \approx V_{I3}^{\text{eff}} / V_{I3}$  can, for  $I \neq 3$ , substantially deviate from unity. Simple approximate (but very accurate) expressions for  $f_{JI} \equiv V_{JI} / V_{JI}^{\text{eff}}$  defined in eq. (1.2) will be given in section 3 (see eq. (3.53)) and the corresponding numerical analysis in section 5.

The elements  $|V_{ub}|$  and  $|V_{cb}|$ , that are affected by these corrections are usually determined from tree level decays under the assumption that new physics contributions to the relevant branching ratios can be neglected. This assumption is clearly violated in the case of supersymmetry at large  $\tan \beta$ . However, in this case the most important  $\tan \beta$  enhanced loop corrections to tree level decays, can be absorbed in the  $V^{\text{eff}}$ . Therefore, the quantities which experimentalists extract from these processes can be identified with  $|V_{ub}^{\text{eff}}|$  and  $|V_{cb}^{\text{eff}}|$  defined in (2.21).

On the other hand, as we will see the ratio  $|V_{ub}| / |V_{cb}|$  is to an excellent approximation not affected by these corrections and  $|V_{ub}| / |V_{cb}| \approx |V_{ub}^{\text{eff}}| / |V_{cb}^{\text{eff}}|$ . It should also be emphasized that

$$V^{\text{eff}} (V^{\text{eff}})^\dagger = \hat{1} \quad (2.22)$$

so that all unitarity relations, in particular the formulae related to the unitarity triangle, expressed usually in terms of  $V_{JI}$ , are also valid for  $V_{JI}^{\text{eff}}$ .

For the  $Z^0$  couplings the rescalings (2.3) amount to the replacements

$$\Delta F_{L(R)}^{Zq} \rightarrow \Delta \hat{F}_{L(R)}^{Zq} \equiv \Delta F_{L(R)}^{Zq} + \frac{1}{2} \Sigma_{VL(R)}^q F_{L(R)}^{Zq} + \frac{1}{2} F_{L(R)}^{Zq} \Sigma_{VL(R)}^q. \quad (2.23)$$

To one-loop accuracy, the subsequent unitary rotations (2.8) do not affect the  $Z^0$  vertices. Flavour changing introduced in higher orders can be treated along the lines discussed in subsection 2.6.

## 2.4 Neutral Higgs-fermion vertices

The one-loop corrections to scalar ( $S^0$ ) neutral Higgs boson vertices induced by the decoupled particles can be written as

$$\mathcal{L}_{\text{eff}}^{S^0} = -\overline{(d_J)_R} (F_L^{dS} + \Delta F_L^{dS})^{JI} (d_I)_L S^0 - \overline{(d_J)_L} (F_R^{dS} + \Delta F_R^{dS})^{JI} (d_I)_R S^0 \quad (2.24)$$

and similarly for the up-type quarks (see Appendix A.3 for the expressions for  $\Delta F_{L,R}^{dS}$ ). For neutral Higgs and Goldstone bosons we have

Figure 3: One-loop corrections to neutral Higgs-quark vertices.

$$(F_{L(R)}^{dS})^{JI} = \eta_{L(R)}^{dS} m_{d_J} \delta^{JI} \equiv (F_{L(R)}^{dS})^J \delta^{JI}. \quad (2.25)$$

with explicit expressions for  $\eta_{L(R)}^{dS}$  given in (3.20) and (3.21). After the operations (2.3) and (2.8) the expressions inside the brackets in eq. (2.24) become respectively

$$F_L^{dS} + \Delta F_L^{dS} + \frac{1}{2} \Sigma_{VR}^d F_L^{dS\text{corr}} + \frac{1}{2} F_L^{dS\text{corr}} \Sigma_{VL}^d + \mathbf{\Delta D}_R^\dagger F_L^{dS\text{corr}} + F_L^{dS\text{corr}} \mathbf{\Delta D}_L \quad (2.26)$$

$$F_R^{dS} + \Delta F_R^{dS} + \frac{1}{2} \Sigma_{VL}^d F_R^{dS\text{corr}} + \frac{1}{2} F_R^{dS\text{corr}} \Sigma_{VR}^d + \mathbf{\Delta D}_L^\dagger F_R^{dS\text{corr}} + F_R^{dS\text{corr}} \mathbf{\Delta D}_R \quad (2.27)$$

where we have defined

$$(F_{L(R)}^{dS\text{corr}})^J \equiv \eta_{L(R)}^{dS} m_{d_J} + (\Delta F_{L(R)}^{dS})^{JJ}. \quad (2.28)$$

Of course, in the phenomenological applications one has to express  $F_L^{dS}$  in terms of the “observable”  $\overline{m}_{d_J}$  by using eq. (2.9):

$$\left(F_L^{dS}\right)^{JI} = \eta_L^{dS} \frac{\overline{m}_{d_J}}{1 + \kappa_{d_J}} \delta^{JI} \approx \eta_L^{dS} \frac{\overline{m}_{d_J}}{1 + \epsilon_{d_J}} \delta^{JI} \left[1 - \frac{1}{2} \left(\Sigma_{VL}^d + \Sigma_{VR}^d\right)^{JJ}\right] \quad (2.29)$$

with an analogous formula for  $\left(F_R^{dS}\right)^{JI}$ . In writing the second expression in (2.29) we have assumed that the vector parts of the fermion self energies do not contain large contributions and neglected terms of order  $\epsilon_d \left(\Sigma_{VL}^d + \Sigma_{VR}^d\right)$  and smaller. We have also defined the quantity  $\epsilon_{d_J}$

$$\epsilon_{d_J} \equiv \frac{\left(\Sigma_{mL}^d\right)^{JJ}}{m_{d_J} \tan \beta} \quad (2.30)$$

which for  $J = 3$  corresponds to  $\epsilon_b$  of ref. [25]. It is also instructive to make contact with the standard perturbative (on-shell) calculation of the one loop  $\bar{d}S^0 d$  vertex which gives [6, 22]

$$\eta_L^{dS} \overline{m}_{d_J} \delta^{JI} + \left(\Delta F_L^{dS}\right)^{JI} - \eta_L^{dS} \Sigma_{mL}^{dJI} . \quad (2.31)$$

By expanding (2.26) strictly to one loop (neglecting the difference between  $m_d$  and  $\overline{m}_d$  in all 1-loop terms) and using the explicit expressions (2.13), (2.14) as well as (2.9) and (2.10) it is easy to see that the two approaches indeed coincide. In particular, to 1-loop accuracy the vertex (2.26) is independent of the vector self energies, both for the diagonal and off-diagonal transitions.

On the other hand, keeping  $\epsilon_{d_J}$  in the denominator in (2.29) resums dominant corrections of order  $\alpha_s(\mu/\overline{m}_{\bar{g}}) \tan \beta$  to all orders of the perturbation expansion [17] which are important for neutral Higgs decays into  $b\bar{b}$  or  $\tau^+\tau^-$  pairs [13, 14, 16]. Thus, the diagonal couplings of scalars to the down-type quarks are

$$\mathcal{L}_{\text{eff}}^{\text{diag}} = -\overline{(d_J)_R} \left( \eta_L^{dS} \frac{\overline{m}_{d_J}}{1 + \epsilon_{d_J} \tan \beta} + \Delta F_L^{dS} \right)^{JJ} (d_J)_L S^0 - \text{H.c.} \quad (2.32)$$

The expression for the flavour non-diagonal vertex can be simplified by taking into account the hierarchy of masses  $m_{d_J}$ :  $m_{d_3} \gg m_{d_2} \gg m_{d_1}$  ( $\overline{m}_{d_3} \gg \overline{m}_{d_2} \gg \overline{m}_{d_1}$ ) and using the expressions (2.15) and (2.16) for the  $\mathbf{\Delta D}_{L(R)}$  matrices. One has also to take into account that (as we will see shortly) in the limit of  $SU(2) \times U(1)$  symmetry  $(\Delta m_d)^{JI} \propto m_{d_J}$  and  $(\Delta m_d^\dagger)^{JI} \propto m_{d_I}$ . In general one gets

$$\mathcal{L}_{\text{eff}}^{\text{off-diag}} = -\overline{(d_J)_R} \left[ X_{RL}^S \right]^{JI} (d_I)_L S^0 - \overline{(d_J)_L} \left[ X_{LR}^S \right]^{JI} (d_I)_R S^0 \quad (2.33)$$

where for  $J > I$

$$[X_{RL}^S]^{JI} = \left( \Delta F_L^{dS} + \frac{1}{2} \Sigma_{VR}^d F_L^{d\text{Scorr}} + \frac{1}{2} F_L^{d\text{Scorr}} \Sigma_{VL}^d \right)^{JI} - \frac{(F_L^{d\text{Scorr}})^J}{\overline{m}_{d_J}} (\Delta m_d)^{JI} \quad (2.34)$$

$$\begin{aligned} [X_{LR}^S]^{JI} &= \left( \Delta F_R^{dS} + \frac{1}{2} \Sigma_{VL}^d F_R^{d\text{Scorr}} + \frac{1}{2} F_R^{d\text{Scorr}} \Sigma_{VR}^d \right)^{JI} \\ &- \frac{(F_R^{d\text{Scorr}})^J}{\overline{m}_{d_J}} (\Delta m_d^\dagger)^{JI} + \left( \frac{(F_R^{d\text{Scorr}})^I}{\overline{m}_{d_I}} - \frac{(F_R^{d\text{Scorr}})^J \overline{m}_{d_I}}{\overline{m}_{d_J}^2} \right) (\Delta m_d)^{JI} \end{aligned} \quad (2.35)$$

and for  $J < I$  the expressions for  $(X_{RL}^S)^{JI}$  and  $(X_{LR}^S)^{JI}$  can be obtained by using the rules (remember that  $(F_L^{d\text{Scorr}})^{J*} = (F_R^{d\text{Scorr}})^J$ ):

$$[X_{RL}^S]^{JI} = [X_{LR}^{S\dagger}]^{JI} = [X_{LR}^S]^{IJ*}, \quad [X_{LR}^S]^{JI} = [X_{RL}^{S\dagger}]^{JI} = [X_{RL}^S]^{IJ*} \quad (2.36)$$

Explicitly for  $J < I$  one gets

$$\begin{aligned} [X_{RL}^S]^{JI} &= \left( \Delta F_L^{dS} + \frac{1}{2} \Sigma_{VR}^d F_L^{d\text{Scorr}} + \frac{1}{2} F_L^{d\text{Scorr}} \Sigma_{VL}^d \right)^{JI} \\ &- (\Delta m_d)^{JI} \frac{(F_L^{d\text{Scorr}})^I}{\overline{m}_{d_I}} + \left( \frac{(F_L^{d\text{Scorr}})^J}{\overline{m}_{d_I}} - \frac{(F_L^{d\text{Scorr}})^I \overline{m}_{d_J}}{\overline{m}_{d_I}^2} \right) (\Delta m_d^\dagger)^{JI} \end{aligned} \quad (2.37)$$

$$[X_{LR}^S]^{JI} = \left( \Delta F_R^{dS} + \frac{1}{2} \Sigma_{VL}^d F_R^{d\text{Scorr}} + \frac{1}{2} F_R^{d\text{Scorr}} \Sigma_{VR}^d \right)^{JI} - \frac{(F_R^{d\text{Scorr}})^I}{\overline{m}_{d_I}} (\Delta m_d^\dagger)^{JI}. \quad (2.38)$$

We observe that for  $J > I$  ( $I > J$ ) the effects of the re-diagonalization in  $X_{LR}$  ( $X_{RL}$ ) are suppressed by a factor  $\sim m_{d_I}/m_{d_J} (m_{d_J}/m_{d_I})$  compared to its effects in  $X_{RL}$  ( $X_{LR}$ ). It has to be remembered that  $m_d$  and  $V$  entering the calculation of  $\Delta F_{L(R)}^{dS}$ ,  $\Delta m_d$  etc. have to be ultimately expressed in terms of  $\overline{m}_d$  and  $V^{\text{eff}}$ .

## 2.5 Charged Higgs-fermion vertices

In the same manner the operations (2.3) and (2.8) imply the following charged scalar ( $H^\pm$ ) and charged Goldstone boson ( $G^\pm$ ) couplings

$$\mathcal{L}_{\text{eff}}^{H^+} = \overline{(u_J)_R} [P_{RL}^H]^{JI} (d_I)_L H^+ + \overline{(u_J)_L} [P_{LR}^H]^{JI} (d_I)_R H^+ + \text{H.c.} \quad (2.39)$$

$$\mathcal{L}_{\text{eff}}^{G^+} = \overline{(u_J)_R} [P_{RL}^G]^{JI} (d_I)_L G^+ + \overline{(u_J)_L} [P_{LR}^G]^{JI} (d_I)_R G^+ + \text{H.c.} \quad (2.40)$$

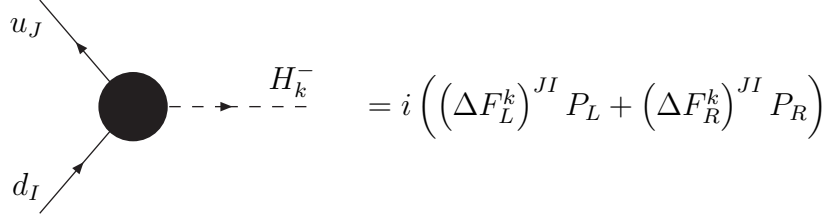


Figure 4: One-loop corrections to charged Higgs-quark vertices.

where ( $i = H^+, G^+$ )

$$\left[ P_{RL}^i \right] = \eta_L^i m_u V^{\text{eff}} + \eta_L^i (\Delta \mathbf{U}_R^\dagger m_u - m_u \Delta \mathbf{U}_L^\dagger) V^{\text{eff}} + \mathbf{U}_R^\dagger \Delta \hat{F}_L^i \mathbf{D}_L \quad (2.41)$$

$$\left[ P_{LR}^i \right] = \eta_R^i V^{\text{eff}} m_d + \eta_R^i V^{\text{eff}} (m_d \Delta \mathbf{D}_R - \Delta \mathbf{D}_L m_d) + \mathbf{U}_L^\dagger \Delta \hat{F}_R^i \mathbf{D}_R \quad (2.42)$$

Here

$$\Delta \hat{F}_L^k = \Delta F_L^k + \frac{1}{2} \Sigma_{VR}^u F_L^k + \frac{1}{2} F_L^k \Sigma_{VL}^d \quad (2.43)$$

$$\Delta \hat{F}_R^k = \Delta F_R^k + \frac{1}{2} \Sigma_{VL}^u F_R^k + \frac{1}{2} F_R^k \Sigma_{VR}^d \quad (2.44)$$

with

$$F_L^k = \eta_L^k m_u V, \quad F_R^k = \eta_R^k V m_d \quad (2.45)$$

and  $\Delta F_{L(R)}^k$  defined in analogy with (2.2) (see Appendix A.3 for the explicit expressions).

Finally

$$\eta_L^H = \frac{g_2}{\sqrt{2}M_W} \cot \beta, \quad \eta_R^H = \frac{g_2}{\sqrt{2}M_W} \tan \beta \quad (2.46)$$

and

$$\eta_L^G = \frac{g_2}{\sqrt{2}M_W}, \quad \eta_R^G = -\frac{g_2}{\sqrt{2}M_W}. \quad (2.47)$$

In writing (2.41) and (2.42) we have used (2.21) in order to convert the CKM matrix in the tree level vertices  $F_{L(R)}^i$  into the effective CKM matrix  $V^{\text{eff}}$ .

In what follows it will be useful to define the parameters  $\epsilon_{JI}^{HL}$ ,  $\epsilon_{JI}^{HR}$ ,  $\epsilon_{JI}^{GL}$  and  $\epsilon_{JI}^{GR}$  through

$$\left[ P_{RL}^H \right]^{JI} = \eta_L^H \overline{m}_{u_J} V_{JI}^{\text{eff}} (1 - \epsilon_{JI}^{HL}), \quad \left[ P_{LR}^H \right]^{JI} = \eta_R^H V_{JI}^{\text{eff}} \overline{m}_{d_I} (1 - \epsilon_{JI}^{HR}), \quad (2.48)$$

$$\left[ P_{RL}^G \right]^{JI} = \eta_L^G \overline{m}_{u_J} V_{JI}^{\text{eff}} (1 + \epsilon_{JI}^{GL}), \quad \left[ P_{LR}^G \right]^{JI} = \eta_R^G V_{JI}^{\text{eff}} \overline{m}_{d_I} (1 + \epsilon_{JI}^{GR}). \quad (2.49)$$

This parametrization of the  $H^+$  and  $G^+$  couplings differs from the parametrization in terms of  $\epsilon'$  factors introduced in ref. [25] but is more natural for our purposes. In

particular it emphasizes the fact that ultimately all vertices should be expressed in terms of  $\overline{m}_i$  and  $V_{JI}^{\text{eff}}$ .

The numerical analysis of the parameters  $\epsilon_{JI}^{HL}$ ,  $\epsilon_{JI}^{HR}$ ,  $\epsilon_{JI}^{GL}$  and  $\epsilon_{JI}^{GR}$  is presented in section 5. While the general formulae for these parameters are rather involved, they simplify considerably in the  $SU(2) \times U(1)$  symmetry limit with the gauge couplings  $g_1$  and  $g_2$  set to zero as we will see in section 3. In particular the parameters  $\epsilon_{JI}^{GL}$  and  $\epsilon_{JI}^{GR}$  vanish in this limit. Therefore  $\epsilon_{JI}^{GL}$  and  $\epsilon_{JI}^{GR}$  should be generally smaller than  $\epsilon_{JI}^{HL}$ , and  $\epsilon_{JI}^{HR}$ . This expectation is confirmed by our numerical analysis presented in section 5.

## 2.6 Chargino-Quark-Squark Vertices

In the approach formulated above charginos and squarks are integrated out and do not appear as explicit degrees of freedom in the low energy effective theory. Their virtual effects are accounted for by corrections  $\Delta m_{d,u}$ , various formfactors  $\Delta F$  and, as already mentioned, by higher dimension operators. Let us consider for definiteness one of several such non-renormalizable operators

$$\Delta \mathcal{L}^{\text{eff}} = -C_{JIMN}^{VLR} \left( \overline{(d_J)_L} \gamma^\mu (d_I)_L \right) \left( \overline{(d_M)_R} \gamma_\mu (d_N)_R \right) \quad (2.50)$$

which is generated by chargino-stop box diagrams in the course of integrating out these particles.  $C_{JIMN}^{VLR}$  are the Wilson coefficients that depend on flavour indices  $J, I, M, N$  and can be calculated by using the original MSSM vertices

$$\mathcal{L}_\chi^{\text{MSSM}} = - \sum_{i=1,2} \overline{\chi_i} \tilde{u}^\dagger \left( c_L^i d_L + c_R^i d_R \right) + \text{H.c.} \quad (2.51)$$

which (in the matrix notation) have the following structure [30]:

$$c_L^i = \left( a^i + b^i \cdot \frac{m_u}{\sin \beta} \right) \cdot V, \quad c_R^i = \frac{h^i}{\cos \beta} \cdot V \cdot m_d \quad (2.52)$$

Here  $a^i$ ,  $b^i$  and  $h^i$  are  $6 \times 3$  matrices that depend on chargino compositions and left-right mixing of squarks. The coefficients like  $C_{JIMN}^{VLR}$  corresponding to definite chiralities of external quark fields are given as sums over squark and chargino indices of appropriate products of  $c_L^i$ ,  $c_R^i$ ,  $(c_L^i)^\dagger$  and  $(c_R^i)^\dagger$  weighted by some functions of chargino and up-type squark masses.

The operations (2.3) and (2.8) performed on the quark fields in the effective Lagrangian affect also the coefficient  $C_{JIMN}^{VLR}$ . Neglecting rescalings (2.3) which are not enhanced by  $\tan \beta$  it is easy to see that the rotations (2.8) amount simply to the multiplication from the right of each  $c_L^i$  and  $c_R^i$  entering  $C_{JIMN}^{VLR}$  by the matrix  $\mathbf{D}_L$  and  $\mathbf{D}_R$ , respectively. From

(2.21) it follows that in the approximation  $\Delta \mathbf{U}_{L(R)} \approx 0$  this has the effect of replacing  $V$  by  $V^{\text{eff}}$  in all  $c_L^i$ . For the factors  $c_R^i$  the effect of the rotation is more complicated:

$$V \cdot m_d \cdot \mathbf{D}_R \approx V^{\text{eff}} \cdot \mathbf{D}_L^\dagger \cdot m_d \cdot \mathbf{D}_R \approx V^{\text{eff}} \cdot m_d + V^{\text{eff}} \cdot (m_d \cdot \Delta \mathbf{D}_R - \Delta \mathbf{D}_L \cdot m_d)$$

Thus, the most important effects of the rotations (2.8) in the non-renormalizable operators can be simply taken into account by calculating their Wilson coefficients using the modified chargino-squark couplings:

$$c_L^i \rightarrow \left( a^i + b^i \cdot \frac{m_u}{\sin \beta} \right) \cdot V^{\text{eff}}, \quad (2.53)$$

$$c_R^i \rightarrow \frac{h^i}{\cos \beta} \cdot \left[ V^{\text{eff}} \cdot m_d + V^{\text{eff}} \cdot (m_d \cdot \Delta \mathbf{D}_R - \Delta \mathbf{D}_L \cdot m_d) \right] \quad (2.54)$$

where  $m_{u_j} \approx \overline{m}_{u_j}$  and  $m_{d_I} = \overline{m}_{d_I} / (1 + \epsilon_{d_I} \tan \beta)$ .

The effective vertices of the effective Lagrangian calculated as described in this section do depend on the renormalization scale  $\mu_R$ . According to the standard reasoning this scale should be of the order of the mass scale of the particles which are integrated out. The couplings and masses of the effective Lagrangian should be then treated as running parameters. For example, the contribution of the Higgs boson exchanges to the Wilson coefficients of the effective Hamiltonians discussed in sec. 6 should be calculated at the scale  $\mu_{R'} \sim M_{\text{Higgs}} \sim M_{H^+}$ . If the  $M_{\text{SUSY}} \gg M_{\text{Higgs}} \sim M_{H^+}$ , the couplings of the effective Lagrangian should be evolved with the effective theory RGEs from  $\mu_R \sim M_{\text{SUSY}}$  down  $\mu_{R'} \sim M_{\text{Higgs}} \sim M_{H^+}$ . In our numerical results we neglect this running as it would not change the results drastically. It should be however taken into account to predict physical quantities in the MSSM with higher accuracy.

Finally let us stress that although in what follows we will restrict our attention to the version of the MSSM in which flavour and CP violation are ruled by the CKM matrix, the effective Lagrangian approach described in this section is more general and can be used [6, 7] also in the case of flavour and CP violation originating in the squark sector.

### 3 The limit of unbroken $SU(2) \times U(1)$ symmetry

In this section we will discuss the approach of ref. [27] that can be considered as a special limit of the more general approach presented in section 2. We will also compare our results with the recent analysis presented in [28] that goes beyond supersymmetry but similarly to [27] is based on the same approximation. In order to relate these approaches



to our approach we consider decoupling of sparticles in the limit of unbroken  $SU(2) \times U(1)$  symmetry. The electroweak symmetry breaking is then taken into account after sparticles are integrated out. The main goal of this section is the derivation of explicit expressions for the flavour changing neutral scalar couplings  $[X_{RL}^S]^{JI}$  and  $[X_{LR}^S]^{JI}$  and the charged scalar couplings  $[P_{RL}^H]^{JI}$ ,  $[P_{LR}^H]^{JI}$ ,  $[P_{RL}^G]^{JI}$  and  $[P_{LR}^G]^{JI}$  at large  $\tan \beta$  in the  $SU(2) \times U(1)$  symmetry limit. This approximation should be valid if the sparticle mass scale is larger than the mass scale of the Higgs boson sector (set by  $M_{H^+}$ ). It should be emphasized that the absence of vacuum expectation values before decoupling implies neglecting the left-right mixing of squarks even for non-vanishing  $A_{u,d}$  and/or  $\mu$  parameters.

In this section following the practice in the existing literature we will assume also the dominance of  $\alpha_s$  and top and bottom Yukawa couplings neglecting the contributions of the electroweak couplings  $g_2$  and  $g_1$ . We will assess the validity of this approximation in section 5.

### 3.1 Minimal Flavour Violation and Flavour Dependence

The large  $\tan \beta$  enhanced corrections in the approach of [27, 28] are governed in the MSSM by four universal parameters that we will denote by  $\epsilon_0$ ,  $\epsilon_Y$ ,  $\epsilon'_0$  and  $\epsilon'_Y$ . These parameters as defined in [27, 28] are flavour independent. Therefore flavour dependence enters the Higgs and chargino couplings only through the CKM matrix  $V_{\text{eff}}$ . This scenario can only be realized if the soft SUSY breaking mass squared matrix  $m_Q^2$  is strictly proportional to the unit matrix. This corresponds to the Minimal Flavour Violation as defined in ref. [28] and to the scenario A in [22].

However, in more realistic situations the diagonal entries  $m_{Q_3}^2$ ,  $m_{U_3}^2$  and  $m_{D_3}^2$  of the matrices  $m_Q^2$ ,  $m_U^2$  and  $m_D^2$  that are related to third generation squarks differ from the entries corresponding to the first two generations to be denoted collectively by  $m^2$ . As pointed out in [1] in this situation some flavour violation (still ruled by the CKM matrix) unavoidably appears in the up- or down-type (or in both) squark mass squared matrices. For  $m^2 \neq m_{Q_3}^2$ , at the phenomenological level, it becomes a matter of choice in which basis  $m_Q^2$  is assumed to be diagonal. The two simplest choices are

$$(\mathcal{M}_D^2)_{\text{LL}} = m_Q^2 + \dots \quad \text{and} \quad (\mathcal{M}_U^2)_{\text{LL}} = V m_Q^2 V^\dagger + \dots \quad (3.1)$$

or

$$(\mathcal{M}_D^2)_{\text{LL}} = V^\dagger m_Q^2 V + \dots \quad \text{and} \quad (\mathcal{M}_U^2)_{\text{LL}} = m_Q^2 + \dots \quad (3.2)$$

where  $m_Q^2$  is diagonal and the ellipses stand for other diagonal terms. In the classification in [22], the settings in (3.1) and (3.2) correspond to scenarios B and C, respectively.

In our calculations in the approach of section 2 we choose the soft SUSY breaking mass parameter  $m_Q^2$  as in (3.1). The scenario (3.2) with flavour violation in the down-type squark mass matrix would require the inclusion of box and Higgs penguin diagrams with gluinos and is beyond the scope of this paper. Note that in SUSY breaking scenarios like minimal SUGRA or gauge mediation, in which proportionality of  $m_Q^2$  to the unit matrix is assumed at some high scale, the renormalization group evolution produces calculable off diagonal terms both in  $(\mathcal{M}_U^2)_{LL}$  and in  $(\mathcal{M}_D^2)_{LL}$ . This is however a secondary effect as the evolution has to generate first the splitting of the diagonal entries of the squark mass matrices. The magnitude of the off diagonal entries is then proportional to this splitting. Due to this fact the effects of the splitting are always more important in flavour changing amplitudes. Our framework should therefore constitute a good approximation to predictions of the SUSY breaking scenarios in which at some high scale the matrices  $m_Q^2$ ,  $m_U^2$  and  $m_D^2$  are proportional to the unit matrix and the trilinear soft parameters  $A_t$  and  $A_b$  are real.

Allowing for different values of the parameters  $m_{Q_3}^2$ ,  $m_{U_3}^2$ ,  $m_{D_3}^2$  and  $m^2$  introduces some flavour dependence into  $\epsilon_0$ ,  $\epsilon_Y$ ,  $\epsilon'_0$ ,  $\epsilon'_Y$  and the formulae for various couplings presented in [27, 28] have to be generalized to account for it. However, for the sake of comparison with [27, 28] we will for the most part of this section treat  $\epsilon_0$ ,  $\epsilon_Y$ ,  $\epsilon'_0$  and  $\epsilon'_Y$  as universal flavour independent quantities and only at the end, in subsection 3.6, we will provide formulae for various couplings that are also valid for flavour dependent  $\epsilon_0$ ,  $\epsilon_Y$ ,  $\epsilon'_0$  and  $\epsilon'_Y$ . As we will see in sec. 5, obtaining a numerically reliable approximation to the results of the complete calculation done as in sec. 2 will require extending the approach of refs. [27, 28] by taking into account both the flavour dependence of  $\epsilon_0$ ,  $\epsilon_Y$ ,  $\epsilon'_0$  and  $\epsilon'_Y$  and the effects of the electroweak couplings  $g_2$  and  $g_1$ . The latter will be automatically included in the formulae presented in sec. 3.6 by defining appropriately flavour dependent factors  $\epsilon_0$ ,  $\epsilon_Y$ ,  $\epsilon'_0$  and  $\epsilon'_Y$  as discussed in section 5. Thus, the analytic expressions of sec. 3.6 are the basis of the approximation that within a few percent reproduces the numerical results of the full approach of section 2 which includes automatically both the  $SU(2) \times U(1)$  breaking effects and the effects of electroweak couplings.

## 3.2 Effective Lagrangians

In this approach below the sparticle mass scale we get the effective Lagrangian whose part relevant for the neutral Higgs boson couplings to the down-type quarks has the form [31, 20]

$$\mathcal{L}_{\text{eff}} = -\epsilon_{ij} H_i^{(d)} \overline{d_R} \cdot (\mathbf{Y}_d + \Delta_d \mathbf{Y}_d) \cdot q_{jL} - H_i^{(u)*} \overline{d_R} \cdot \Delta_u \mathbf{Y}_d \cdot q_{iL} + \text{H.c.} \quad (3.3)$$

where  $\epsilon_{21} = -\epsilon_{12} = 1$  and  $\mathbf{Y}_{d,u}$  are Yukawa coupling matrices. As in the papers [27, 28] we make further assumption (which by itself is not related to the symmetry limit) that the effects of the electroweak gauge couplings  $g_1$  and  $g_2$  are negligible. We will examine numerically the validity of this approximation in sec. 5. With this assumption the only diagrams giving rise to the correction  $\Delta_u \mathbf{Y}_d$  are shown in Figs. 5a and 5b. The loop induced term  $-\epsilon_{ij} H_i^{(d)} \Delta_d \mathbf{Y}_d$  is always subleading in the large  $\tan\beta$  limit and can be neglected. In the basis in which

$$\mathbf{Y}_d = \text{diag}(y_d), \quad \mathbf{Y}_u = \text{diag}(y_u) \cdot V \quad (3.4)$$

the correction  $\Delta_u \mathbf{Y}_d$  can be easily seen to have the structure [27]

$$(\Delta_u \mathbf{Y}_d)^{JI} = -y_{d_J} \left( \epsilon_0 \delta^{JI} + \epsilon_Y y_t^2 V^{3J*} V^{3I} \right) \equiv -y_{d_J} \left( \tilde{\epsilon}_J \delta^{JI} + \epsilon_Y y_t^2 \lambda_0^{JI} \right) \quad (3.5)$$

where the contributions proportional to  $y_u^2$  and  $y_c^2$  have been neglected,

$$\tilde{\epsilon}_J \equiv \epsilon_0 + \epsilon_Y y_t^2 V^{3J*} V^{3J} \approx \epsilon_0 + \epsilon_Y y_t^2 \delta^{J3} \quad (3.6)$$

and

$$\lambda_0^{JI} = V^{3J*} V^{3I} \quad \text{for } J \neq I \quad \text{and} \quad \lambda_0^{JJ} = 0 \quad \text{for } J = I. \quad (3.7)$$

The approximation in (3.6) is justified by the hierarchical structure of the elements of the CKM matrix. The correction  $\Delta_d \mathbf{Y}_d$  has the same structure (3.5) as  $\Delta_u \mathbf{Y}_d$  but is subleading for large  $\tan\beta$ .

As follows from figs. 5a and 5b, in  $(\Delta_u \mathbf{Y}_d)^{JI}$  the correction  $\epsilon_0$  depends on the gluino mass and the masses of the  $\tilde{D}_j^c$  and  $\tilde{Q}_J$  squarks, while  $\epsilon_Y$  depends on the  $\mu$  parameter and the masses of the  $\tilde{Q}_J$  and  $\tilde{U}_3^c$  squarks. Note that in this limit the parameter  $\mu$  plays the role of the mass of the higgsinos. The dependence of  $\epsilon_0(\tilde{D}_j^c, \tilde{Q}_J)$  and  $\epsilon_Y(\tilde{Q}_J, \tilde{U}_3^c)$  on the generation indices can be neglected if the squark masses are not significantly split. It will be taken into account in sec. 3.6

Decomposing the two Higgs doublets as

$$\begin{aligned} H_1^{(d)} &= \frac{v_d}{\sqrt{2}} + \frac{1}{\sqrt{2}} \left( c_\alpha H^0 - s_\alpha h^0 + i s_\beta A^0 - i c_\beta G^0 \right) \\ H_2^{(u)*} &= \frac{v_u}{\sqrt{2}} + \frac{1}{\sqrt{2}} \left( s_\alpha H^0 + c_\alpha h^0 - i c_\beta A^0 - i s_\beta G^0 \right) \end{aligned} \quad (3.8)$$

(where  $c_\alpha \equiv \cos \alpha$ , etc.) we find first

$$\mathcal{L}_{\text{mass}}^{(d)} = \bar{d}_R \cdot \left( \frac{v_d}{\sqrt{2}} y_d + \frac{v_d}{\sqrt{2}} \Delta_d \mathbf{Y}_d - \frac{v_u}{\sqrt{2}} \Delta_u \mathbf{Y}_d \right) \cdot d_L + \text{H.c.} \quad (3.9)$$

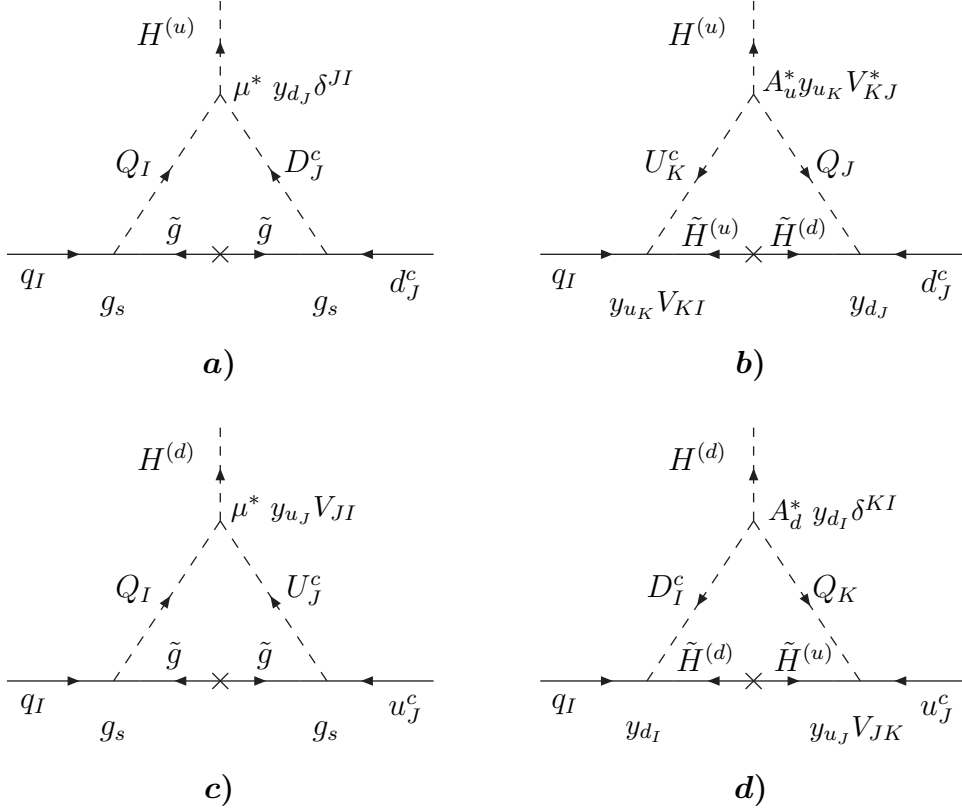


Figure 5: Vertex corrections in the  $SU(2) \times U(1)$  symmetry limit for vanishing electroweak gauge couplings. Diagrams a) and b) give rise to corrections  $(\Delta_u \mathbf{Y}_d)^{JI}$ . Corrections  $(\Delta_d \mathbf{Y}_d)^{JI}$  are generated by similar diagrams with outgoing  $H^{(u)}$  replaced by incoming  $H^{(d)}$  and factors  $\mu^*$  and  $A_u^*$  in diagrams a) and b) replaced by  $A_d$  and  $\mu$ , respectively. Diagrams c) and d) give rise to corrections  $(\Delta_d \mathbf{Y}_u)^{JI}$ . Corrections  $(\Delta_u \mathbf{Y}_u)^{JI}$  are generated by similar diagrams with outgoing  $H^{(d)}$  replaced by incoming  $H^{(u)}$  and factors  $\mu^*$  and  $A_d^*$  in diagrams c) and d) replaced by  $A_u$  and  $\mu$ , respectively.

Comparison with (2.4) gives then

$$(\Delta m_d)^{JI} = -\frac{v_d}{\sqrt{2}} (\Delta_d \mathbf{Y}_d - \tan \beta \Delta_u \mathbf{Y}_d)^{JI} \approx \frac{v_d}{\sqrt{2}} \tan \beta (\Delta_u \mathbf{Y}_d)^{JI}. \quad (3.10)$$

In our conventions

$$m_{d_J} = -\frac{v_d}{\sqrt{2}} y_{d_J}, \quad m_{u_J} = \frac{v_u}{\sqrt{2}} y_{u_J} \quad (3.11)$$

and  $v_d^2 / \cos^2 \beta = v_u^2 / \sin^2 \beta = 1 / \sqrt{2} G_F \approx (246 \text{ GeV})^2$ . Consequently

$$\begin{aligned} (\Delta m_d)^{JI} &= m_{d_J} \tan \beta (\tilde{\epsilon}_J \delta^{JI} + \epsilon_Y y_t^2 \lambda_0^{JI}) \\ (\Delta m_d^\dagger)^{JI} &= m_{d_I} \tan \beta (\tilde{\epsilon}_I \delta^{JI} + \epsilon_Y y_t^2 \lambda_0^{JI}) \\ \kappa_{d_J} &\approx \epsilon_{d_J} \tan \beta = \tilde{\epsilon}_J \tan \beta \end{aligned} \quad (3.12)$$

with  $\epsilon_{d_J}$  defined in (2.30) and  $\tilde{\epsilon}_J$  given in (3.6). The last equation tells us that in the approximation considered here  $\epsilon_{d_J} = \tilde{\epsilon}_J$ . Thus using (2.9) we have

$$m_{d_J} = \frac{\overline{m}_{d_J}}{1 + \tilde{\epsilon}_J \tan \beta}, \quad (3.13)$$

with  $\overline{m}_{d_J}$  denoting the running quark masses as discussed in Section 2. Note that the large  $\tan \beta$  corrections to  $m_d$  and  $m_s$  in contrast to  $m_b$  do not involve the top Yukawa coupling.

Similarly the corrections to the up-type quarks Yukawa coupling can be summarized by the effective Lagrangian

$$\mathcal{L}_{\text{eff}} = -\epsilon_{ij} H_i^{(u)} \overline{u}_R \cdot (\mathbf{Y}_u + \Delta_u \mathbf{Y}_u) \cdot q_{jL} - H_i^{(d)*} \overline{u}_R \cdot \Delta_d \mathbf{Y}_u \cdot q_{iL} + \text{H.c.} \quad (3.14)$$

The correction  $\Delta_d \mathbf{Y}_u$  is generated by the diagrams shown in figs. 5c and 5d. In the basis (3.4) one has

$$(\Delta_d \mathbf{Y}_u)^{JI} = y_{u_J} V_{JI} \left( \epsilon'_0 + \epsilon'_Y y_{d_I}^2 \right). \quad (3.15)$$

where the factor  $\epsilon'_0$  depends on the masses of gluino and  $\tilde{U}_J^c$  and  $\tilde{Q}_I$  squarks, while  $\epsilon'_Y$  depends on the  $\mu$  parameter and the masses of  $\tilde{Q}_I$  and  $\tilde{D}_I^c$  squarks. For squark masses not significantly split the generation dependence of  $\epsilon'_0(\tilde{U}_J^c, \tilde{Q}_I)$  and  $\epsilon'_Y(\tilde{Q}_I, \tilde{D}_I^c)$  on the generation indices can be dropped. The correction  $\Delta_u \mathbf{Y}_u$  has the same general structure. The mass term for the up-type quarks takes then the form

$$\mathcal{L}_{\text{mass}}^{(u)} = -\overline{u}_R \cdot \left( \frac{v_u}{\sqrt{2}} y_u V + \frac{v_u}{\sqrt{2}} \Delta_u \mathbf{Y}_u + \frac{v_d}{\sqrt{2}} \Delta_d \mathbf{Y}_u \right) \cdot u_L + \text{H.c.} \quad (3.16)$$

Note that the effects of the correction  $\Delta_d \mathbf{Y}_u$  are suppressed by  $\tan \beta$  with respect to the effects of the correction  $\Delta_u \mathbf{Y}_u$  which itself is not  $\tan \beta$  enhanced with respect to the tree level mass term. The corrected mass term (3.16) is diagonalized by the rotations

$$u_L \rightarrow V^\dagger \cdot \mathbf{U}_L u_L, \quad \overline{u}_R \rightarrow \overline{u}_R \mathbf{U}_R^\dagger \quad (3.17)$$

that with  $\mathbf{U}_{L,R} = \mathbf{1} + \Delta\mathbf{U}_{L,R}$  satisfy the conditions (2.17) and (2.18) with

$$(\Delta m_u)^{JI} = \frac{v_u}{\sqrt{2}} \left( \Delta_u \mathbf{Y}_u \cdot V^\dagger + \cot \beta \Delta_d \mathbf{Y}_u \cdot V^\dagger \right)^{JI} \quad (3.18)$$

Since  $\Delta m_u$  is not  $\tan \beta$  enhanced,  $\mathbf{U}_{L,R}$  are in general very close to unit matrices. Consequently

$$m_{u,J} \approx \bar{m}_{u,J} . \quad (3.19)$$

### 3.3 Neutral Higgs-fermion vertices

Using the effective Lagrangian (3.3) and the decomposition (3.8) it is easy to identify in the  $SU(2) \times U(1)$  symmetry limit with zero  $g_1$  and  $g_2$  the vertex corrections  $\Delta F_{L(R)}^{dS}$  for  $S^0 = H^0, h^0, A^0$  and  $G^0$  defined in eq. (2.24). We find:

$$\begin{aligned} (F_L^{dS})^J &= \frac{m_{dJ}}{v_d} x_d^S = (F_R^{dS})^{J*} \\ (\Delta F_L^{dS})^{JI} &= \frac{m_{dJ}}{v_d} \left( \tilde{\epsilon}_J \delta^{JI} + \epsilon_Y y_t^2 \lambda_0^{JI} \right) x_u^S = (\Delta F_R^{dS})^{IJ*} \end{aligned} \quad (3.20)$$

where

$$x_d^S = (c_\alpha, -s_\alpha, i s_\beta, -i c_\beta), \quad x_u^S = (s_\alpha, c_\alpha, -i c_\beta, -i s_\beta) \quad (3.21)$$

for  $S^0 = H^0, h^0, A^0$  and  $G^0$ , respectively. In obtaining (3.20) we have set  $\Delta_d \mathbf{Y}_d$  to zero as done in refs. [27] and [28]. We will proceed in the same manner in deriving the formulae for the neutral Higgs couplings below. However, at the end of this subsection we will list for completeness the corrections to these formulae due to a non-vanishing  $\Delta_d \mathbf{Y}_d$ .

It is now easy to check that the diagonal part (2.32) of the  $\bar{d}S^0 d$  vertex is

$$[X^S]^{JJ} \equiv \left( \eta_L^{dS} \frac{\bar{m}_{dJ}}{1 + \epsilon_{dJ} \tan \beta} + \Delta F_L^{dS} \right)^{JJ} = \frac{\bar{m}_{dJ}}{v_d(1 + \tilde{\epsilon}_J \tan \beta)} \left( x_d^S + \tilde{\epsilon}_J x_u^S \right) . \quad (3.22)$$

For the flavour changing couplings  $[X_{RL}^S]^{JI}$  with  $J > I$ , neglecting  $\Sigma_{VL}^d$  and  $\Sigma_{VR}^d$  and ignoring the contribution of  $\Delta_d \mathbf{Y}_d$  one gets from (2.34)

$$\begin{aligned} [X_{RL}^S]^{JI} &= \frac{m_{dJ}}{v_d} \epsilon_Y y_t^2 \lambda_0^{JI} \left[ x_u^S - \frac{\tan \beta}{1 + \tilde{\epsilon}_J \tan \beta} x_d^S - \frac{\tilde{\epsilon}_J \tan \beta}{1 + \tilde{\epsilon}_J \tan \beta} x_u^S \right] \\ &= \frac{\bar{m}_{dJ}}{v_d(1 + \tilde{\epsilon}_J \tan \beta)^2} \epsilon_Y y_t^2 \lambda_0^{JI} \left( x_u^S - x_d^S \tan \beta \right) \end{aligned} \quad (3.23)$$

in agreement with equation (9) of ref. [27]. Notice that effects of the genuine vertex correction  $\Delta F_L^{dS}$  (proportional to  $x_u^S$ ) are subleading compared to the effects of the rotation  $\Delta \mathbf{D}_L \propto \Delta m_d$ . In the case of split mass parameters  $m_Q^2$ , the factor  $\epsilon_Y$  in (3.23) depends on  $m_Q^2$  of the  $J$ -th generation and  $m_U^2$  of the third generation.

Similarly, neglecting  $\Delta_d \mathbf{Y}_d$  we find from (2.35) an explicit expression for  $[X_{LR}^S]^{JI}$  with  $J > I$

$$\begin{aligned} [X_{LR}^S]^{JI} &= \frac{m_{d_I}}{v_d} \epsilon_Y y_t^2 \lambda_0^{JI} \left[ x_u^{S*} - \tan \beta \frac{m_{d_J}}{\overline{m}_{d_J}} \epsilon_Y y_t^2 \delta^{J3} x_u^{S*} - \tan \beta \frac{\overline{m}_{d_I} m_{d_J}^2}{m_{d_I} \overline{m}_{d_J}^2} (x_d^{S*} + \tilde{\epsilon}_J x_u^{S*}) \right] \\ &= \frac{\overline{m}_{d_I}}{v_d (1 + \tilde{\epsilon}_J \tan \beta)^2} \epsilon_Y y_t^2 \lambda_0^{JI} (x_u^{S*} - x_d^{S*} \tan \beta) . \end{aligned} \quad (3.24)$$

that has not been given in [27]. In particular this formula does not follow from the equation (9) of this paper, that for  $J > I$  is valid only for the  $[X_{RL}^S]^{JI}$  couplings. The expression (3.24) has been derived under the assumption that  $\epsilon_Y(\tilde{Q}_J, \tilde{U}_3^c) \approx \epsilon_Y(\tilde{Q}_I, \tilde{U}_3^c)$ . Note, that in this case  $[X_{LR}^S]^{JI}$  can be obtained from  $[X_{RL}^S]^{JI}$  by simply replacing  $\overline{m}_{d_J}$  by  $\overline{m}_{d_I}$  and complex conjugation of  $x_d^S$  and  $x_u^S$  without any other changes in the indices. The couplings  $[X_{RL}^S]^{JI}$  and  $[X_{LR}^S]^{JI}$  for  $J < I$  can be found by applying the rule (2.36) to (3.24) and (3.23), respectively.

In the same approximation it is easy to derive the relation between the CKM matrix  $V_{JI}$  of the MSSM and the effective matrix  $V_{JI}^{\text{eff}}$ . Using the hierarchy of quark masses and CKM matrix entries (and neglecting  $\Delta \mathbf{U}_L$ ) one obtains from eqs. (2.21), (2.13), (3.12) the relations [24, 20, 27]

$$\begin{aligned} V_{JI} &= V_{JI}^{\text{eff}} \begin{bmatrix} 1 + \tilde{\epsilon}_3 \tan \beta \\ 1 + \epsilon_0 \tan \beta \end{bmatrix} \quad \text{for } (JI) = (13), (23), (31) \text{ and } (32), \\ V_{JI} &= V_{JI}^{\text{eff}} \quad \text{otherwise.} \end{aligned} \quad (3.25)$$

We can now summarize the results for the neutral Higgs-quark vertices. In the case of  $B$ -physics the pairs  $(J, I) = (3, 2), (3, 1), (2, 3)$  and  $(1, 3)$  matter. Combining (3.23), (3.24), the corresponding formulae for  $J < I$ , and (3.25) and neglecting the dependence of  $\epsilon_0$  and  $\epsilon_J$  on the generation indices we find the final formulae for the neutral Higgs couplings relevant for  $B$ -physics that exhibit all large  $\tan \beta$  enhanced corrections:

$$[X_{RL}^S]^{JI} = \frac{g_2}{2M_W \cos \beta} \frac{\overline{m}_{d_J} V_{\text{eff}}^{3J*} V_{\text{eff}}^{3I}}{(1 + \tilde{\epsilon}_3 \tan \beta)(1 + \epsilon_0 \tan \beta)} \epsilon_Y y_t^2 (x_u^S - x_d^S \tan \beta) , \quad (3.26)$$

$$[X_{LR}^S]^{JI} = \frac{g_2}{2M_W \cos \beta} \frac{\overline{m}_{d_I} V_{\text{eff}}^{3J*} V_{\text{eff}}^{3I}}{(1 + \tilde{\epsilon}_3 \tan \beta)(1 + \epsilon_0 \tan \beta)} \epsilon_Y y_t^2 (x_u^{S*} - x_d^{S*} \tan \beta) , \quad (3.27)$$

that are valid for both  $J > I$  and  $J < I$ .

In the case of  $K$ -physics the pairs  $(J, I) = (2, 1)$  and  $(1, 2)$  matter and we find

$$[X_{RL}^S]^{JI} = \frac{g_2}{2M_W \cos \beta} \overline{m}_{d_J} V_{\text{eff}}^{3J*} V_{\text{eff}}^{3I} \frac{(1 + \tilde{\epsilon}_3 \tan \beta)^2}{(1 + \epsilon_0 \tan \beta)^4} \epsilon_Y y_t^2 (x_u^S - x_d^S \tan \beta) . \quad (3.28)$$

$$[X_{LR}^S]^{JI} = \frac{g_2}{2M_W \cos \beta} \overline{m}_{d_I} V_{\text{eff}}^{3J*} V_{\text{eff}}^{3I} \frac{(1 + \tilde{\epsilon}_3 \tan \beta)^2}{(1 + \epsilon_0 \tan \beta)^4} \epsilon_Y y_t^2 (x_u^{S*} - x_d^{S*} \tan \beta) . \quad (3.29)$$

It is evident from (3.21) and (3.26)-(3.29) that the flavour violating couplings of  $G^0$  vanish in this limit.

Finally, we would like to list the corrections to (3.20), (3.22), (3.23) and (3.24) that result from

$$(\Delta_d \mathbf{Y}_d)^{JI} = -y_{d_J} \left( \tilde{e}_J \delta^{JI} + e_Y y_t^2 \lambda_0^{JI} \right) \quad (3.30)$$

with  $e_0$ ,  $e_Y$  and  $\tilde{e}_J$  replacing  $\epsilon_0$ ,  $\epsilon_Y$  and  $\tilde{\epsilon}_J$  in  $\Delta_u \mathbf{Y}_d$ , respectively. We find:

$$\delta \left( \Delta F_L^{dS} \right)^{JI} = -\frac{m_{d_J}}{v_d} \left( \tilde{e}_J \delta^{JI} + e_Y y_t^2 \lambda_0^{JI} \right) x_d^S \quad (3.31)$$

and

$$\left( x_d^S + \tilde{\epsilon}_J x_u^S \right) \rightarrow \left( x_d^S - \tilde{e}_J x_d^S + \tilde{\epsilon}_J x_u^S \right) \quad (3.32)$$

in (3.22). In  $[X_{RL}^S]^{JI}$  and  $[X_{LR}^S]^{JI}$  the correction  $\Delta_d \mathbf{Y}_d$  produces the following subleading terms:

$$\delta [X_{RL}^S]^{JI} = \frac{\overline{m}_{d_J}}{v_d (1 + \tilde{\epsilon}_J \tan \beta)^2} y_t^2 \lambda_0^{JI} [-e_Y + (e_0 \epsilon_Y - e_Y \epsilon_0) \tan \beta] x_d^S \quad (3.33)$$

$$\delta [X_{LR}^S]^{JI} = \frac{\overline{m}_{d_I}}{v_d (1 + \tilde{\epsilon}_J \tan \beta)^2} y_t^2 \lambda_0^{JI} [-e_Y + (e_0 \epsilon_Y - e_Y \epsilon_0) \tan \beta] x_d^{S*} \quad (3.34)$$

which are smaller than the  $x_d^S \tan \beta$  terms in eqs. (3.24), (3.23) but can be of the same order of magnitude as the  $x_u^S$  ones. The analysis of sec. 5 shows that the above terms are not numerically important.

### 3.4 Charged Higgs-fermion vertices

In the same approximation we can consider also the corrections to the charged Higgs boson and charged Goldstone boson couplings. In order to find explicit expressions for the charged scalar ( $H^\pm$ ) and charged Goldstone boson ( $G^\pm$ ) couplings defined in (2.39) and (2.40), we combine the effective Lagrangians (3.3) and (3.14). Performing the rotations (2.6) and (3.17) we find

$$\begin{aligned} \mathcal{L}_{\text{eff}}^{\text{tot}} = & \overline{u}_R \mathbf{U}_R^\dagger \left[ H_1^{(u)} \left( y_u + \Delta_u \mathbf{Y}_u \cdot V^\dagger \right) - H_2^{(d)*} \Delta_d \mathbf{Y}_u \cdot V^\dagger \right] \mathbf{U}_L \cdot V^{\text{eff}} d_L \\ & + \overline{u}_L V^{\text{eff}} \cdot \mathbf{D}_L^\dagger \left[ -H_2^{(d)*} \left( y_d + (\Delta_d \mathbf{Y}_d)^\dagger \right) - H_1^{(u)} (\Delta_u \mathbf{Y}_d)^\dagger \right] \mathbf{D}_R d_R \end{aligned} \quad (3.35)$$

where we have used the definition (2.21) of  $V^{\text{eff}}$ .

Expressing  $H_2^{(d)*}$  and  $H_1^{(u)}$  in terms of  $H^+$  and  $G^+$  as follows

$$H_2^{(d)*} = H^+ \sin \beta - G^+ \cos \beta, \quad H_1^{(u)} = H^+ \cos \beta + G^+ \sin \beta \quad (3.36)$$



we calculate, the couplings  $[P_{RL}^H]^{JI}$ ,  $[P_{LR}^H]^{JI}$ ,  $[P_{RL}^G]^{JI}$ ,  $[P_{LR}^G]^{JI}$  in (2.39) and (2.40) and the parameters  $\epsilon_{JI}^{HL}$ ,  $\epsilon_{JI}^{HR}$ ,  $\epsilon_{JI}^{GL}$  and  $\epsilon_{JI}^{GR}$  defined by eqs. (2.48) and (2.49).

For  $G^+$  couplings, using (3.36) and comparing terms in square brackets of eq. (3.35) with eqs. (3.9), (3.10), (3.16), (3.18) we find

$$\begin{aligned} \mathcal{L}_{\text{eff}}^{G^+} &= \frac{\sqrt{2}}{v} G^+ \bar{u}_R \mathbf{U}_R^\dagger [m_u + \Delta m_u] \mathbf{U}_L \cdot V^{\text{eff}} d_L \\ &\quad - \frac{\sqrt{2}}{v} G^+ \bar{u}_L V^{\text{eff}} \cdot \mathbf{D}_L^\dagger [m_d + (\Delta m_d)^\dagger] \mathbf{D}_R d_R. \end{aligned} \quad (3.37)$$

Subsequently using the relations (2.7), (2.17), we easily find ( $\sqrt{2}/v = g_2/\sqrt{2}M_W$ ):

$$\mathcal{L}_{\text{eff}}^{G^+} = \frac{g_2}{\sqrt{2}M_W} G^+ \bar{u}_R \bar{m}_u V^{\text{eff}} d_L - \frac{g_2}{\sqrt{2}M_W} G^+ \bar{u}_L V^{\text{eff}} \bar{m}_d d_R. \quad (3.38)$$

This compared with (2.49) implies

$$[P_{RL}^G]^{JI} = \frac{g_2}{\sqrt{2}M_W} \bar{m}_{u_J} V_{JI}^{\text{eff}}, \quad \epsilon_{JI}^{GL} = 0. \quad (3.39)$$

$$[P_{LR}^G]^{JI} = -\frac{g_2}{\sqrt{2}M_W} V_{JI}^{\text{eff}} \bar{m}_{d_I}, \quad \epsilon_{JI}^{GR} = 0. \quad (3.40)$$

The vanishing of  $\epsilon_{JI}^{GL}$  and  $\epsilon_{JI}^{GR}$  is easy to understand. Indeed, in the effective Lagrangian constructed before the electroweak symmetry breaking and defined by eqs. (3.3) and (3.14) the Higgs mechanism must operate in the standard way (e.g. in the  $R_\xi$  gauge the tree level exchange of  $G^+$  must cancel the gauge dependence of the amplitude generated by the  $W^+$  exchange) which requires that the  $G^+$  couplings to quarks be precisely as in the SM with the mass parameters corresponding to the tree-level quark masses in the effective theory (that is  $\bar{m}_{d(u)}$ ) and that the CKM matrix in the  $G^+$  couplings is the same as the one in the  $W^+$  couplings (that is  $V^{\text{eff}}$ ). The same argument shows that  $\epsilon_{JI}^{GL}$  and  $\epsilon_{JI}^{GR}$  must vanish in the  $SU(2) \times U(1)$  symmetry limit also without the approximation of vanishing electroweak gauge couplings.

For  $H^+$  couplings, from (3.35) and (3.36) we find

$$\begin{aligned} \mathcal{L}_{\text{eff}}^{H^+} &= \frac{\sqrt{2}}{v} H^+ \bar{u}_R \mathbf{U}_R^\dagger \left[ \cot \beta \left( m_u + \frac{v_u}{\sqrt{2}} \Delta_u \mathbf{Y}_u \cdot V^\dagger \right) - \tan \beta \frac{v_d}{\sqrt{2}} \Delta_d \mathbf{Y}_u \cdot V^\dagger \right] \mathbf{U}_L \cdot V^{\text{eff}} d_L \\ &\quad + \frac{\sqrt{2}}{v} H^+ \bar{u}_L V^{\text{eff}} \cdot \mathbf{D}_L^\dagger \left[ \tan \beta \left( m_d - \frac{v_d}{\sqrt{2}} (\Delta_d \mathbf{Y}_d)^\dagger \right) - \cot \beta \frac{v_u}{\sqrt{2}} (\Delta_u \mathbf{Y}_d)^\dagger \right] \mathbf{D}_R d_R \end{aligned} \quad (3.41)$$

We observe that in the first line of eq. (3.41)  $\Delta_d \mathbf{Y}_u$  cannot be neglected as it is multiplied by  $\tan \beta$ . On the other hand  $\Delta_u \mathbf{Y}_u$  can be neglected and  $\mathbf{U}_{L,R}$  can be approximated by unit matrices. Consequently we find for the  $\bar{u}_R H^+ d_L$  vertex

$$[P_{RL}^H]^{JI} \approx \frac{g_2}{\sqrt{2}M_W} \cos \beta \left[ V_{\text{eff}}^{JI} - \tan \beta \left( \epsilon'_0 V_{\text{eff}}^{JI} + \epsilon'_Y V^{JM} y_{d_M}^2 V^{KM*} V_{\text{eff}}^{KI} \right) \right] \quad (3.42)$$

Approximating next  $m_{u,J}$  by  $\overline{m}_{u,J}$  and expressing  $V$  through  $V^{\text{eff}}$  by means of (3.25), we find

$$[P_{RL}^H]^{JI} = \frac{g_2}{\sqrt{2}} \frac{m_{\overline{u}_J}}{M_W} \cos \beta V_{\text{eff}}^{JI} \left[ 1 - \tan \beta \left( \epsilon'_0 + \epsilon'_Y y_b^2 \delta^{I3} \right) - \Delta_{IJ} \right], \quad (3.43)$$

and consequently

$$\epsilon_{JI}^{HL} = \tan \beta \left( \epsilon'_0 + \epsilon'_Y y_b^2 \delta^{I3} \right) + \Delta_{JI} \quad (3.44)$$

where

$$\Delta_{JI} = y_b^2 y_t^2 \frac{\epsilon_Y \epsilon'_Y \tan^2 \beta}{1 + \epsilon_0 \tan \beta} \times \begin{cases} +1 & (J, I) = (1, 3), (2, 3) \\ -1 & (J, I) = (3, 1), (3, 2) \\ 0 & \text{otherwise} \end{cases} \quad (3.45)$$

This agrees with ref. [28], where the presence of  $\Delta_{JI}$  has been pointed out.

In calculating the  $\overline{u}_L H^+ d_R$  vertex in (3.41) we observe that the effects of  $\Delta_d \mathbf{Y}_d$  are not  $\tan \beta$  enhanced with respect to the tree level coupling and can therefore be neglected. The second term involving  $\Delta_u \mathbf{Y}_d$  is suppressed for large  $\tan \beta$  with respect to the first term and can also be neglected. Consequently

$$[P_{LR}^H]^{JI} \approx \frac{g_2}{\sqrt{2} M_W} \tan \beta \left[ V_{\text{eff}}^{JI} m_{d_I} + V_{\text{eff}}^{JK} (m_d \Delta \mathbf{D}_R - \Delta \mathbf{D}_L m_d)^{KI} \right]. \quad (3.46)$$

Using the formulae (2.15), (2.16), (3.12), (3.25) and retaining only terms dominant for large  $\tan \beta$  (and unsuppressed by quark mass ratios or small CKM matrix elements), we find

$$[P_{LR}^H]^{JI} = \frac{g_2}{\sqrt{2} M_W} \tan \beta V_{\text{eff}}^{JI} \frac{\overline{m}_{d_I}}{1 + \tilde{\epsilon}_J \tan \beta}, \quad \epsilon_{JI}^{HR} = \frac{\tilde{\epsilon}_J \tan \beta}{1 + \tilde{\epsilon}_J \tan \beta} \quad (3.47)$$

for all  $(J, I)$  with  $\tilde{\epsilon}_J$  defined in (3.6).

Inspecting (3.47) we find that in the case of the vertices involving  $V_{ts}^{\text{eff}}$  and  $V_{td}^{\text{eff}}$  the corrections depend on the top Yukawa coupling  $y_t^2$  while the corrections to vertices  $V_{cb}^{\text{eff}}$  and  $V_{ub}^{\text{eff}}$  do not.

We would like to emphasize that whereas the rule (3.47) for  $(J \neq 3, I)$  and accidentally for  $J = I = 3$  is equivalent to expressing in the tree level formulae  $V_{JI}$  and  $m_{d_I}$  through  $V_{JI}^{\text{eff}}$  and  $\overline{m}_{d_I}$  respectively, for  $J = 3$  and  $I = 1, 2$  it is more involved. Expressing in these cases only  $V_{JI}$  and  $m_{d_I}$  through  $V_{JI}^{\text{eff}}$  and  $\overline{m}_{d_I}$ , would give  $(1 + \tilde{\epsilon}_3 \tan \beta)/(1 + \epsilon_0 \tan \beta)^2$  as opposed to the correct result  $1/(1 + \tilde{\epsilon}_3 \tan \beta)$ .

### 3.5 Chargino-Quark-Squark Vertices

As argued in subsection 2.6, to account for rotations (2.8) performed on the quark fields in the higher dimensional operators resulting from integrating out charginos, their Wilson coefficients should be calculated by using the modified chargino-quark-squark couplings.

Modifications of  $c_L^i$  given in (2.53) are trivial. In the  $SU(2) \times U(1)$  symmetry limit the modifications (2.54) of  $c_R^i$  can be easily given in closed form if we note that they are exactly as in the expression (3.46) for the couplings  $[P_{LR}^H]^{JI}$ . Thus, in  $c_R^i$  in (2.52) one should replace as in (3.47)

$$V^{JI} m_{d_I} \rightarrow V_{\text{eff}}^{JI} \frac{\overline{m}_{d_I}}{1 + \tilde{\epsilon}_J \tan \beta} . \quad (3.48)$$

### 3.6 Introducing Flavour Dependence

Let us next generalize the main results of this section to the case of flavour dependent  $\epsilon_0$ ,  $\epsilon_Y$ ,  $\epsilon'_0$  and  $\epsilon'_Y$ . In this case (3.5) and (3.12) are replaced by

$$(\Delta_u \mathbf{Y}_d)^{JI} = -y_{d_J} \left( \epsilon_0^{(J)} \delta^{JI} + \epsilon_Y^{(JI)} y_t^2 V^{3J*} V^{3I} \right) \equiv -y_{d_J} \left( \tilde{\epsilon}_J \delta^{JI} + \epsilon_Y^{(JI)} y_t^2 \lambda_0^{JI} \right) \quad (3.49)$$

$$(\Delta m_d)^{JI} = m_{d_J} \tan \beta \left( \tilde{\epsilon}_J \delta^{JI} + \epsilon_Y^{(JI)} y_t^2 \lambda_0^{JI} \right) \quad (3.50)$$

where now

$$\tilde{\epsilon}_J = \epsilon_0^{(J)} + \epsilon_Y^{(33)} y_t^2 \delta^{J3} \quad (3.51)$$

and it is  $\tilde{\epsilon}_J$  given in (3.51) that enters the relation (3.13).

In agreement with the typical pattern of the soft SUSY breaking mass parameters, in what follows we will assume that

$$\epsilon_Y^{(11)} = \epsilon_Y^{(12)} = \epsilon_Y^{(21)} = \epsilon_Y^{(22)} , \quad \epsilon_Y^{(31)} = \epsilon_Y^{(32)} , \quad \epsilon_Y^{(13)} = \epsilon_Y^{(23)} . \quad (3.52)$$

With this assumption, instead of the relation (3.25) for  $(JI) = (13), (23), (31)$  and  $(32)$  we find:

$$V_{JI} = V_{JI}^{\text{eff}} \left[ \frac{1 + \tilde{\epsilon}_3 \tan \beta}{1 + \tilde{\epsilon}_0 \tan \beta} \right] \quad (3.53)$$

with  $\tilde{\epsilon}_J$  given in (3.51) and  $\tilde{\epsilon}_0$  defined through

$$\tilde{\epsilon}_0 = \epsilon_0^{(3)} + y_t^2 (\epsilon_Y^{(33)} - \epsilon_Y^{(31)}) = \tilde{\epsilon}_3 - y_t^2 \epsilon_Y^{(31)} \quad (3.54)$$

Note that  $\tilde{\epsilon}_0$  differs from  $\epsilon_0^{(J)}$  that enters (3.51).

Similarly we find for  $J > I$

$$\left[ X_{RL}^S \right]^{JI} = \frac{\overline{m}_{d_J}}{v_d (1 + \tilde{\epsilon}_J \tan \beta)^2} \epsilon_Y^{(JI)} y_t^2 \lambda_0^{JI} \left( x_u^S - x_d^S \tan \beta \right) \quad (3.55)$$

$$\left[ X_{LR}^S \right]^{JI} = \frac{\overline{m}_{d_I}}{v_d (1 + \tilde{\epsilon}_J \tan \beta)^2} \epsilon_Y^{(IJ)} y_t^2 \lambda_0^{JI} r_{JI} \left( x_u^{S*} - x_d^{S*} \tan \beta \right) . \quad (3.56)$$

where

$$r_{JI} = \frac{1 + [\tilde{\epsilon}_J + (\tilde{\epsilon}_I - \tilde{\epsilon}_J)(\epsilon_Y^{(JI)}/\epsilon_Y^{(IJ)})] \tan \beta}{(1 + \tilde{\epsilon}_I \tan \beta)}. \quad (3.57)$$

$[X_{RL}^S]^{JI}$  and  $[X_{LR}^S]^{JI}$  for  $J < I$  can be obtained by using the rules in (2.36). These improvements can be easily incorporated in the formulae (3.26)–(3.29) taking into account that in expressing  $\lambda_0^{JI}$  through  $V_{\text{eff}}^{JI}$ , the formula (3.53) instead of (3.25) should be used.

Next for the right-handed charged Higgs couplings we find

$$[P_{LR}^H]^{JI} = \frac{g_2}{\sqrt{2}M_W} \tan \beta V_{\text{eff}}^{JI} \frac{\overline{m}_{d_I}}{1 + \epsilon_0^{(I)} \tan \beta}, \quad J = 1, 2 \quad I = 1, 2 \quad (3.58)$$

$$[P_{LR}^H]^{33} = \frac{g_2}{\sqrt{2}M_W} \tan \beta V_{\text{eff}}^{33} \frac{\overline{m}_{d_3}}{1 + \tilde{\epsilon}_3 \tan \beta}, \quad (3.59)$$

$$[P_{LR}^H]^{J3} = \frac{g_2}{\sqrt{2}M_W} \tan \beta V_{\text{eff}}^{J3} \frac{\overline{m}_{d_3}}{1 + \tilde{\epsilon}_0 \tan \beta}, \quad J = 1, 2 \quad (3.60)$$

with  $\tilde{\epsilon}_0$  defined in (3.54). Finally

$$[P_{LR}^H]^{3I} = \frac{g_2}{\sqrt{2}M_W} \tan \beta V_{\text{eff}}^{JI} \overline{m}_{d_I} \left[ \frac{1}{1 + \epsilon_0^{(I)} \tan \beta} - \frac{\epsilon_Y^{(3I)} y_t^2 \tan \beta}{(1 + \tilde{\epsilon}_0 \tan \beta)(1 + \tilde{\epsilon}_3 \tan \beta)} + \frac{(\epsilon_Y^{(3I)} - \epsilon_Y^{(I3)}) y_t^2 \tan \beta}{(1 + \tilde{\epsilon}_0 \tan \beta)(1 + \epsilon_0^{(I)} \tan \beta)} \right] \quad I = 1, 2 \quad (3.61)$$

Flavour dependence in the formulae (3.43)–(3.45) for the couplings  $[P_{RL}^H]^{JI}$  will be introduced in sec. 5.3.

### 3.7 Summary

In this section we have derived explicit expressions for the flavour changing neutral scalar couplings  $[X_{RL}^S]^{JI}$  and  $[X_{LR}^S]^{JI}$  and the charged scalar couplings  $[P_{RL}^H]^{JI}$ ,  $[P_{LR}^H]^{JI}$ ,  $[P_{RL}^G]^{JI}$  and  $[P_{LR}^G]^{JI}$  at large  $\tan \beta$  in the  $SU(2) \times U(1)$  symmetry limit assuming the dominance of  $\alpha_s$  and the top and bottom Yukawa couplings. The main results are given in (3.23), (3.24), (3.26)–(3.29), (3.39), (3.40), (3.43) and (3.47). The important formula [20, 27] that relates  $V_{JI}$  to  $V_{\text{eff}}^{JI}$  is given in (3.25). We have also indicated how these formulae should be changed to account for flavour violating effects in the case of split squark mass parameters. This set of formulae allow to calculate scalar contributions to any flavour violating process. In addition we have presented the rules for incorporating large  $\tan \beta$  effects in the Wilson coefficients of the higher dimension operators generated in the course of integrating out sparticles.

## 4 Comparison with the Literature

The formulae presented in sections 2 and 3 generalize and in certain cases correct those present in the literature. Let us discuss this in details.

The results in section 2 are new as they go beyond the limit of zero electroweak gauge couplings and also beyond the  $SU(2) \times U(1)$  symmetry limit. We devote the next section to the detailed comparison of the approximation of sec. 3 and the complete approach of sec. 2. Our results of section 3 agree with the recent analysis in [28] if one makes the following replacements in our formulae

$$\epsilon'_0 \rightarrow -\epsilon'_0, \quad \epsilon_Y y_t^2 \rightarrow \epsilon_1, \quad \epsilon'_Y y_b^2 \rightarrow -\epsilon'_1 \quad (4.1)$$

with  $\epsilon_0$  unchanged. We would like also to compare our results with those of [25] in order to have a dictionary between the two notations. This will prove helpful for discussing  $\bar{B} \rightarrow X_s \gamma$  decay.

The explicit expressions for  $[P_{RL}^{H(G)}]^{JI}$  with  $J = 3, I = 1, 2, 3$  and for  $[P_{LR}^{H(G)}]^{JI}$  with  $J = 1, 2, 3$  and  $I = 3$  given in eq. (17) of ref. [25] do not take into account the modifications of the CKM factors summarized in (3.25). However, correcting the formula (17) of [25] has to be done with care. In particular, identifying  $V$  used in that paper with  $V_{\text{eff}}$  would generally give wrong results for  $[P_{LR}^{H(G)}]^{JI}$ , while it is correct for  $[P_{RL}^{H(G)}]^{JI}$  if the term  $\Delta_{JI}$  given in eq. (3.45) is neglected.

In order to see this explicitly let us observe that the couplings  $[P_{RL}^{H(G)}]^{JI}$  involve left-handed down quarks that enter also the  $W^\pm$ -quark couplings. As the corrections resulting from rotating the  $u_L$  and  $u_R$  fields can be neglected, the CKM matrix in  $[P_{RL}^{H(G)}]^{JI}$  after the rotations (2.8) becomes automatically  $V^{\text{eff}}$  except for  $V$  in the last term in eq. (3.42). Approximating  $V$  in the latter term with  $V^{\text{eff}}$  we find  $[P_{RL}^H]^{JI}$  in (3.43) with  $\Delta_{JI}$  set to zero. This result, obtained in the  $SU(2) \times U(1)$  symmetry limit, agrees then with  $[P_{RL}^H]^{JI}$  in equation (17) of [25] provided the CKM matrix there is identified with  $V^{\text{eff}}$ . We find also the relation between  $\epsilon_{JI}^{HL}$  introduced by us and the parameters  $\epsilon'_J(I)$  in [25]:

$$\epsilon_{JI}^{HL} = \epsilon'_J(I) \tan \beta \quad J = t, \quad I = d, s, b, \quad (\Delta_{JI} \rightarrow 0). \quad (4.2)$$

However, as emphasized in ref. [28],  $\Delta_{JI}$  cannot be generally neglected for  $|\epsilon_Y \tan \beta|$  and  $|\epsilon'_Y \tan \beta|$  larger than 0.5 and it could be important for  $\epsilon'_0 \approx -\epsilon'_Y$  when the  $\mathcal{O}(\tan \beta)$  term in  $\epsilon_{JI}^{HL}$  is small.

However, we will see in section 5 that even with the  $\Delta_{JI}$  term included,  $\epsilon_{JI}^{HL}$  obtained in the approach of sec. 3 deviate rather significantly from  $\epsilon_{JI}^{HL}$  computed as in sec. 2. The replacement of  $\epsilon'_0 + \epsilon'_Y y_b^2 \delta^{I3}$  in eq. (3.44) obtained in the strict  $SU(2) \times U(1)$  symmetry

limit and neglecting couplings other than  $\alpha_s$  and Yukawas by  $\epsilon'_J(I)$  given in eq. (16) of [25] does not help much. To get a reliable approximation one has to include additional terms that depend on the electroweak gauge couplings which are numerically important but have been neglected in all previous analyses. In contrast to  $[P_{RL}^H]^{JI}$ , the coupling  $[P_{RL}^G]^{JI}$  of the charged Goldstone boson as used in ref. [25] agrees with ours if  $V$  of [25] is interpreted as  $V_{\text{eff}}$ . As we will see,  $\epsilon_{JI}^{GL}$  computed in the approach of sec. 2 are indeed negligible.

In the case of  $[P_{LR}^{H(G)}]^{JI}$  the right-handed down quarks are rotated differently from the left-handed down quarks present in the  $W^\pm$ -quark couplings and this mismatch results in additional  $\tan\beta$  enhanced corrections. Interpreting  $V$  in  $[P_{LR}^{H(G)}]^{JI}$  in equation (17) in [25] as  $V^{\text{eff}}$ , would generally miss them. However, it turns out that for  $J = 1, 2, 3$  and  $I = 3$  considered in [25], the results correct in the  $SU(2) \times U(1)$  symmetry limit can be obtained by identifying  $V$  in  $[P_{LR}^{H(G)}]^{JI}$  of this paper not with  $V_{\text{eff}}$  as in the case of  $[P_{RL}^{H(G)}]^{JI}$  but with the original CKM matrix  $V$ . Indeed, expressing the  $V$  elements in  $[P_{LR}^{H(G)}]^{JI}$  of [25] in terms of  $V^{\text{eff}}$  by using the rules in (3.25), the formulae for these couplings given in [25] can be transformed into ours provided the following replacements are simultaneously made:

$$\frac{V^{JI}}{V_{\text{eff}}^{JI}} \frac{1}{1 + \epsilon_I \tan\beta} \rightarrow 1 - \epsilon_{JI}^{HR} \quad J = u, c, t, \quad I = b \quad (4.3)$$

in the case of  $[P_{LR}^H]^{JI}$  and

$$\frac{V^{JI}}{V_{\text{eff}}^{JI}} \frac{1 + \epsilon'_I(J) \tan\beta}{1 + \epsilon_I \tan\beta} \rightarrow 1 + \epsilon_{JI}^{GR} \quad J = u, c, t \quad I = b \quad (4.4)$$

in the case of  $[P_{LR}^{H(G)}]^{JI}$  (note that  $\epsilon_I$  of [25] corresponds to  $\tilde{\epsilon}_I$  in our paper). As in the  $SU(2) \times U(1)$  symmetry limit

$$\epsilon'_b(t) = \epsilon_b = \tilde{\epsilon}_3, \quad \epsilon'_b(c) = \epsilon'_b(u) = \epsilon_0, \quad (4.5)$$

with  $\tilde{\epsilon}_3$  and  $\epsilon_0$  defined in (3.6), the formulae given above reduce indeed to the corresponding formulae for the parameters  $\epsilon_{JI}^{H(G)R}$  given in (3.40) and (3.47). It should be emphasized that the factor  $V^{JI}/V_{\text{eff}}^{JI}$  in (4.4) that we introduced here is essential for vanishing of  $\epsilon_{JI}^{GR}$  in the  $SU(2) \times U(1)$  symmetry limit as required by general arguments. We will see, however, in the next section that for split squark masses the formula (3.47) for  $\epsilon_{JI}^{HR}$  has to be modified along the lines of section 3.6 in order to approximate well the results of the complete calculation. We shall also explain in more detail the status of the recipe (4.4).

## 5 The Size of the Large $\tan\beta$ Corrections: Full Calculation and the $SU(2) \times U(1)$ Limit

This section is devoted to the numerical evaluation and the assessment of the importance of the corrections discussed in sections 2 and 3. We will also compare results of the complete diagrammatic calculation of these corrections with the approximation based on the  $SU(2) \times U(1)$  symmetry limit discussed in section 3. This will allow to test the quality of the latter approach and to find its limitations. We will also present analytic expressions for various couplings that approximate the full approach much better than the formulae of section 3.

### 5.1 Full Calculation

The one-loop contributions of sparticles to quark self-energies  $\Sigma_{mL(R)}^q(0)$ ,  $\Sigma_{VL(R)}^q(0)$  and various vertex formfactors  $\Delta F_{L(R)}$  at vanishing external momenta, that are the main ingredients of the full method of section 2, can be easily calculated by using the Feynman rules of the MSSM collected in [30] and the standard one-loop functions. We recall the relevant expressions in the Appendix A.1.

In order to find the original mass parameters  $m_{d_J}$  and the original CKM matrix  $V^{JJ}$  that enter these rules we proceed as follows. We begin by computing  $\epsilon_{d_J}$  defined in (2.30). Since to a good approximation  $(\Sigma_{mL}^d)^{JJ} \propto m_{d_J}$  the quark mass cancels out in the ratio in (2.30). Therefore, in the actual calculation of  $\epsilon_{d_J}$  the MSSM mass parameters  $m_{d_J}$  can be replaced by  $\overline{m}_{d_J}$  that are known experimentally. Note also, that to compute diagonal self energies one can use experimentally known  $V^{\text{eff}}$  instead of the yet unknown  $V$ . Having obtained  $\epsilon_{d_J}$  in this manner we can calculate  $m_{d_J} \approx \overline{m}_{d_J}/(1 + \epsilon_{d_J} \tan\beta)$ .

In order to find  $V$  we proceed iteratively: starting with  $m_{d_J}$  and  $V = V^{\text{eff}}$  we compute  $\Delta' m_d$  by means of (2.5) and (2.11) and subsequently using (2.13) and (2.14) we find the rotations  $\mathbf{D}_{L,R} = \mathbf{1} + \mathbf{\Delta D}_{L,R}$ . This allows to find  $V$  in the first approximation by inverting the relation (2.21) in which  $\mathbf{\Delta U}_L$  can be set to zero. This is next used to compute  $\Delta' m_d$  anew and so on. The procedure converges quickly yielding  $V$  and the rotations  $\mathbf{D}_{L,R}$ . Having these, we can compute all the necessary formfactors  $\Delta F_{L,R}$  and the couplings  $X_{RL}$ ,  $X_{LR}$ ,  $P_{RL}$  and  $P_{LR}$ .

The simple and transparent expressions derived in secs. 3.2-3.5 are very convenient, as they make the effects of large  $\tan\beta$  explicit and allow for easy qualitative discussion of the dominant effects. However, as the comparison with the complete calculation will reveal, they are not very accurate numerically and it is desirable to improve the accuracy of the approach of section 3 retaining, however, its simplicity. It turns out that for the

CKM matrix and the couplings  $[X_{RL}]$ ,  $[X_{LR}]$ , and  $[P_{LR}^H]$  this can be achieved by simply using the expressions (3.53)-(3.61) with  $\tilde{\epsilon}_J$  and  $\epsilon_Y^{(JI)}$  calculated directly from the full one loop correction  $\Delta m_d$  to the down-quark mass matrix given in (2.5):

$$y_t^2 \epsilon_Y^{(JI)} = \frac{(\Delta m_d)^{JI}}{m_{d_J} \lambda_0^{JI} \tan \beta} \quad \text{for } J \neq I, \quad \tilde{\epsilon}_J = \frac{(\Delta m_d)^{JJ}}{m_{d_J} \tan \beta}. \quad (5.1)$$

The complete formula for  $(\Delta m_d)^{JI}$  is given in (2.5) with the relevant expressions for quark self-energies given in the Appendix A.2. Note that with  $\epsilon_Y^{(JI)}$  and  $\tilde{\epsilon}_J$  all parameters entering (3.53)-(3.61), in particular  $\tilde{\epsilon}_0$  in (3.54), can be calculated. In this manner also the effects of the electroweak couplings  $g_1$  and  $g_2$  present in  $(\Delta m_d)^{JI}$  are automatically taken into account. Simple but accurate expressions for the couplings  $[P_{RL}^H]$  can also be given. They will be discussed separately below.

## 5.2 The neutral Higgs boson sector

In order to implement the formulae of section 3 we need the quantities  $\epsilon_0$ ,  $\epsilon_Y$  defined by eq. (3.5) and  $\epsilon'_0$ ,  $\epsilon'_Y$  of eq. (3.15). Evaluating diagrams shown in fig. 5 we find

$$\epsilon_0 = -\frac{2\alpha_s}{3\pi} \frac{\mu}{m_{\tilde{g}}} H_2(x^{Q/g}, x^{D/g}), \quad \epsilon_Y = \frac{1}{16\pi^2} \frac{A_t}{\mu} H_2(x_l^{Q/\mu}, x_l^{U/\mu}) \quad (5.2)$$

$$\epsilon'_0 = -\frac{2\alpha_s}{3\pi} \frac{\mu}{m_{\tilde{g}}} H_2(x^{Q/g}, x^{U/g}), \quad \epsilon'_Y = \frac{1}{16\pi^2} \frac{A_b}{\mu} H_2(x_l^{Q/\mu}, x_l^{D/\mu}) \quad (5.3)$$

where  $x^{Q/g} \equiv m_Q^2/m_{\tilde{g}}^2$ ,  $x^{D/g} \equiv m_D^2/m_{\tilde{g}}^2$ ,  $x_l^{Q/\mu} \equiv m_Q^2/|\mu|^2$  etc., and  $m_Q^2$ ,  $m_D^2$ ,  $m_U^2$ ,  $A_t$ , and  $A_b$  are the parameters of the soft supersymmetry breaking in the MSSM Lagrangian.<sup>3</sup> The function  $H_2(x, y)$  is defined as

$$H_2(x, y) = \frac{x \ln x}{(1-x)(x-y)} + \frac{y \ln y}{(1-y)(y-x)}. \quad (5.4)$$

As discussed in sec. 3, for squark mass parameters  $m_Q^2$ ,  $m_D^2$ ,  $m_U^2$  having different values for different generations (e.g. if the the third generation squarks are split from the others as happens in the minimal SUGRA scenario)  $\epsilon_0$ ,  $\epsilon_Y$ ,  $\epsilon'_0$  and  $\epsilon'_Y$  depend on the generation indices. We have given the relevant expressions in subsection 3.6. In our comparison of the approximate and full methods, we parametrize the squark spectrum with four independent mass parameters:  $m^2 \equiv m_{Q_{1,2}}^2 = m_{D_{1,2}}^2 = m_{U_{1,2}}^2$  for the squarks of the first two generations and  $m_{Q_3}^2$ ,  $m_{D_3}^2$ ,  $m_{U_3}^2$  for the third one. Consequently, in eqs. (3.26)-(3.29)

<sup>3</sup>Our convention for  $A_u$  and  $A_d$  parameters is fixed by the form of the left-right squark mixing terms in the squark mass squared matrices which read  $-m_u(A_u + \mu \cot \beta)$  and  $-m_d(A_d + \mu \tan \beta)$  for the up and down squarks, respectively.



$\tilde{\epsilon}_3$  always depends on the third generation squark masses but as in sec. 3.6 we distinguish  $\epsilon_0$  arising from expressing  $V_{JI}$  in terms of  $V_{JI}^{\text{eff}}$ , which also depends on the third generation squark masses, and  $\epsilon_0$  that result from expressing  $m_{d_{1,2}}$  in terms of  $\overline{m}_{d_{1,2}}$  which depends on  $m^2$ .

The formulae (5.2) for  $\epsilon_0$  and  $\epsilon_Y$  apply in the strict limit of  $SU(2) \times U(1)$  symmetry supplemented by the approximation  $g_1 = g_2 = 0$ . Under these conditions only the higgsino of mass  $|\mu|$  couples to quarks through Yukawa couplings. In application to the relation between  $m_{d_J}$  and  $\overline{m}_{d_J}$  and to the neutral Higgs boson couplings it is easy to take into account the contribution of the true charginos. Simplifying appropriately the full expression for  $(\Sigma_{mL}^d)^{JJ}$  (or the full expression for the one loop vertex diagram in which  $H^0$  or  $h^0$  couples to the up-type squarks and the charginos connect the external  $d$ -quarks) and comparing with the  $\epsilon_Y$  contribution to  $\Delta m_d$  (to  $\Delta F_L^{dS}$ ) one gets

$$\epsilon_Y = \frac{1}{16\pi^2} \sum_{l=1}^2 Z_-^{2l} \frac{A_t}{m_{C_l}} Z_+^{2l} H_2(x_l^{Q/C}, x_l^{U/C}) \quad (5.5)$$

where  $x_l^{Q/C} \equiv m_Q^2/m_{C_l}^2$  etc., and the matrices  $Z_+$  and  $Z_-$  are defined in ref. [30]. Similarly one could take into account also the left-right mixing of squarks. The formula (5.5) goes beyond the  $SU(2) \times U(1)$  symmetry limit in that it takes into account the mixing of higgsinos and gauginos which depends on vacuum expectation values and on the gauge couplings  $g_1$  and  $g_2$  and can be suitably extended to include also the mixing of left and right-handed squarks proportional to VEVs. However, it still neglects  $g_1$  and  $g_2$  in the couplings of charginos to quarks and the contribution of the neutralinos.

The magnitude of  $\epsilon_0$  and  $\epsilon_Y$  can be easily estimated from eq. (5.2) remembering that  $H_2(1,1) = -1/2$  and that  $H_2(x,x)$  varies between  $-0.18$  for  $x = 4$  and  $-1.7$  for  $x = 0.1$ . Figures 6a,b show the comparison of  $\epsilon_{d_2} \approx \epsilon_{d_1}$  and of  $\epsilon_{d_3}$  computed from the full one-loop self energies (eq. (2.30)) with  $\epsilon_0$  and  $\tilde{\epsilon}_3$ , respectively, for a sample of points in the MSSM parameter space corresponding to sparticles heavier than 500 GeV. As seen in figs. 6a and 6b, typically  $|\epsilon_{d_3}|$  and  $|\epsilon_{d_2}|$  ( $|\epsilon_0|$  and  $|\tilde{\epsilon}_3|$ ) are of order  $\sim 5 \times 10^{-3}$  and reach  $\sim 1 \times 10^{-2}$  only for very special combinations of squark and gluino masses,  $|\mu|$  and/or  $|A_t|$ .

The two distinct bands seen in panels a) and b) of the figure 6 correspond to  $\mu < 0$  ( $\epsilon_0 < \epsilon_{d_2} < 0$  and  $\tilde{\epsilon}_3 < \epsilon_{d_3}$ ) and  $\mu > 0$  ( $\epsilon_0 > \epsilon_{d_2} > 0$  and  $\tilde{\epsilon}_3 > \epsilon_{d_3}$ ). The discrepancy between  $\epsilon_0$  ( $\tilde{\epsilon}_3$ ) and  $\epsilon_{d_2}$  ( $\epsilon_{d_3}$ ) (quantified by the deviation of the bands from the diagonal) is partly due to the absence in  $\epsilon_0$  given by (5.2) of the neutralino contribution to the  $d$ -quark self energies but mostly to the fact that in the full approach the chargino couplings depend also on the gauge coupling constants so that charginos do contribute also to  $\epsilon_0$  and hence also to  $\epsilon_{d_1}$  and  $\epsilon_{d_2}$ . Neglecting the contribution of  $\Delta_d \mathbf{Y}_d$  in the formula (3.10) corresponds in the full approach to neglecting the contribution of  $A_b$  (of  $\mu$ ) to the mixing of the left

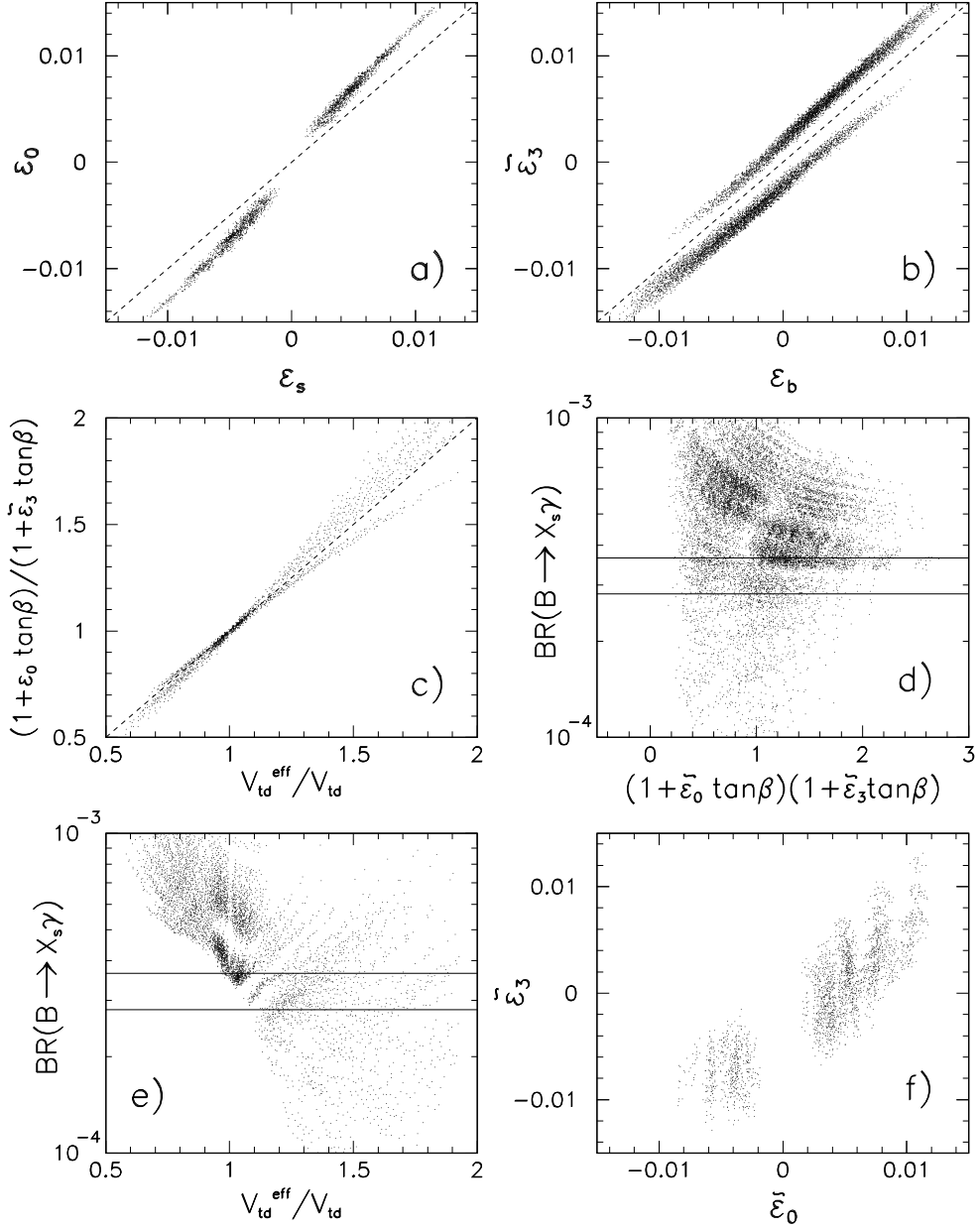


Figure 6: Comparison of the results obtained in the complete calculation with the ones obtained in the approximation based on the  $SU(2) \times U(1)$  symmetry limit for a sample of the sparticle mass spectra for  $\tan\beta = 50$  and  $M_A = 200$  GeV. See the text for further explanations.

and right sbottoms (stops) and is justified for  $|A_b| \ll |\mu| \tan \beta$  and  $|\mu| \ll A_t \tan \beta$ . More detailed comparison shows that the differences between  $\epsilon_0$  ( $\tilde{\epsilon}_3$ ) and  $\epsilon_{d_2}$  ( $\epsilon_{d_3}$ ) are of order 15%-20% when the epsilons assume phenomenologically relevant values.

The gap in values of  $\epsilon_{d_2}$  ( $\epsilon_0$ ) seen in panel a) of fig. 6 reflects the existence of a lower bound on  $\mu m_{\tilde{g}}$  in the scan which follows from the imposed condition  $m_{C_1}, m_{\tilde{g}} > 500$  GeV. Note also, that while  $\epsilon_0$  and  $\epsilon_Y$  as given by (5.2) or (5.5) are UV finite,  $\epsilon_{d_I}$  have to be renormalized in the  $\overline{\text{MS}}$  scheme. We have checked however, that the variation of  $\epsilon_{d_I}$  with the renormalization scale  $Q$  is very small for  $500 \text{ GeV} < Q < m_{\tilde{g}}$ .

Figure 6c shows the comparison of<sup>4</sup>  $V_{td}^{\text{eff}}/V_{td}$  obtained from the complete expression (2.21) and in the approximation (3.25) for a sample of sparticle parameters and  $\tan \beta = 50$ . It is to be noted that the approximation (3.25) with  $\epsilon_0$  and  $\epsilon_Y$  computed as in eqs. (5.2) and (5.5), works only qualitatively.

Figures 6a - 6c show that in general the effects of the electroweak couplings are non-negligible. They could be included in the framework of the  $SU(2) \times U(1)$  symmetry limit by computing diagrams with gaugino exchange but since the full expression for the supersymmetric contribution to the down quark self energy are simple enough, it is more practical to use the formulation of section 3.6 with  $\epsilon_Y^{(JI)}$  and  $\tilde{\epsilon}_J$  computed as in (5.1). The formula (3.53) improved in this way gives perfect approximation to the ratios  $V_{td}^{\text{eff}}/V_{td}$  etc. obtained in the approach of sec. 2. Obviously,  $\tilde{\epsilon}_J$  given by (5.1) coincide with the factors  $\epsilon_{d_J}$  of sec. 2.

The panel d) of figure 6 shows for  $M_A = 200$  GeV and  $\tan \beta = 50$  the correlation<sup>5</sup> of  $BR(\bar{B} \rightarrow X_s \gamma)$  with the factor  $(1 + \tilde{\epsilon}_0 \tan \beta)(1 + \tilde{\epsilon}_3 \tan \beta)$  that enters the denominator of the flavour violating neutral Higgs boson couplings (3.26) and (3.27) improved as in sec. 3.6. We have used here the eq. (5.1) to determine  $\tilde{\epsilon}_0$  and  $\tilde{\epsilon}_3$ . We observe that the experimentally acceptable value of  $BR(\bar{B} \rightarrow X_s \gamma)$  can be realized both for  $(1 + \tilde{\epsilon}_0 \tan \beta)(1 + \tilde{\epsilon}_3 \tan \beta)$  greater than one and smaller than one corresponding respectively to the suppression and the enhancement of the actual scalar FCNC compared to the naive one loop estimates of ref. [6, 22, 23].

In contrast, it is interesting to observe in the panel e) of figure 6 that the correlation between  $V_{td}^{\text{eff}}/V_{td}$  and  $\bar{B} \rightarrow X_s \gamma$  has quite different implications. Here the requirement of acceptable rate of the  $\bar{B} \rightarrow X_s \gamma$  decay eliminates (for  $M_A = 200$  GeV and  $\tan \beta = 50$ ) all points with  $V_{td}^{\text{eff}}/V_{td} < 1$ .

Both facts can be qualitatively understood by investigating signs of  $\tilde{\epsilon}_0$  and  $\epsilon_Y^{(31)}$  and remembering that, as follows from eqs. (5.2),  $\tilde{\epsilon}_0 \approx \epsilon_0 \propto \mu$  and  $\epsilon_Y^{(31)} \approx \epsilon_Y \propto -\mu A_t$

<sup>4</sup>We have checked that the full approach based on eq. (2.21) also gives  $V_{td}^{\text{eff}}/V_{td} \approx V_{ts}^{\text{eff}}/V_{ts} \approx V_{ub}^{\text{eff}}/V_{ub} \approx V_{cb}^{\text{eff}}/V_{cb}$ .

<sup>5</sup>For details of the  $BR(\bar{B} \rightarrow X_s \gamma)$  calculation see sec. 6.

(the function  $H_2$  is negative). Let us consider the case  $\tilde{\epsilon}_0 < 0$ ,  $\tilde{\epsilon}_3 > 0$  which according to eq. (3.53) leads to  $V_{td}^{\text{eff}}/V_{td} < 1$ . This requires  $\mu < 0$  and  $A_t > 0$ . However, the relative sign of the chargino-stop and  $H^+$  contributions to the amplitude of the  $\bar{B} \rightarrow X_s \gamma$  decay is opposite to the sign of  $\mu A_t$ . Therefore,  $\mu A_t > 0$  is a necessary condition for the cancellation to occur [26]. Hence, for  $\tilde{\epsilon}_0 < 0$ ,  $\tilde{\epsilon}_3 > 0$  no cancellation between the chargino-stop and  $H^+$  contributions is possible which explains why  $V_{td}^{\text{eff}}/V_{td} < 1$  is incompatible with the  $BR(\bar{B} \rightarrow X_s \gamma)$  constraint.

On the other hand, for  $(1 + \tilde{\epsilon}_0 \tan \beta)(1 + \tilde{\epsilon}_3 \tan \beta) < 1$  (enhancement of the flavour changing scalar couplings) that holds always for  $\mu < 0$  such a cancellation is possible for  $A_t < 0$ . This is further illustrated in figure 6f which shows the correlation of  $\tilde{\epsilon}_0$  and  $\tilde{\epsilon}_3$  for those sparticle parameters which for  $\tan \beta = 50$  and  $M_A = 200$  GeV give  $2.81 \times 10^{-4} < BR(\bar{B} \rightarrow X_s \gamma) < 3.65 \times 10^{-4}$ . It should be stressed that the frequently used argument [27] that obtaining acceptable  $\bar{B} \rightarrow X_s \gamma$  rate requires  $\mu > 0$ , which implies the suppression of the scalar FCNC, applies only in particular SUSY breaking scenarios. For example, in the minimal SUGRA, due to the fixed point structure of the relevant RGEs, not too large values of  $A_0$  (common value of  $A_t$ ,  $A_b$  etc. at the high scale) always lead to a fixed sign (positive in our convention) of  $A_t$ . However, fixed sign of  $A_t$  needs not be a common feature of all SUSY breaking scenarios and can be reversed even in the minimal SUGRA if the initial value  $|A_0|$  is sufficiently large (see e.g. ref. [32]). It is therefore justified to study the phenomenological consequences of both possibilities:  $(1 + \tilde{\epsilon}_0 \tan \beta)(1 + \tilde{\epsilon}_3 \tan \beta)$  greater than one and smaller than one.

Finally, let us stress that in the case of the enhancement of the scalar flavour changing couplings the value of  $(1 + \epsilon_0 \tan \beta)(1 + \tilde{\epsilon}_3 \tan \beta)$  with  $\epsilon_0$  and  $\tilde{\epsilon}_3$  calculated from eqs. (5.2), (5.5) is smaller than  $(1 + \tilde{\epsilon}_0 \tan \beta)(1 + \tilde{\epsilon}_3 \tan \beta)$  with  $\tilde{\epsilon}_0$  and  $\tilde{\epsilon}_3$  calculated using (5.1) by 10%–35% which means that the naive approximation gives too big an enhancement. Similarly, in the case of the suppression of the scalar flavour changing couplings the value of  $(1 + \epsilon_0 \tan \beta)(1 + \tilde{\epsilon}_3 \tan \beta)$  obtained by means of (5.2) and (5.5) is larger by 10%–25% than the corresponding factor calculated using (5.1). Thus the approximation of sec 3. overestimates the effects of resummed large  $\tan \beta$  corrections in the neutral Higgs boson couplings.

This is reflected in figure 7a where we show the comparison of the couplings  $[X_{RL}^H]^{32}$  of  $H^0$  to the down quarks obtained from the complete calculation and from the approximate formulae (3.26) with  $\epsilon_0$  and  $\epsilon_Y$  computed by means of eqs. (5.2), (5.5). In this figure positive (negative) values of  $[X_{RL}^H]^{32}$  correspond to negative (positive) value of the product  $\mu A_t$ . Clearly visible shorter band corresponds to positive  $\mu$  (suppression of the flavour changing scalar couplings by the factor  $(1 + \epsilon_0 \tan \beta)(1 + \tilde{\epsilon}_3 \tan \beta)$ ) and the longer one to  $\mu < 0$  (enhancement). For points for which the coupling  $[X_{RL}^H]^{32}$  has a non-negligible value

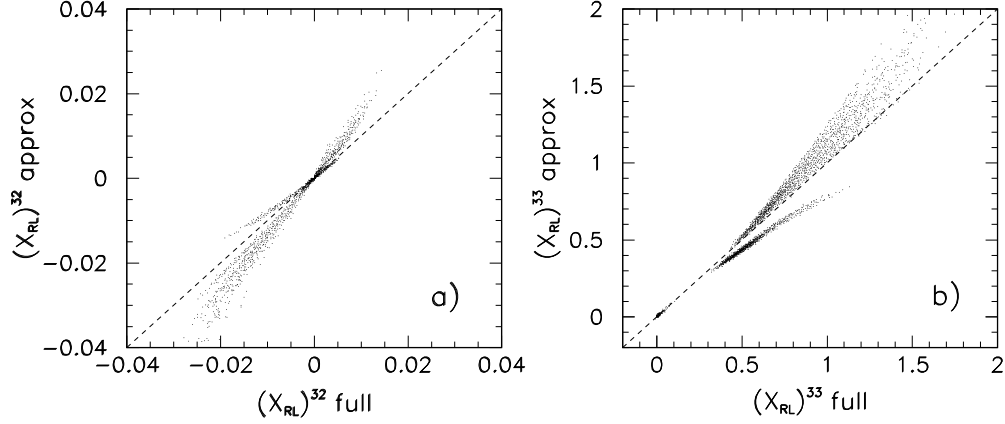


Figure 7: As in figure 6 but for the couplings  $[X_{RL}]^{JI}$  of  $H^0$  to the down quarks.

the difference between the full and approximate calculation varies between 10%–25% for  $\mu > 0$  (suppression) and 10%–40% for  $\mu < 0$  (enhancement). Other flavour changing couplings:  $[X_{RL}^H]^{31}$ ,  $[X_{RL}^H]^{23}$  etc. exhibit similar behaviour. For completeness, in figure 7b we show the comparison of the diagonal couplings  $[X_{RL}^H]^{33}$  of  $H^0$  obtained from the complete calculation and from the approximate formulae (3.22).

Similarly as in the case of the ratio  $V_{td}^{\text{eff}}/V_{td}$ , the quality of the approximation of section 3 seen in figure 7 can be greatly improved by using the formulae (3.22) and (3.26), (3.27) improved according to the rules of sec. 3.6 with  $\tilde{\epsilon}_0$  and  $\tilde{\epsilon}_J$  and  $\epsilon_Y^{(JI)}$  computed as in eqs. (5.1). Since the  $\tan\beta$  enhanced parts of the flavour changing couplings are proportional to  $A_t$ , such an approximation is not good only if the parameter  $A_t$  is small but then also the couplings  $[X_{RL}^S]^{JI}$ ,  $[X_{LR}^S]^{JI}$  for  $J \neq I$  become phenomenologically uninteresting.

For (almost) degenerate squarks of the first two generations the approximation of subsection 3.6 for couplings  $[X_{RL}^S]^{JI}$  and  $[X_{LR}^S]^{IJ}$  where  $I = 3$  and/or  $J = 3$  with  $\tilde{\epsilon}_0$  and  $\tilde{\epsilon}_J$  and  $\epsilon_Y^{(JI)}$  given by eqs. (5.1) could break down also for unrealistically large differences  $m^2 - m_{Q_3}^2$ . This is because, as we have explained in section 3.1, we are working in the scenario in which the left-left block of the up-type squark mass squared matrix is  $Vm_Q^2V^\dagger$  and is therefore not diagonal in the generation space as we allow for  $m_{Q_3}^2 \neq m^2 \equiv m_{Q_1}^2 = m_{Q_2}^2$ . However, due to the special structure of the CKM matrix this flavour violation remains negligible as long as  $|(m_{Q_3}^2 - m^2)V_{tb}V_{cb}^*|$  remains small compared to  $m_{Q_3}^2$ . If this

condition is not satisfied then, the couplings of stops to charginos and down quarks depart from the simple structure (2.52) and in consequence  $(\Delta' m_d)^{JI}$  is no longer proportional to  $\lambda_0^{JI}$ . Since in our scans  $|(m_{Q_3}^2 - m^2)V_{tb}V_{cb}^*| \ll m_{Q_3}^2$  the effects of this additional flavour violation never manifest themselves. The main effects of flavour violation arise then from flavour dependence of  $\epsilon_0$  and  $\epsilon_Y$  and when the approximate formulae (3.26)-(3.29) are modified according to the prescriptions of section 3.6 with epsilon parameters calculated by means of (5.1) they always agree very well with the results of the full calculation.

### 5.3 Charged Higgs Couplings

In this subsection we will assess the magnitude of the factors  $\epsilon_{JI}^{HL}$ ,  $\epsilon_{JI}^{HR}$  and  $\epsilon_{JI}^{GL}$ ,  $\epsilon_{JI}^{GR}$  introduced in subsection 2.5 to parametrize the corrections to the charged Higgs and Goldstone boson couplings and test the quality of the approximations developed in subsection 3.3.

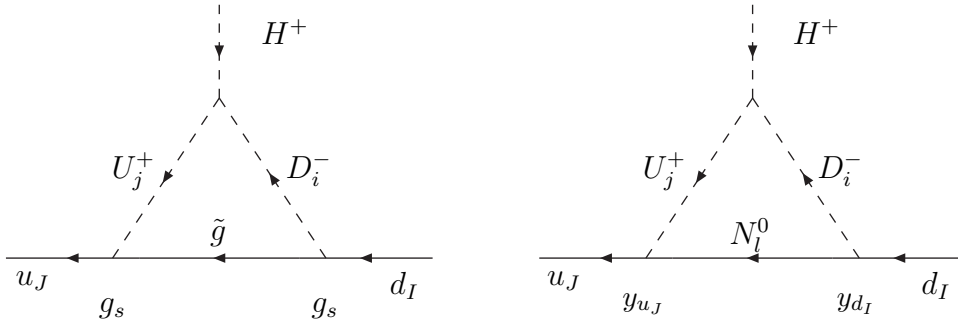


Figure 8: Dominant corrections to the charged Higgs boson couplings to quarks.

The factors  $\epsilon'_0$ ,  $\epsilon'_Y$ , given in eq. (5.3) entering the expression (3.44) for  $\epsilon_{JI}^{HL}$  obtained in the  $SU(2) \times U(1)$  symmetry limit and for vanishing electroweak gauge couplings can be easily extended beyond this approximation. Improvement analogous to the replacement of  $\epsilon_Y$  of eq. (5.2) by  $\epsilon_Y$  of eq. (5.5) in the neutral Higgs boson sector has been given in ref. [25]. Simplifying appropriately the full MSSM expressions for the diagrams shown in fig. 8 allows to replace  $\mu$  by the contribution of the four neutralino mass eigenstates and to take into account the mixing of the left and right squarks of the third generation. As a result  $\epsilon'_0 + \epsilon'_Y y_b^2$  in the formulae (3.15) and (3.44) for  $(\Delta_d \mathbf{Y}_u)^{JI}$  and  $\epsilon_{JI}^{HL}$ , respectively are replaced by the flavour dependent quantity  $\epsilon'_J(I)$  of [25]:

$$\epsilon'_J(I) = -\frac{2\alpha_s}{3\pi} \frac{\mu}{\tilde{m}_g} \left[ c_u^2 c_d^2 H_2(x_2^{u/g}, x_1^{d/g}) + s_u^2 c_d^2 H_2(x_1^{u/g}, x_1^{d/g}) \right]$$

$$\begin{aligned}
& + c_{\tilde{u}}^2 s_{\tilde{d}}^2 H_2(x_2^{u/g}, x_2^{d/g}) + s_{\tilde{u}}^2 s_{\tilde{d}}^2 H_2(x_1^{u/g}, x_2^{d/g})] \\
& - \frac{y_b^2}{16\pi^2} \sum_{l=1}^4 Z^{3l} \frac{A_b}{m_{N_l}} Z^{4l} [c_{\tilde{u}}^2 c_{\tilde{b}}^2 H_2(x_{1l}^{u/N}, x_{2l}^{b/N}) + s_{\tilde{u}}^2 c_{\tilde{b}}^2 H_2(x_{2l}^{u/N}, x_{2l}^{b/N}) \\
& + c_{\tilde{u}}^2 s_{\tilde{b}}^2 H_2(x_{1l}^{u/N}, x_{1l}^{b/N}) + s_{\tilde{u}}^2 s_{\tilde{b}}^2 H_2(x_{2l}^{u/N}, x_{1l}^{b/N})] \delta^{I3}
\end{aligned} \tag{5.6}$$

where  $x_k^{u/g} \equiv M_{\tilde{u}_k}^2/m_g^2$  ( $x_k^{d/g} \equiv M_{\tilde{d}_k}^2/m_g^2$ ),  $k = 1, 2$  with  $\tilde{u}_k$  ( $\tilde{d}_k$ ) being the up (down) squark of the  $J$ -th ( $I$ -th) generation and  $c_{\tilde{u}}$  and  $c_{\tilde{d}}$  etc. denoting cosines and sines of the appropriate mixing angles. (For the first two generations  $c_{\tilde{u},\tilde{d}} \approx 1$ ,  $s_{\tilde{u},\tilde{d}} \approx 0$ .) Similarly,  $x_{kl}^{u/N} \equiv M_{\tilde{u}_k}^2/m_{N_l}^2$ ,  $k = 1, 2$ ,  $l = 1, 4$  etc. In the formula (5.6)  $y_b$  is given by

$$y_b = -\frac{\sqrt{2}}{v_d} \frac{\bar{m}_b}{(1 + \tilde{\epsilon}_3 \tan \beta)}. \tag{5.7}$$

Using the identity  $Z_N^{3j} m_{N_l} Z_N^{4j} = -\mu^*$  it is easy to see that in the  $SU(2) \times U(1)$  limit  $\epsilon'_J(I) \rightarrow \epsilon'_0 + \epsilon'_Y y_b^2$ .

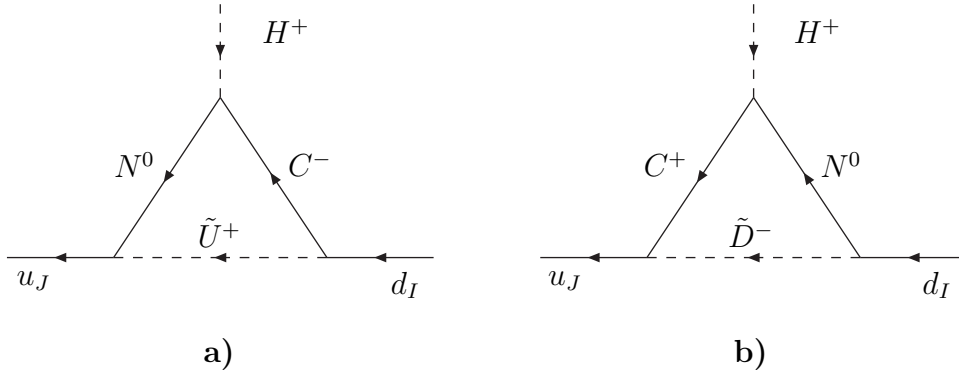


Figure 9: Additional important corrections to the charged Higgs boson couplings to quarks.

Similarly as in the case of the replacement of  $\epsilon_Y$  of eq. (5.2) by that of eq. (5.5), the use of  $\epsilon'_J(I)$  does not improve the approximation to  $\epsilon_{JI}^{HL}$  obtained in the full approach of sec. 2.5. This is because while going beyond the  $SU(2) \times U(1)$  symmetry limit in taking into account vacuum expectation value dependent particle mixing, it still neglects contributions which are present in the  $SU(2) \times U(1)$  symmetry limit for nonzero gauge couplings  $g_1$  and  $g_2$ . The latter effects can be incorporated taking into account also the  $SU(2) \times U(1)$  symmetry breaking effects by computing diagrams shown in fig. 9 (in the  $SU(2) \times U(1)$  symmetry limit they correspond to diagrams shown in 10 contributing to

$\Delta_d \mathbf{Y}_u$  for nonzero  $g_1$  and  $g_2$ ). Taking into account their dominant parts (which are finite) amounts to adding to  $\epsilon'_J(I)$  the following terms:

$$\begin{aligned}\delta_a \epsilon'_J(I) &= \frac{1}{16\pi^2} \frac{g_2^2}{\sqrt{2}c_W} \sum_{j,l} Z_+^{1l} Z_N^{1j} a^{lj} \frac{m_{N_j}}{m_{C_l}} H_2(x_{jl}^{N/C}, x_{jl}^{Q/C}) \\ &\quad + \frac{1}{16\pi^2} \frac{2g_2^2 s_W}{3c_W^2} \sum_{j,l} Z_+^{2l} Z_N^{4j} a^{lj} \frac{m_{N_j}}{m_{C_l}} H_2(x_{jl}^{N/C}, x_{jl}^{U/C}) \\ \delta_b \epsilon'_J(I) &= -\frac{1}{16\pi^2} \frac{g_2^2}{2c_W^2} \sum_{j,l} Z_+^{2l} \left( \frac{1}{3} s_W Z_N^{1j} - c_W Z_N^{2j} \right) a^{lj} \frac{m_{N_j}}{m_{C_l}} H_2(x_{jl}^{N/C}, x_{jl}^{Q/C})\end{aligned}$$

where  $x_{jl}^{N/C} = m_{N_j}^2/m_{C_l}^2$ ,  $x_{jl}^{Q/C} = m_{Q_j}^2/m_{C_l}^2$ , etc. and  $a^{lj} = Z_-^{2l}(s_W Z_N^{1j} + c_W Z_N^{2j}) - \sqrt{2} Z_-^{1l} Z_N^{3j}$ .

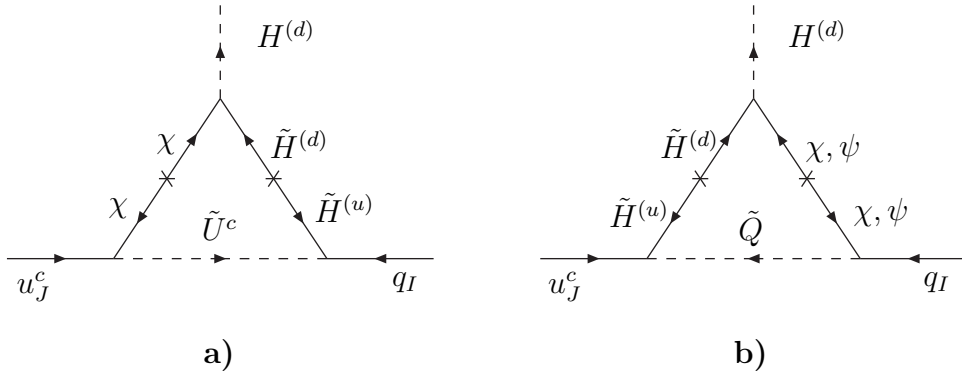


Figure 10: Additional contribution to  $\Delta_d \mathbf{Y}_u$  for nonzero electroweak gauge couplings.  $\chi$  and  $\psi$  denote  $U(1)$  and  $SU(2)$  gauginos, respectively.

Only the sum of all these corrections including the delta term (3.45) reproduces the correction  $\epsilon_{JI}^{HL}$  computed as in sec 2.5:

$$\epsilon_{JI}^{HL} \approx \tan \beta [\epsilon'_J(I) + \delta_a \epsilon'_J(I) + \delta_b \epsilon'_J(I)] + \Delta_{JI} \quad (5.8)$$

While in most cases the term proportional to  $\alpha_s$  in  $\epsilon'_J(I)$  is dominant, the term  $\delta_a \epsilon'_J(I) + \delta_b \epsilon'_J(I)$  is usually more important than the term  $\Delta_{JI}$  and even than  $y_b^2$  dependent part of the  $\epsilon'_J(I)$  term. Let us also stress that the quality of the approximation of  $\epsilon_{JI}^{HL}$  by the rhs depends crucially on how well  $\tilde{\epsilon}_3$  approximates the factor  $\epsilon_{d_3}$  (2.30) needed to obtain  $y_b$  and how well epsilons reproduce the ratio  $V^{JI}/V_{\text{eff}}^{JI}$ . Since the approximations of secs. 3.2-3.3 are usually not better than 15%-20%, the contributions to the lhs and rhs of eq. (5.8) not proportional to  $\alpha_s$  usually differ by about 20%-50%. Reliable approximation



can be obtained only by using in (3.45)  $\tilde{\epsilon}_0$  and  $\epsilon_Y^{(32)}$  computed as in eq. (5.1) instead of  $\epsilon_0$  and  $\epsilon_Y$ . The approximation (5.8) works then to an accuracy 5%-10%. This is demonstrated in figure 11 where in panels a and b (panels c and d) we compare  $\epsilon_{33}^{HL}$  ( $\epsilon_{32}^{HL}$ ) calculated as in section 2.5 with the approximation based on the formula (3.44) and with the approximation based on eq. (5.8), respectively. In panel a (and c) we have used in the  $\Delta_{JI}$  term (3.45)  $\epsilon_0$  and  $\epsilon_Y$  given by eqs. (5.2), (5.5) whereas in panel b (and d)  $\tilde{\epsilon}_0$  and  $\epsilon_Y^{(32)}$  from the formula (5.1). The difference between the results of the full and approximate calculations is quantified by the deviation of the points from the diagonal line. The dramatic improvement of the approximation is clearly seen in panels b and d of figure 11.

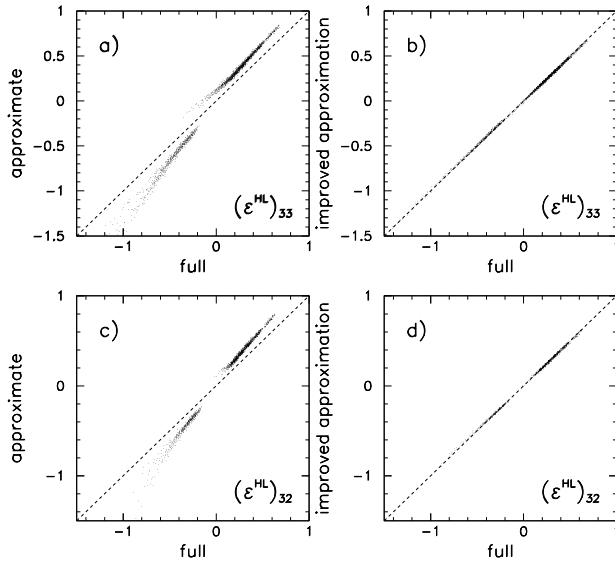


Figure 11: As in figure 6 but for the corrections  $\epsilon_{33}^{HL}$  and  $\epsilon_{32}^{HL}$  to the couplings of  $H^+$  to the left-handed down quarks. Only points yielding acceptable  $BR(\bar{B} \rightarrow X_s \gamma)$  are shown.

Next we consider the correction  $\epsilon_{JI}^{HR}$ . As in the approximation based on the  $SU(2) \times U(1)$  symmetry limit, also in the complete calculation of sec. 2.5 it is entirely determined by the rotations in the down quark sector (the genuine vertex corrections and the contribution of the vector self energies are negligible) and can be obtained from the formula (3.46) with exact matrices  $\mathbf{D}_L$  and  $\mathbf{D}_R$ . The quality of the approximation (3.47) depends therefore crucially on how well the matrices  $\mathbf{D}_L$  and  $\mathbf{D}_R$  are approximated. For split squarks the full flavour dependence of the correction  $(\Delta m_d)^{JI}$  is due also to the flavour

dependence of  $\epsilon_0$  and  $\epsilon_Y$  and, consequently, the matrices  $\mathbf{D}_L$  and  $\mathbf{D}_R$  obtained in the strict  $SU(2) \times U(1)$  symmetry limit with universal  $\epsilon_0$  and  $\epsilon_Y$  deviate from the true ones. To obtain a reliable approximation for  $\epsilon_{JI}^{HR}$  in the more realistic situation, in which squarks from the third generation are split from the others, one has to use flavour dependent expressions (3.58)-(3.61) and the improved formulae in (5.1). The results of this improvement are shown in figure 12 where we compare  $\epsilon_{32}^{HR}$  obtained in the full approach based on eqs. (2.42), (2.44) with the approximation (3.47) using universal  $\epsilon_0$  and  $\epsilon_Y$  obtained from eqs. (5.2) and (5.5) (panel a) and with the  $\epsilon_{32}^{HR}$  obtained from eqs. (3.61) and (5.1) (panel b).

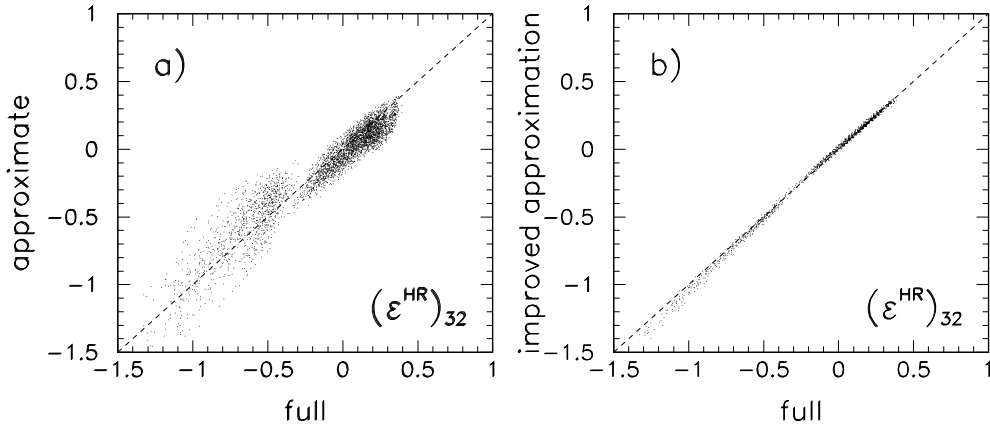


Figure 12: As in figure 6 but for the corrections  $\epsilon_{32}^{HR}$  to the couplings of  $H^+$  to the right-handed down quarks. Only points yielding acceptable  $BR(\bar{B} \rightarrow X_s \gamma)$  are shown.

Finally we consider the corrections of the charged Goldstone bosons to quarks defined in eq. (2.49). As we argued, in the  $SU(2) \times U(1)$  symmetry limit  $\epsilon_{JI}^{GL} = \epsilon_{JI}^{GR} = 0$  also for nonzero electroweak gauge couplings  $g_1$  and  $g_2$ . To understand our results, it is important to stress at this point that integrating out sparticles and constructing the effective Lagrangian in the  $SU(2) \times U(1)$  symmetry limit without making any assumption about dominance of some particular couplings (like  $\alpha_s$ , or  $y_t$ ) requires also the inclusion of the vector parts of the quark self energies and of all vertex diagrams, in particular the ones shown in fig. 10. In other words, the whole procedure of sec. 2 has to be used with the exception that the Higgs boson vacuum expectation values are equal zero. The

argument for vanishing  $\epsilon_{JI}^{GL}$  and  $\epsilon_{JI}^{GR}$  applies then up to  $1/M_{\text{SUSY}}^2$  corrections.

To go beyond the  $SU(2) \times U(1)$  symmetry limit we write the factors  $\epsilon_{JI}^{GL}$  and  $\epsilon_{JI}^{GR}$  as

$$\epsilon_{GL}^{JI} = \frac{\sqrt{2}M_W}{g_2} \frac{[\mathbf{U}_R^\dagger \cdot (\Delta\hat{F}_L^G \cdot V^\dagger - \frac{g_2}{\sqrt{2}M_W}\Delta m_u) \cdot \mathbf{U}_L]^{JK} V_{\text{eff}}^{KI}}{\bar{m}_{u_j} V_{\text{eff}}^{JI}} \quad (5.9)$$

$$\epsilon_{GR}^{JI} = -\frac{\sqrt{2}M_W}{g_2} \frac{V_{\text{eff}}^{JK} [\mathbf{D}_L^\dagger \cdot (V^\dagger \cdot \Delta\hat{F}_R^G + \frac{g_2}{\sqrt{2}M_W}(\Delta m_d)^\dagger) \cdot \mathbf{D}_R]^{KI}}{V_{\text{eff}}^{JI} \bar{m}_{d_I}} \quad (5.10)$$

where  $\Delta\hat{F}_{L,R}^G$  are defined in eqs. (2.43), (2.44). (Similar expressions can be written down for corrections  $\epsilon_{HL}^{JI}$  and  $\epsilon_{HR}^{JI}$ .) As can be seen by using the formula (3.35), in the  $SU(2) \times U(1)$  symmetry limit  $\Delta\hat{F}_L^G = \frac{g_2}{\sqrt{2}M_W}\Delta m_u V$ ,  $\Delta\hat{F}_R^G = -\frac{g_2}{\sqrt{2}M_W}V(\Delta m_d)^\dagger$  and the corrections indeed vanish. (It is also easy to see that  $\Sigma_{VL}^u$  and  $\Sigma_{VR}^d$  cancel out in (5.9) and in (5.10), respectively.) Because both,  $V^\dagger\Delta\hat{F}_R^G$  and  $(g_2/\sqrt{2}M_W)(\Delta m_d)^\dagger$  contain contributions  $\propto \tan\beta$ , any mismatch between them could in principle give rise to  $\tan\beta$  enhanced terms in  $\epsilon_{JI}^{GR}$  and this motivated the authors of ref. [25] to keep the correction  $\epsilon_{JI}^{GR}$  in their  $BR(\bar{B} \rightarrow X_s\gamma)$  calculation (no such enhancement was expected in  $\epsilon_{JI}^{GL}$ ). Exact numerical evaluation of the formulae (5.9), (5.10) reveals, however, that the cancellation between  $\Delta\hat{F}_L^G \cdot V^\dagger$  and  $-(g_2/\sqrt{2}M_W)\Delta m_d$  in (5.9) and between  $V^\dagger \cdot \Delta\hat{F}_R^G$  and  $(g_2/\sqrt{2}M_W)(\Delta m_d)^\dagger$  in (5.10) is surprisingly accurate when these quantities are calculated as in sec. 2 which means that the  $SU(2) \times U(1)$  symmetry breaking corrections to  $\Delta\hat{F}_{L,R}^G$  and  $\Delta m_{u,d}$  are tiny compared to the corrections introduced by switching on the electroweak gauge couplings. We find that  $|\epsilon_{JI}^{GL}|$  and  $|\epsilon_{JI}^{GR}|$  are of the same order of magnitude and are  $\sim \mathcal{O}(10^{-4})$  in most of the parameter space (for sparticles heavier than 500 GeV and  $\tan\beta = 50$ ). These are small corrections compared to 1 and do not influence appreciably the phenomenology we are going to discuss. Note also, that approximating  $\Delta m_d$  or  $\Delta\hat{F}_{L,R}^G$  by dropping some ‘‘small’’ terms or using simplified couplings in the vertices as compared to the ones given in ref. [30] spoils this delicate cancellation and generates  $|\epsilon_{JI}^{GL,R}| \sim 10^{-(1-2)}$  !

Finally let us explain the status of the rules (4.3) and (4.4). As long as one considers only  $\mathcal{O}(\alpha_s)$  corrections to the effective Lagrangian couplings the rules (4.3) and (4.4) are the true equalities. This has to be so, because when the charged Goldstone boson vertices corrected as in [25] are used in the one loop expressions for the Wilson coefficients  $C_{7,8}$  of the (chromo)magnetic operators they reproduce correctly [26] appropriate  $\tan\beta$  enhanced terms in the two loop contributions to  $C_{7,8}$  calculated in [33]. The ideology of the effective Lagrangian serves then only to correctly resum these terms. Indeed, in this case  $V^{\text{eff}} = V$ ,  $\mathbf{D}_{L,R} = \mathbf{I}$  and inserting  $\Delta\hat{F}_R^G$  in the form

$$(\Delta\hat{F}_R^G)^{JI} = -\frac{g}{\sqrt{2}M_W} V^{JI} m_{d_I} \epsilon'_I(J) \tan\beta \quad (5.11)$$

as in ref. [25] in (5.10) one recovers the rule (4.4).<sup>6</sup> However, when the corrections depending on the top Yukawa coupling to the vertices of the effective Lagrangian are taken into account, the true formula (5.10) for  $\epsilon_{JI}^{GR}$  is more involved and cannot be obtained from the rule (4.4) just by including the terms  $\propto y_t^2$  to  $\epsilon'_I(J)$  as in [25]. Formulae (4.3) and (4.4) are then only the substitution rules allowing to translate the formulae of [25] into ours.

## 6 $\Delta M_{d,s}$ , $B_{d,s}^0 \rightarrow \mu^+ \mu^-$ and $\bar{B} \rightarrow X_s \gamma$

The  $B_{s,d}^0 \rightarrow \mu^+ \mu^-$  decays and the  $B_s^0$ - $\bar{B}_s^0$  mixing attracted recently a renewed attention due to the observation that for large values of  $\tan \beta$  their amplitudes can receive very large contributions from diagrams depicted in figures 13 and 14 in which the black blobs represent the flavour changing couplings  $[X_{RL}^S]^{JI}$  and  $[X_{LR}^S]^{JI}$  discussed in the preceding sections. These contributions have been found to *increase* by orders of magnitude the branching ratios for the rare decays  $B_{s,d}^0 \rightarrow \mu^+ \mu^-$  [20, 6, 21, 22] and to *decrease* substantially the  $B_s^0$ - $\bar{B}_s^0$  mass difference  $\Delta M_s$  [23].

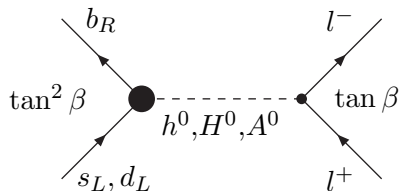


Figure 13: Diagrams giving dominant contribution to  $B_{s,d}^0 \rightarrow l^+ l^-$  amplitudes at large  $\tan \beta$ .

As demonstrated in [20, 6, 21, 22], for  $\tan \beta \sim 50$  and non-negligible values of the parameter  $A_t$  the  $B_{s,d}^0 \rightarrow \mu^+ \mu^-$  amplitudes are totally dominated by the diagram of fig. 13. In the absence of any other constraints on the MSSM parameter space, the corresponding branching ratios, which behave as  $|A_t \tan^3 \beta / M_A^2|^2$ , can be enhanced by up to three orders of magnitude relative to the SM predictions and can even exceed the

---

<sup>6</sup>However, calculating  $\epsilon'_I(J)$  from the triangle diagram of fig. 1a of [25] with simplified  $G^+$  couplings to up and down squarks would result in  $\epsilon_{JI}^{GR} \sim 10^{-2}$ , much bigger than  $\mathcal{O}(10^{-4})$  obtained with the full  $G^+$  couplings given in [30]. In particular, we have found that for non-negligible sbottom mixing (if, say,  $|A_b| \sim |A_t|$ ) neglecting in this vertex terms  $\propto y_t^2$  and  $\propto g_2^2$  has dramatic effect on the cancellation in (5.10). On the other hand, neglecting simultaneously the contributions of the vector self energies to  $\Delta \hat{F}_R^G$  and to  $\Delta m_d$  does not affect it.

present experimental bounds:

$$BR(B_d^0 \rightarrow \mu^+ \mu^-) < 2.1 \times 10^{-7} \quad \text{BaBar [34]}, \quad (6.1)$$

$$BR(B_s^0 \rightarrow \mu^+ \mu^-) < 2.0 \times 10^{-6} \quad \text{CDF [35]}. \quad (6.2)$$

The  $B_{s,d}^0 - \bar{B}_{s,d}^0$  mass difference in turn receives several contributions:

$$\Delta M_s = |(\Delta M_s)^{\text{SM}} + (\Delta M_s)^{H^\pm} + (\Delta M_s)^{\chi^\pm} + (\Delta M_s)^{\text{DP}}| \equiv (\Delta M_s)^{\text{SM}} |1 + f_s| \quad (6.3)$$

(by definition  $\Delta M_s$  is a positive definite quantity). For large  $\tan \beta$  and non-negligible  $A_t$  the contribution  $(\Delta M_s)^{\text{DP}}$  of the double scalar penguin (DP) shown in fig. 14 is the dominant correction to the SM contribution  $(\Delta M_s)^{\text{SM}}$ . Both,  $(\Delta M_s)^{\text{DP}}$  and the contribution  $(\Delta M_s)^{H^\pm}$  of the box-diagrams with top and charged Higgs bosons  $H^\pm$  have the signs opposite to  $(\Delta M_s)^{\text{SM}}$ . While generally smaller than  $(\Delta M_s)^{\text{SM}}$ , their sum leads for large  $\tan \beta$  to a significant decrease of the predicted  $\Delta M_s$  (i.e. to  $f_s < 0$ ) independently of the choice of supersymmetric parameters. We will assess the relative magnitudes of the double penguin, charged Higgs and chargino box diagrams in secs. 6.1.3, 6.1.4.

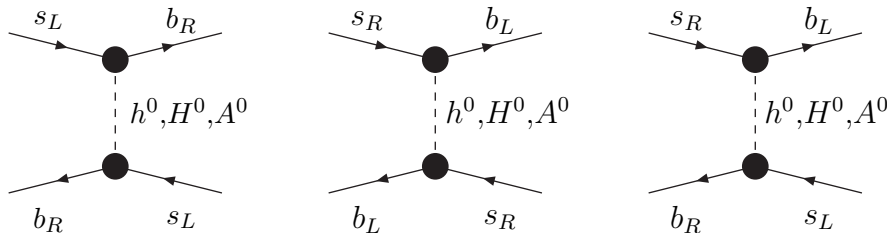


Figure 14: Double penguin diagrams contributing to  $\Delta M_s$ .

As is evident from the comparison of figures 13 and 14 there must exist a strong correlation between the enhancement of  $BR(B_{s(d)}^0 \rightarrow \mu^+ \mu^-)$  and the suppression of  $\Delta M_s$ . In particular for  $0 < (1 + f_s) < 1$  the experimental lower bound  $\Delta M_s > 15/\text{ps}$  puts an upper bound on the possible enhancement of  $BR(B_{s(d)}^0 \rightarrow \mu^+ \mu^-)$ . Of interest is also the case  $(1 + f_s) < 0$  corresponding to a very large negative  $(\Delta M_s)^{\text{DP}}$  (that can be realized for very special values of supersymmetric parameters) which has quite different implications than the case  $0 < (1 + f_s) < 1$ . The main result concerning this correlation has been presented in [29]. Our purpose now is to explore it in more detail investigating in particular its dependence on the MSSM parameters and elucidating the impact of the  $\tan \beta$  enhanced corrections to  $\Delta M_s$  on the standard Unitarity Triangle (UT) analysis which is necessary to determine the CKM matrix element  $V_{td}$  needed to predict accurately  $BR(B_d^0 \rightarrow \mu^+ \mu^-)$ .

Large  $\tan\beta$  effects manifest themselves also in the transition  $\bar{B} \rightarrow X_s\gamma$ , which being already relatively well measured, plays an important role in constraining the allowed region in the space of supersymmetric parameters [25, 33, 26]. Exploring the correlation between the increase of  $BR(B_{s(d)}^0 \rightarrow \mu^+\mu^-)$  and suppression of  $\Delta M_s$  it is therefore important to incorporate this constraint in the analysis.<sup>7</sup>

In this section we collect the formulae for  $BR(B_{s(d)}^0 \rightarrow \mu^+\mu^-)$  and  $(\Delta M_s)^{\text{DP}}$  in the large  $\tan\beta$  limit and discuss the importance of various contributions. We recall also the UT analysis and include a subsection devoted to the calculation of  $BR(\bar{B} \rightarrow X_s\gamma)$ . As in [23, 29] we will concentrate on the scenario with heavy sparticles and the mass scale of the Higgs sector close to the electroweak scale but will comment also on possible effects of lighter sparticles. The numerical analysis of the correlation of the enhancement of  $BR(B_{s(d)}^0 \rightarrow \mu^+\mu^-)$  and the suppression of  $\Delta M_s$  will be the subject of the next section.

## 6.1 Formulae for calculating $\Delta M_s$

### 6.1.1 The Effective Hamiltonian

The effective Hamiltonian for  $B_s^0$ - $\bar{B}_s^0$  mixing has the form as follows

$$\mathcal{H}_{\text{eff}}^{\Delta B=2} = \frac{G_F^2 M_W^2}{16\pi^2} (V_{\text{eff}}^{tb*} V_{\text{eff}}^{ts})^2 \sum_i C_i(\mu) Q_i. \quad (6.4)$$

Here  $Q_i$  are the  $\Delta B = 2$  operators and  $G_F$  is the Fermi constant. It should be stressed that with the improvements in the calculation of Higgs boson vertices the factorization of the CKM elements in (6.4) is only approximate. Still, it is an excellent approximation to the full calculation and allows for a transparent discussion of the unitarity triangle (UT). The set of dimension six  $\Delta B = 2$  operators consists of

$$\begin{aligned} Q^{\text{VLL}} &= (\bar{b}_L \gamma_\mu s_L) (\bar{b}_L \gamma^\mu s_L) \\ Q_1^{\text{LR}} &= (\bar{b}_L \gamma_\mu s_L) (\bar{b}_R \gamma_\mu s_R) \\ Q_2^{\text{LR}} &= (\bar{b}_R s_L) (\bar{b}_L s_R) \\ Q_1^{\text{SLL}} &= (\bar{b}_R s_L) (\bar{b}_R s_L) \\ Q_2^{\text{SLL}} &= (\bar{b}_R \sigma_{\mu\nu} s_L) (\bar{b}_R \sigma^{\mu\nu} s_L) \end{aligned} \quad (6.5)$$

where  $\sigma_{\mu\nu} = \frac{1}{2}[\gamma_\mu, \gamma_\nu]$  and the colour indices are contracted within the brackets. The additional operators  $Q^{\text{VRR}}$ ,  $Q_1^{\text{SRR}}$  and  $Q_2^{\text{SRR}}$  are obtained from  $Q^{\text{VLL}}$ ,  $Q_1^{\text{SLL}}$  and  $Q_2^{\text{SLL}}$  by

---

<sup>7</sup>Large  $\tan\beta$  effects have been also investigated in  $(g-2)_\mu$ . However, they depend on the slepton sector parameters which can be correlated with the squark sector ones only within a particular scenario like e.g. minimal supergravity [36] or gauge mediation.

replacing  $L$  with  $R$ . Similar Hamiltonians, with appropriate changes of the quark fields and the CKM matrix elements describe also  $B_d^0-\bar{B}_d^0$  and  $K^0-\bar{K}^0$  transitions. In the SM only the Wilson coefficients of  $Q^{\text{VLL}}$  are relevant and the details of their contributions are well known (see e.g. [37]).

The basic formula for the  $B_q^0-\bar{B}_q^0$  mass difference reads

$$\Delta M_q = \frac{G_F^2 M_W^2}{6\pi^2} M_{B_q} \eta_B F_{B_q}^2 \hat{B}_{B_q} |V_{tq}^{\text{eff}}|^2 |F_{tt}^q| \quad (6.6)$$

where  $q = s$  or  $d$ . We recall also that [23]

$$\begin{aligned} F_{tt}^s &= \left[ S_0(x_t) + \frac{1}{4r} C_{\text{new}}^{\text{VLL}}(\mu_S) \right] \\ &+ \frac{1}{4r} C_1^{\text{VRR}}(\mu_S) + \bar{P}_1^{\text{LR}} C_1^{\text{LR}}(\mu_S) + \bar{P}_2^{\text{LR}} C_2^{\text{LR}}(\mu_S) \\ &+ \bar{P}_1^{\text{SLL}} \left[ C_1^{\text{SLL}}(\mu_S) + C_1^{\text{SRR}}(\mu_S) \right] + \bar{P}_2^{\text{SLL}} \left[ C_2^{\text{SLL}}(\mu_S) + C_2^{\text{SRR}}(\mu_S) \right] \end{aligned} \quad (6.7)$$

with  $r = 0.985$  [38] describing  $\mathcal{O}(\alpha_s)$  QCD corrections to  $S_0(x_t)$  in the SM and  $\eta_B = 0.55$ . The factor  $f_s$  introduced in eq. (6.3) is given by  $1 + f_s \equiv F_{tt}^s/S_0(x_t)$ . Next

$$\bar{P}_i^a = \frac{P_i^a}{4\eta_B \hat{B}_{B_s}} \quad (6.8)$$

where  $\hat{B}_{B_s}$  is the non-perturbative parameter related to the matrix elements of  $Q^{\text{VLL}}$ . The coefficients  $P_i^a$  include NLO QCD renormalization group factors [39, 40, 41] that sum up large logarithms between  $\mu_S$  and  $\mu_b = \mathcal{O}(m_b)$  scales. Explicit formulae for  $P_i^a$  in terms of these QCD factors and non-perturbative parameters  $B_i$  can be found in [41, 23].

In [23], except for  $B^{\text{VLL}}$ , we have set the non-perturbative parameters  $B_i$  in the B-system to unity as the results of lattice calculations were not available at that time. Meanwhile all these parameters have been calculated in [42]. Translating these results into our operator basis by means of the formulae given in [41] we find

$$B^{\text{VLL}} = 0.87, \quad B_1^{\text{LR}} = 1.75, \quad B_2^{\text{LR}} = 1.16, \quad B_1^{\text{SLL}} = 0.80, \quad B_2^{\text{SLL}} = 0.71 \quad (6.9)$$

for  $\mu_b = 4.6$  GeV. This gives

$$P_1^{\text{LR}} = -2.03, \quad P_2^{\text{LR}} = 2.56, \quad P_1^{\text{SLL}} = -1.06, \quad P_2^{\text{SLL}} = -2.05 \quad (6.10)$$

and using (6.8) with  $\hat{B}_{B_s} = 1.3$  we find

$$\bar{P}_1^{\text{LR}} = -0.71, \quad \bar{P}_2^{\text{LR}} = 0.90, \quad \bar{P}_1^{\text{SLL}} = -0.37, \quad \bar{P}_2^{\text{SLL}} = -0.72. \quad (6.11)$$

We observe substantial suppression of  $4\bar{P}_1^{\text{SLL}}$  relative to the vacuum insertion estimates used in [23, 27] that resulted in  $-0.53$ . The formula for  $\varepsilon_K$  in terms of  $F_{tt}^\varepsilon$  as well as the expressions analogous to (6.7) for  $F_{tt}^\varepsilon$  can be found in ref. [23].

In our numerical analysis of section 7 we have included complete expressions for all the one loop box diagrams contributing to Wilson coefficients  $C_i(\mu_S)$  relevant for  $B_{s,d}^0\bar{B}_{s,d}^0$  mass difference and  $\varepsilon_K$  as well as the complete expressions for the contribution of the double penguin diagrams shown in fig. 14. In the box diagrams involving charged Higgs and Goldstone bosons we have used vertices with corrections  $\epsilon_{JI}^{HL(R)}$  and  $\epsilon_{JI}^{GL(R)}$  calculated as in sec. 2. Similarly, in the diagrams shown in fig. 14 we have used full flavour changing vertices  $[X_{RL}^S]^{JI}$ ,  $[X_{LR}^S]^{JI}$  as given in eqs. (2.34), (2.35), (2.37) and (2.38). The necessary formulae are collected in the Appendix A. In the numerical calculation for the scale  $\mu_S$  we have taken  $\mu_S = M_{H^+}$ .

Let us now concentrate on the most important of new contributions to the Wilson coefficients  $C_i$  relevant for  $\Delta M_s$ .

### 6.1.2 Double Penguin Diagrams

As shown in [19, 20, 23] in supersymmetry with large  $\tan\beta$  contribution of the double-penguin diagrams shown in fig. 14 to the Wilson coefficients of the operators  $Q_2^{\text{LR}}$ ,  $Q_1^{\text{SLL}}$  and  $Q_1^{\text{SRR}}$  can be substantial. Their Wilson coefficients  $C_i$  relevant for the  $B_s^0\bar{B}_s^0$  mixing are then determined from the matching conditions:

$$\frac{G_F^2 M_W^2}{16\pi^2} (V_{\text{eff}}^{tb*} V_{\text{eff}}^{ts})^2 C_2^{\text{LR}} = i \sum_{S^0=h^0, H^0, A^0} \frac{i}{-M_{S^0}^2} (-i)^2 [X_{RL}^S]^{bs} [X_{LR}^S]^{bs} \quad (6.12)$$

with  $X_{RL}^S X_{LR}^S$  replaced by  $X_{RL}^S X_{RL}^S$  and  $X_{LR}^S X_{LR}^S$  for  $C_1^{\text{SLL}}$  and  $C_1^{\text{SRR}}$ , respectively. In these cases a combinatorial factor 1/2 has to be included on the r.h.s of (6.12). The contribution of the neutral Goldstone boson  $G^0$  can be neglected as  $X_{LR}^G$  and  $X_{RL}^G$  vanish in the  $SU(2) \times U(1)$  symmetry limit. (See eqs. (3.23) and (3.24).)

In what follows it will be convenient to introduce the “reduced” couplings  $[\bar{X}_{RL}^S]^{JI}$  defined by

$$[X_{RL}^S]^{bs} \equiv G_F^{3/2} 2^{7/4} V_{\text{eff}}^{tb*} V_{\text{eff}}^{ts} [\bar{X}_{RL}^S]^{bs} \quad (6.13)$$

with the same definition for  $[\bar{X}_{LR}^S]^{bs}$ .

In the approximation of sec. 3, using (3.26) and (3.27) we find for  $J = 3 = b$ ,  $I = 2 = s$

$$[\bar{X}_{RL}^S]^{bs} = \frac{\bar{m}_b \bar{m}_t^2 \epsilon_Y \tan\beta}{(1 + \tilde{\epsilon}_3 \tan\beta)(1 + \epsilon_0 \tan\beta)} (x_u^S - x_d^S \tan\beta) \quad (6.14)$$

and

$$[\bar{X}_{LR}^S]^{bs} = \frac{\bar{m}_s \bar{m}_t^2 \epsilon_Y \tan\beta}{(1 + \tilde{\epsilon}_3 \tan\beta)(1 + \epsilon_0 \tan\beta)} (x_u^{S*} - x_d^{S*} \tan\beta) \quad (6.15)$$

where we used the approximations  $1/\cos\beta \approx \tan\beta$ ,  $y_t^2 \approx 2\sqrt{2}G_F \bar{m}_t^2$  valid for  $\tan\beta \gg 1$ .  $x_u^S$  and  $x_d^S$  are defined in (3.21). Following the numerical analysis performed in sec. 5.2



reliable approximation to the results of the complete calculation requires, however, using the formulae of section 3.6 with the epsilon parameters extracted as in eq. (5.1). Still, the simple formulae (5.2) used in (6.14), (6.15) describe well the qualitative behaviour of the double penguin contribution.

From (6.12) and (6.13) we find then the double penguin contributions to the Wilson coefficients in question:

$$C_2^{LR} = -\frac{G_F (16\pi^2)^2}{\sqrt{2} M_W^2 \pi^2} \sum_{S^0=h^0, H^0, A^0} \frac{1}{M_{S^0}^2} [\overline{X}_{RL}^S]^{bs} [\overline{X}_{LR}^S]^{bs} \quad (6.16)$$

and

$$C_1^{SLL} = -\frac{1}{2} \frac{G_F (16\pi^2)^2}{\sqrt{2} M_W^2 \pi^2} \sum_{S^0=h^0, H^0, A^0} \frac{1}{M_{S^0}^2} [\overline{X}_{RL}^S]^{bs} [\overline{X}_{RL}^S]^{bs} \quad (6.17)$$

with  $C_1^{SRR}$  obtained from  $C_1^{SLL}$  by interchanging  $L$  and  $R$ .

Using formulae (6.14) and (6.15) we find

$$[\overline{X}_{RL}^S]^{bs} = \frac{\overline{m}_b \overline{m}_t^2 \epsilon_Y \tan^2 \beta}{(1 + \tilde{\epsilon}_3 \tan \beta)(1 + \epsilon_0 \tan \beta)} [\sin(\alpha - \beta), \cos(\alpha - \beta), -i] \quad (6.18)$$

$$[\overline{X}_{LR}^S]^{bs} = \frac{\overline{m}_s \overline{m}_t^2 \epsilon_Y \tan^2 \beta}{(1 + \tilde{\epsilon}_3 \tan \beta)(1 + \epsilon_0 \tan \beta)} [\sin(\alpha - \beta), \cos(\alpha - \beta), i] \quad (6.19)$$

for  $S^0 = [H^0, h^0, A^0]$ . Consequently the dominant,  $\mathcal{O}(\tan^4 \beta)$ , contributions to  $C_2^{LR}$ ,  $C_1^{SLL}$  and  $C_1^{LRR}$ , that come solely from the double penguin diagrams read

$$C_2^{LR} \approx -\frac{G_F \overline{m}_b \overline{m}_s \overline{m}_t^4}{\sqrt{2} \pi^2 M_W^2} \frac{\tan^4 \beta \epsilon_Y^2 (16\pi^2)^2}{(1 + \tilde{\epsilon}_3 \tan \beta)^2 (1 + \epsilon_0 \tan \beta)^2} \mathcal{F}^+, \quad (6.20)$$

$$C_1^{SLL} \approx -\frac{G_F \overline{m}_b^2 \overline{m}_t^4}{2\sqrt{2} \pi^2 M_W^2} \frac{\tan^4 \beta \epsilon_Y^2 (16\pi^2)^2}{(1 + \tilde{\epsilon}_3 \tan \beta)^2 (1 + \epsilon_0 \tan \beta)^2} \mathcal{F}^-, \quad (6.21)$$

$$C_1^{SRR} = \frac{\overline{m}_s^2}{\overline{m}_b^2} C_1^{SLL}. \quad (6.22)$$

(Note that  $\epsilon_Y$  as given by eq. (5.2) is equal  $X_{Ct}/16\pi^2$  of ref. [23] and  $G_F/\sqrt{2} = \pi\alpha_{EM}/2s_W^2 M_W^2$ .) Here

$$\mathcal{F}^\pm \equiv \frac{\sin^2(\alpha - \beta)}{M_{H^0}^2} + \frac{\cos^2(\alpha - \beta)}{M_{h^0}^2} \pm \frac{1}{M_{A^0}^2} \approx \frac{1}{M_{H^0}^2} \pm \frac{1}{M_{A^0}^2} \quad (6.23)$$

where we have used the fact that in the MSSM for  $\tan \beta \gg 1$  and  $M_{A^0} > M_Z$  one has  $\sin^2(\alpha - \beta) \approx 1$  and  $\cos^2(\alpha - \beta) \approx 0$ . Because  $M_{A^0} \approx M_{H^0}$ , it follows, that for large

$\tan\beta$  the  $H^0$  and  $A^0$  contributions to  $C_1^{\text{SLL}}$  and  $C_1^{\text{SRR}}$  cancel each other [20] and the contribution of  $h^0$  can be neglected. It is therefore the coefficient  $C_2^{\text{LR}}$  that receives the largest contribution from double penguin diagrams [23]. Their contribution to the Wilson coefficients relevant for the  $B_d^0$ - $\bar{B}_d^0$  mixing (for  $\varepsilon_K$ ) are given by the same formulae with  $m_s$  replaced by  $m_d$  ( $m_s$  replaced by  $m_d$  and  $m_b$  replaced by  $m_s$ ). Our result for  $C_2^{\text{LR}}$  agrees with the corrected version of eq. (42) of [27] where the presence of additional  $\tan\beta$  factors involving  $\tilde{\varepsilon}_3$  and  $\varepsilon_0$ , not included in [23] has been pointed out.

An important feature of the double penguin contribution to  $C_2^{\text{LR}}$ , (and also to  $C_1^{\text{SLL}}$  and  $C_1^{\text{SRR}}$ ) is its fixed negative sign that is the same as the sign of the contribution of the charged Higgs boson box diagrams at large  $\tan\beta$  [23]. Because the strong correction factor  $\bar{P}_2^{\text{LR}}$  in (6.7) is positive the double penguin contribution interferes destructively with the SM ones and leads to  $1 + f_s < 1$ . Another interesting feature is its strong dependence on the left-right mixing of the top squarks as  $\epsilon_Y^2 \propto A_t^2$ .

Using the general formulae given in refs. [23, 41] and collected in the preceding subsection we find the contribution of the double penguin diagrams to  $\Delta M_s$ :

$$(\Delta M_s)^{DP} = \frac{G_F^2 M_W^2}{24\pi^2} M_{B_s} F_{B_s}^2 |V_{ts}^{\text{eff}}|^2 P_2^{\text{LR}} C_2^{\text{LR}}(\mu_S). \quad (6.24)$$

For  $\mu_S = \mathcal{O}(m_t)$  the factor  $P_2^{\text{LR}}$  summarizing renormalization group effects between  $\mu_b \leq \mu \leq \mu_S$  and including the relevant hadronic matrix elements is  $P_2^{\text{LR}} \approx 2.5$ .

Identifying  $C_2^{\text{LR}}$  in (6.20) with  $C_2^{\text{LR}}(\mu_S)$  we find for large  $\tan\beta$

$$\begin{aligned} (\Delta M_s)^{DP} = & -12.0/ps \times \left[ \frac{\tan\beta}{50} \right]^4 \left[ \frac{P_2^{\text{LR}}}{2.50} \right] \left[ \frac{F_{B_s}}{230 \text{ MeV}} \right]^2 \left[ \frac{|V_{ts}|}{0.040} \right]^2 \\ & \times \left[ \frac{\bar{m}_b(\mu_S)}{3.0 \text{ GeV}} \right] \left[ \frac{\bar{m}_s(\mu_S)}{0.06 \text{ GeV}} \right] \left[ \frac{\bar{m}_t^4(\mu_S)}{M_W^2 M_A^2} \right] \frac{(16\pi^2)^2 \epsilon_Y^2}{(1 + \tilde{\varepsilon}_3 \tan\beta)^2 (1 + \varepsilon_0 \tan\beta)^2} \end{aligned} \quad (6.25)$$

### 6.1.3 Charged Higgs Box Diagram Contributions

The formulae for the charged Higgs boson ( $H^\pm, G^\pm$ ) box diagram contributions to the Wilson coefficients of the effective Hamiltonians describing  $B_{s,d}^0$ - $\bar{B}_{s,d}^0$  mixing have been presented in section 4.1 of [23] and have been confirmed in [27]. They do not, however take into account the corrections to the  $H^+$  couplings discussed in sections 2.5 and 3.4. The corrections  $\epsilon_{JI}^{\text{HL}}$  and  $\epsilon_{JI}^{\text{HR}}$  can be easily incorporated in those expressions of eqs. (4.4) and (4.5) of [23] that contain a single  $D_0$  or a single  $D_2$ -function. To this end it suffices to make the following replacements

$$a_{L(R)}^{Jlk=1} \rightarrow \left[ P_{RL(LR)}^H \right]^{JI} / V_{\text{eff}}^{JI} \quad a_{L(R)}^{Jlk=2} \rightarrow \left[ P_{RL(LR)}^G \right]^{JI} / V_{\text{eff}}^{JI} \quad (6.26)$$

The two expressions in eqs. (4.4) and (4.5) of [23] which contain three  $D_2$ -functions have been obtained by using the unitarity of the CKM matrix. Therefore, in this case the

replacement (6.26) has to be supplemented by multiplication of the second and third  $D_2$ -function in the square bracket in (4.4) of [23] by  $r$  and  $r^2$ , respectively and by  $r^2$  and  $r^4$  in (4.5) of [23] where  $r = (1 + \tilde{\epsilon}_3 \tan \beta)/(1 + \tilde{\epsilon}_1 \tan \beta)$  as follows from the formula (3.47). For completeness we give the relevant expressions in the Appendix A.4.

In this section we would like to assess the magnitude of the charged Higgs boson box diagram contribution to  $\Delta M_s$  and  $\Delta M_d$  with the corrections  $\epsilon_{JI}^{HL(R)}$  included (as follows from the numerical analysis of sec. 5, the impact of the corrections  $\epsilon_{JI}^{GL(R)}$  is negligible) and compare it with the magnitude of the contribution of the double penguin diagrams.

As found in [23] the largest contribution to  $\Delta M_s$  of the charged Higgs box diagrams, arises from the coefficient  $C_2^{LR}$ . This contribution is proportional to  $\overline{m}_s \overline{m}_b \tan^2 \beta$  and its sign is opposite to the SM contribution. The analogous contributions to  $\Delta M_d$  and  $\varepsilon_K$  are much smaller being proportional to  $\overline{m}_d \overline{m}_b \tan^2 \beta$  and  $\overline{m}_d \overline{m}_s \tan^2 \beta$ , respectively.

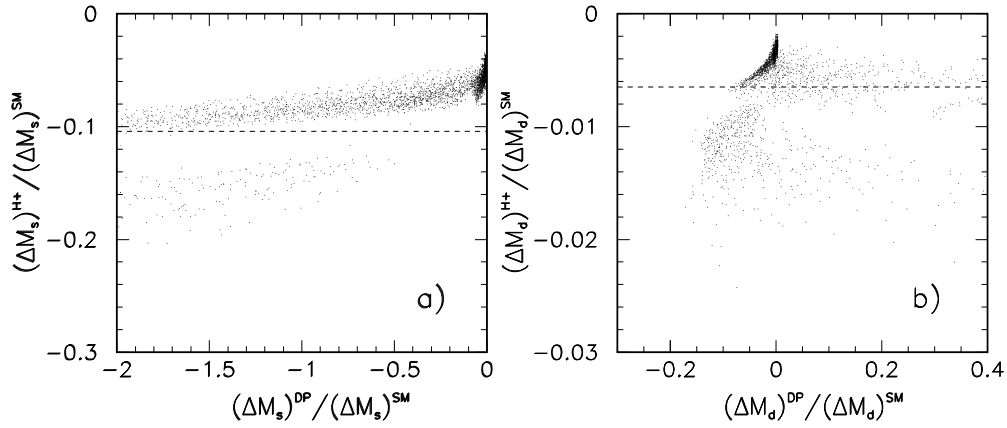


Figure 15: Comparison of the double penguin and charged Higgs boson box diagram contributions to the ratios  $\Delta M_s/(\Delta M_s)^{\text{SM}}$  (panel a) and  $\Delta M_d/(\Delta M_d)^{\text{SM}}$  (panel b) for  $M_A = 200$  GeV and  $\tan \beta = 50$ . Only points giving acceptable  $BR(\bar{B} \rightarrow X_s \gamma)$  are shown. Dashed lines show the ratios  $(\Delta M_s)^{H^+}/(\Delta M_s)^{\text{SM}}$  and  $(\Delta M_d)^{H^+}/(\Delta M_d)^{\text{SM}}$  in the absence of radiative corrections to the charged Higgs boson vertices.

An order of magnitude estimate of the charged Higgs boson box diagram contribution to  $\Delta M_s$  for  $M_{H^+} \approx \overline{m}_t$  can be obtained by taking into account only the contribution to

$C_2^{LR}$  in (6.7) of the box diagram with two  $H^\pm$ :

$$(\Delta M_s)_{H^\pm}^{LR} \approx -\frac{G_F^2 M_W^2}{18\pi^2} M_{B_s} F_{B_s}^2 P_2^{LR} \frac{\overline{m}_b \overline{m}_s}{M_W^2} \frac{\tan^2 \beta}{(1 + \tilde{\epsilon}_3 \tan \beta)^2} \quad (6.27)$$

where  $P_2^{LR} \approx 2.56$  and the factor  $(1 + \tilde{\epsilon}_3 \tan \beta)^2$  in the denominator comes from the rule (3.47). One should remember, however, that the box diagram with the  $W^\pm H^\mp$  exchange also gives the contribution  $\propto \tan^2 \beta$  and with the same sign as the one with  $H^\pm H^\mp$  exchange [23].

In figure 15 we compare for our scan over the MSSM parameter space the relative magnitude of the (complete) charged Higgs boson contributions to  $\Delta M_s$  and  $\Delta M_d$  with the contributions of the double penguin diagrams. We observe that in the case of  $\Delta M_s$  the contributions of the box-diagrams is much smaller than that of the double penguin diagrams for most of the points in the parameter space. The latter contribution is always negative and in a large portion of the parameter space exceeds also the SM one. The upper (lower) branch of points seen in panel a of figure 15a corresponds to  $\mu > 0$  ( $\mu < 0$ ). In fact, for points corresponding to unnaturally large  $A_t$  combined with negative values of  $\mu$  leading to enhancement of the effective couplings, the ratio  $(\Delta M_s)^{DP}/(\Delta M_s)^{SM}$  can reach values even as big as  $-10$ . The same points lead also to  $(\Delta M_d)^{DP}/(\Delta M_d)^{SM} \lesssim -0.2$ . They are excluded as they lead to unacceptably big  $BR(B_s^0 \rightarrow \mu^+ \mu^-)$  - see sec. 6.3. In contrast, the double penguin contribution to  $\Delta M_d$  can be also positive. This is because in this case the suppression by  $\overline{m}_b \overline{m}_d$  of the Wilson coefficient  $C_2^{LR}$  is stronger than the suppression of  $C_1^{SLL}$  by the factor  $\mathcal{F}^-$  in eq. (6.21). Since  $\overline{P}_1^{SLL}$  in (6.7) is negative this leads to positive contribution to  $(\Delta M_d)^{DP}/(\Delta M_d)^{SM}$ . As is seen from fig. 15 for some special values of the MSSM parameters  $(\Delta M_d)^{DP}/(\Delta M_d)^{SM}$  can reach  $\sim \pm 0.2$  but is much smaller in most of the parameter space. The contribution of the box diagrams involving  $H^\pm$  to  $\Delta M_d$  for large  $\tan \beta$  is always negligible compared to the SM and double penguin contributions.

#### 6.1.4 Chargino Box Diagram Contributions

In the scenario considered in [23] and in the present paper supersymmetric particles are heavier than the Higgs bosons and the chargino box contribution  $(\Delta M_s)^{\chi^\pm}$  is small as it is suppressed by  $1/M_{\text{USY}}^2$ . We have checked that in our scan, with all sparticles heavier than 500 GeV, the ratio  $(\Delta M_s)^{\chi^\pm}/(\Delta M_s)^{SM}$  can reach only 0.02 for acceptable values of the  $\overline{B} \rightarrow X_s \gamma$  rate. However, we find some differences with the formulae derived in [27] and we want to devote this subsection to clarify this issue.<sup>8</sup>

<sup>8</sup>P.H.Ch. would like to thank Gino Isidori for the discussion which allowed to identify the source of the discrepancy.

The contributions of box diagrams with chargino exchanges to  $\Delta M_{s,d}$  at large  $\tan\beta$  have been calculated in [23, 27] but only in [27] they have been presented in details. These authors have found that the most important contribution of these diagrams is present in the coefficient  $C_1^{SLL}$  that behaves as  $\overline{m}_t^4 \overline{m}_b^2 \tan^2\beta$  and contributes to  $\Delta M_{s,d}$  with the same sign as the SM contribution. As stressed in [27], if the sparticles are light this contribution could be relevant also for  $\Delta M_d$  due to the absence of the suppression factor  $\overline{m}_d$ . These statements have to be revised, however.

First of all, let us notice that, as follows from the exact formulae for the chargino contributions collected in the Appendix A.4, the Wilson coefficient  $C_2^{SLL}$  in (6.4) has exactly the same dependence on the chargino couplings as does  $C_1^{SLL}$ . In fact, the term in the chargino box amplitude which has that combination of the chargino couplings gives rise to a single scalar left-left operator which, however, has colour indices contracted differently than the operators in the basis (6.5) used also in [27]. Making the Fierz transformation of this operator gives rise to the  $\mathcal{O}_1^{SLL}$  and  $\mathcal{O}_2^{SLL}$  operators with the Wilson coefficients given in the Appendix A.4. The authors of ref. [27] incorrectly identified the scalar left-left operator with wrong contraction of the colour indices with  $\mathcal{O}_1^{SLL}$ . This has the following consequences. Firstly, our  $C_1^{SLL}$  has an additional factor  $-1/2$  which results from the Fierz transformation. This reverses the sign of the contribution of  $C_1^{SLL}$  and decreases it by one half as compared to ref. [27]. Secondly,  $C_2^{SLL} = -(1/4)C_1^{SLL}$  also contributes to the mass difference and further reduces the effects of  $C_1^{SLL}$ . More precisely, using (6.7) and (6.8) the  $\tan^2\beta$  contribution of charginos to (6.6) enters in the combination

$$P_1^{SLL}C_1^{SLL}(\mu_S) + P_2^{SLL}C_2^{SLL}(\mu_S) \approx \frac{1}{2}P_1^{SLL}C_1^{SLL}(\mu_S)$$

where we have used the fact that  $P_2^{SLL} \approx 2P_1^{SLL}$  (see eq. (6.10)). This reduces the  $\tan^2\beta$  contribution of charginos by roughly another 1/2.

Thus, our dominant at large  $\tan\beta$  part of the chargino contribution to  $\Delta M_{s,d}$  is effectively smaller by a factor of approximately 4 compared to the one of ref. [27] and has opposite sign compared to the SM contribution. Neglecting the gauge coupling constants as well as the Yukawa couplings other than top and bottom one gets for the dominant chargino box diagram contribution

$$C_1^{SLL}(\mu_S) = -2 \frac{\overline{m}_b^2 \overline{m}_t^4 A_t^2}{M_W^2 M_{\tilde{t}_1}^4} \frac{\tan^2\beta}{(1 + \tilde{\epsilon}_3 \tan\beta)^2} \sum_{i,j=1}^2 Z_-^{2i} m_{C_i} Z_+^{2i} Z_-^{2j} m_{C_j} Z_+^{2j} \times [D_0(1, 1) - 2D_0(1, 2) + D_0(2, 2)] \quad (6.28)$$

where  $\tilde{t}_1$  is the heavier stop and  $D_0(l, k)$  stands for  $D_0(m_{C_i}, m_{C_j}, M_{\tilde{t}_k}, M_{\tilde{t}_l})$ . The epsilon factor in the denominator appears here in agreement with the rule (3.48). With all these

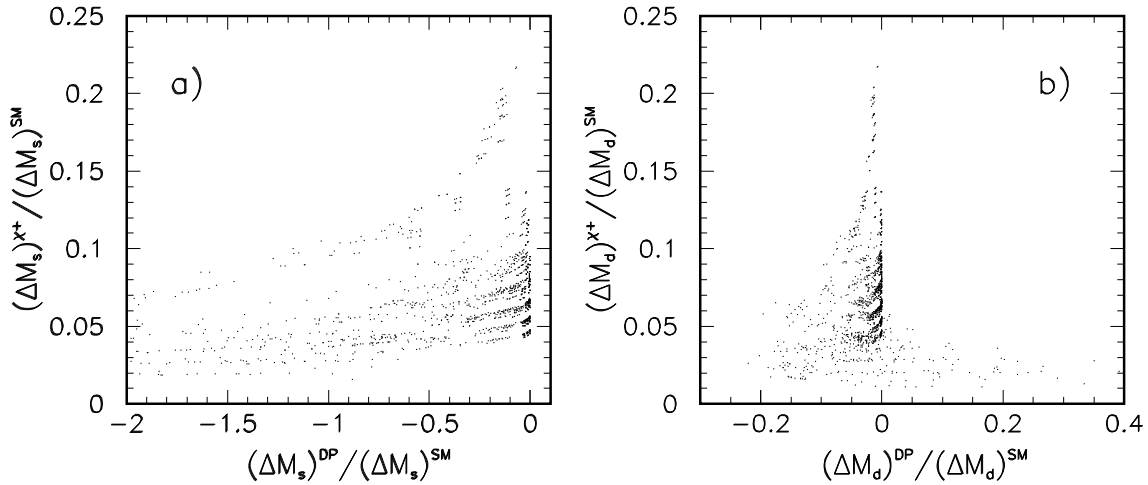


Figure 16: Comparison of the double penguin and chargino box diagram contributions to the ratios  $\Delta M_s/(\Delta M_s)^{\text{SM}}$  (panel a) and  $\Delta M_d/(\Delta M_d)^{\text{SM}}$  (panel b) for  $M_A = 200$  GeV and  $\tan \beta = 50$ . Only points giving acceptable  $BR(\bar{B} \rightarrow X_s \gamma)$  are shown. In this scan we allowed for charginos and stop as light as 100 GeV.

corrections we find that even for  $\tan \beta \sim 50$  the contribution of charginos to  $\Delta M_{s,d}$  is in general dominated by the  $C^{\text{VLL}}$  Wilson coefficient which has the same sign as the SM. Only for very big values of  $A_t$  can the chargino contribution to the Wilson coefficients of the scalar operators compete with the contribution of the standard VLL one.

In figure 16 we show the relative magnitude of the chargino box and double penguin contributions to  $\Delta M_s$  and  $\Delta M_d$  for a scan which included charginos and stop as light as 100 GeV. The biggest contribution of charginos allowed by  $\bar{B} \rightarrow X_s \gamma$  constraint is  $\sim 0.2$  of the SM one. If the  $\bar{B} \rightarrow X_s \gamma$  constraint is relaxed, the ratios  $(\Delta M_s)^{\chi^\pm}/(\Delta M_s)^{\text{SM}}$  and  $(\Delta M_d)^{\chi^\pm}/(\Delta M_d)^{\text{SM}}$  can reach  $\sim 0.3$ . The anti-correlation of the chargino and double penguin contribution is clearly seen in figure 16 (it is even better visible if the points with unacceptable  $BR(\bar{B} \rightarrow X_s \gamma)$  are retained). The reason for it is simple: the biggest double penguin contribution arises for small values of  $(1 + \tilde{\epsilon}_3 \tan \beta)$  when also the contribution the scalar left-left operators generated by boxes is enhanced and cancels the contribution of the  $\mathcal{O}^{\text{VLL}}$  generated by the chargino box diagrams. The biggest total chargino box contribution arises when  $(1 + \tilde{\epsilon}_3 \tan \beta)$  is as big as possible to suppress their negative contribution through the scalar left-left operators. For  $\mu < 0$  this requires  $A_t > 0$  which is incompatible with  $BR(\bar{B} \rightarrow X_s \gamma)$  constraint. For  $\mu > 0$  the biggest values of  $(1 + \tilde{\epsilon}_3 \tan \beta)$  are obtained for  $A_t < 0$  which again leads to unacceptable  $\bar{B} \rightarrow X_s \gamma$  rate. (Cf. the signs

of  $\epsilon_Y$  and  $\epsilon_0$  in eqs. (5.2).)

## 6.2 The $B_{s,d}^0 \rightarrow \mu^+ \mu^-$ Decay

The effective Hamiltonians describing these decays has the form

$$H_{\text{eff}} = -\frac{2G_F}{\sqrt{2}} \frac{\alpha}{2\pi \sin^2 \theta_W} V_{tb}^{\text{eff}*} V_{tq}^{\text{eff}} [c_A \mathcal{O}_A + c'_A \mathcal{O}'_A + c_S \mathcal{O}_S + c'_S \mathcal{O}'_S + c_P \mathcal{O}_P + c'_P \mathcal{O}'_P], \quad (6.29)$$

where  $q = s$  or  $d$  and

$$\mathcal{O}_A = (\bar{b}_L \gamma^\mu q_L) (\bar{l} \gamma_\mu \gamma_5 l), \quad \mathcal{O}'_A = (\bar{b}_R \gamma^\mu q_R) (\bar{l} \gamma_\mu \gamma_5 l), \quad (6.30)$$

$$\mathcal{O}_S = m_b (\bar{b}_R q_L) (\bar{l} l), \quad \mathcal{O}'_S = m_q (\bar{b}_L q_R) (\bar{l} l), \quad (6.31)$$

$$\mathcal{O}_P = m_b (\bar{b}_R q_L) (\bar{l} \gamma_5 l), \quad \mathcal{O}'_P = m_q (\bar{b}_L q_R) (\bar{l} \gamma_5 l). \quad (6.32)$$

For large  $\tan \beta$  the contributions from neutral Higgs scalars dominate. Using the Lagrangian (2.33) for the  $q = s$  case and neglecting  $m_s$  with respect to  $m_b$  we find

$$\mathcal{H}_{\text{eff}} = \frac{G_F}{\sqrt{2}} \frac{4\pi\alpha}{M_W^2 \sin^2 \theta_W} m_\mu V_{tb}^{\text{eff}*} V_{tq}^{\text{eff}} \sum_{S=h^0, H^0, A^0} \frac{1}{M_S^2} \left( \bar{b}_R [\bar{X}_{RL}^S]^{bs} s_L \right) (\bar{l} [Z^S] l) \quad (6.33)$$

with the reduced coupling  $[\bar{X}_{RL}^S]^{bs}$  defined in (6.13) and

$$[Z^{H^0}] = -\frac{\cos \alpha}{\cos \beta}, \quad [Z^{h^0}] = \frac{\sin \alpha}{\cos \beta}, \quad [Z^{A^0}] = i \tan \beta \gamma_5. \quad (6.34)$$

Comparing (6.33) with (6.29) and using (6.14) we find

$$c_S \approx \frac{m_\mu \bar{m}_t^2}{4M_W^2} \frac{16\pi^2 \epsilon_Y \tan^3 \beta}{(1 + \tilde{\epsilon}_3 \tan \beta)(1 + \epsilon_0 \tan \beta)} \left[ \frac{\sin(\alpha - \beta) \cos \alpha}{M_{H^0}^2} - \frac{\cos(\alpha - \beta) \sin \alpha}{M_{h^0}^2} \right]. \quad (6.35)$$

$$c_P \approx -\frac{m_\mu \bar{m}_t^2}{4M_W^2} \frac{16\pi^2 \epsilon_Y \tan^3 \beta}{(1 + \tilde{\epsilon}_3 \tan \beta)(1 + \epsilon_0 \tan \beta)} \left[ \frac{1}{M_{A^0}^2} \right]. \quad (6.36)$$

The contributions of the operators  $\mathcal{O}'_S$  and  $\mathcal{O}'_P$  are strongly suppressed by  $m_s$  with respect to  $\mathcal{O}_S$  and  $\mathcal{O}_P$ . Consequently following [43] we can write to an excellent approximation

$$\begin{aligned} BR(B_s \rightarrow \mu^+ \mu^-) &= 2.32 \times 10^{-6} \left[ \frac{\tau_{B_s}}{1.5 \text{ ps}} \right] \left[ \frac{F_{B_s}}{230 \text{ MeV}} \right]^2 \left[ \frac{|V_{ts}|}{0.040} \right]^2 \\ &\times \left[ |\tilde{c}_S|^2 + |\tilde{c}_P + 0.04(c_A - c'_A)|^2 \right] \end{aligned} \quad (6.37)$$

where  $\tilde{c}_S$  and  $\tilde{c}_P$  are the dimensionless Wilson coefficients

$$\tilde{c}_S = M_{B_s} c_S, \quad \tilde{c}_P = M_{B_s} c_P. \quad (6.38)$$

The coefficients  $c_A$  and  $c'_A$  receive contributions from  $Z^0$ -penguin diagrams and box diagrams and are weighted by the muon mass. For large  $\tan\beta$  they can be safely neglected with respect to  $\tilde{c}_S$  and  $\tilde{c}_P$  that grow like  $\tan^3\beta$  and are not chirally suppressed by the muon mass.

In the large  $\tan\beta$  limit the contribution of  $h^0$  to  $c_S$  can be neglected and setting  $M_{H^0}^2 \approx M_{A^0}^2$  we find from (6.35) and (6.36)

$$c_S = c_P \quad (6.39)$$

with  $c_P$  given in (6.36). Consequently we find the branching ratio

$$\begin{aligned} BR(B_s \rightarrow \mu^+ \mu^-) &= 3.5 \times 10^{-5} \left[ \frac{\tan\beta}{50} \right]^6 \left[ \frac{\tau_{B_s}}{1.5 \text{ ps}} \right] \left[ \frac{F_{B_s}}{230 \text{ MeV}} \right]^2 \left[ \frac{|V_{ts}|}{0.040} \right]^2 \\ &\times \frac{\bar{m}_t^4}{M_A^4} \frac{(16\pi^2 \epsilon_Y)^2}{(1 + \tilde{\epsilon}_3 \tan\beta)^2 (1 + \epsilon_0 \tan\beta)^2}. \end{aligned} \quad (6.40)$$

This result agrees with [27]. Moreover one has

$$\frac{BR(B_d^0 \rightarrow \mu^+ \mu^-)}{BR(B_s^0 \rightarrow \mu^+ \mu^-)} = \left[ \frac{\tau_{B_d}}{\tau_{B_s}} \right] \left[ \frac{F_{B_d}}{F_{B_s}} \right]^2 \left[ \frac{|V_{td}^{\text{eff}}|}{|V_{ts}^{\text{eff}}|} \right]^2 \left[ \frac{M_{B_d}}{M_{B_s}} \right]^5 \quad (6.41)$$

that is, the ratio of the branching fractions can depend on the SUSY parameters only weakly through  $|V_{td}^{\text{eff}}/V_{ts}^{\text{eff}}|$  which should be consistently determined from the unitarity triangle analysis.

The presence of additional  $\tan\beta$  dependence in the denominators of eqs. (6.25) and (6.40), not included in [23] and [20, 6, 22, 21], has been pointed out in [27]. While we confirm these additional factors, we would like to emphasize that depending on the sign of the supersymmetric parameter  $\mu$  they can suppress  $\Delta M_s^{DP}$  and  $BR(B_s^0 \rightarrow \mu^+ \mu^-)$  relative to the estimates in the papers in question, as stressed in [27], but can also provide additional enhancements.

### 6.3 Correlation between $B_{s,d}^0 \rightarrow \mu^+ \mu^-$ and $\Delta M_s^{DP}$

We are now in the position to give an explicit formula for a correlation between the neutral Higgs contributions to  $B_s^0 \rightarrow \mu^+ \mu^-$  and  $\Delta M_s^{DP}$  that we have pointed out in [23, 29]. Indeed from (6.25) and (6.40) we find

$$BR(B_s^0 \rightarrow \mu^+ \mu^-) = \kappa 10^{-6} \left[ \frac{\tan\beta}{50} \right]^2 \left[ \frac{200 \text{ GeV}}{M_{A^0}} \right]^2 \left[ \frac{|\Delta M_s^{DP}|}{2.12/\text{ps}} \right] \quad (6.42)$$



where

$$\kappa = \left[ \frac{2.50}{F_2^{LR}} \right] \left[ \frac{3.0\text{GeV}}{\overline{m}_b(\mu_S)} \right] \left[ \frac{0.06\text{GeV}}{\overline{m}_s(\mu_S)} \right] \left[ \frac{\tau_{B_s}}{1.5 \text{ ps}} \right] \approx 1. \quad (6.43)$$

This relation depends sensitively on  $M_{A^0}$  and  $\tan\beta$  but it does not depend on  $\epsilon_0$  and  $\tilde{\epsilon}_3$ . From (6.41) a similar correlation between  $BR(B_d^0 \rightarrow \mu^+\mu^-)$  and  $\Delta M_s^{DP}$  follows. If the flavour dependence in the epsilon parameters is taken into account as in section 3.6 and formulae (3.55) and (3.56) are used, the r.h.s of (6.42) is multiplied by the factor  $\epsilon^{(32)}/(\epsilon^{(23)}r_{32})$  which, however, does not depart significantly from unity. In our numerical analysis of section 7 we use the formulae of the full approach anyway.

In order to understand these results better, let us now assume that  $\Delta M_s$  has been measured and that appropriate supersymmetric parameters can be found for which the MSSM considered here agrees with  $(\Delta M_s)^{\text{exp}}$ . If  $0 < (1 + f_s) < 1$  this implies  $(\Delta M_s)^{\text{exp}} < (\Delta M_s)^{\text{SM}}$ . Then combining (6.3) and (6.42) we find [29]

$$\begin{aligned} BR(B_s^0 \rightarrow \mu^+\mu^-) &= 8.5 \cdot 10^{-6} \kappa \left[ \frac{\tan\beta}{50} \right]^2 \left[ \frac{200\text{GeV}}{M_{A^0}} \right]^2 \left[ \frac{(\Delta M_s)^{\text{SM}}}{18.0/\text{ps}} \right] \\ &\times \left[ 1 \mp \frac{(\Delta M_s)^{\text{exp}}}{(\Delta M_s)^{\text{SM}}} - \frac{|(\Delta M_s)^{H^\pm}|}{(\Delta M_s)^{\text{SM}}} + \frac{(\Delta M_s)^{\chi^\pm}}{(\Delta M_s)^{\text{SM}}} \right]. \end{aligned} \quad (6.44)$$

with “ $\mp$ ” corresponding to  $0 < (1 + f_s) < 1$  and  $(1 + f_s) < 0$ , respectively. Using (6.41) analogous expression for  $BR(B_d^0 \rightarrow \mu^+\mu^-)$  can be found. In writing (6.44) we have taken into account that  $(\Delta M_s)^{\text{DP}}$  is always negative and that for large  $\tan\beta$   $(\Delta M_s)^{H^\pm}$  is negative and  $(\Delta M_s)^{\chi^\pm}$  mostly positive. Formula (6.44) is valid provided the expression in square brackets is positive and larger than  $10^{-3}$ . Otherwise, other contributions, in particular those coming from  $Z^0$ -penguins have to be taken into account. In our numerical analysis we take them into account anyway.

Formula (6.44) demonstrates very clearly that if  $(\Delta M_s)^{\text{exp}}$  will turn out to be close or larger than the SM value, the order of magnitude enhancements of  $BR(B_{s,d}^0 \rightarrow \mu^+\mu^-)$  in the scenario of the MSSM considered here with  $0 < (1 + f_s) < 1$  will be excluded. On the other hand large enhancements of  $BR(B_{s,d}^0 \rightarrow \mu^+\mu^-)$  are in principle still possible if the double-penguin contribution is so large that  $(1 + f_s) < 0$  and the “+” sign in (6.44) applies. For  $\tan\beta < 50$  obtaining  $(1 + f_s) < 0$  and the right magnitude of  $\Delta M_s$  requires  $\mu < 0$  so that the couplings (3.26) are enhanced by the  $\epsilon$ -factors in the denominator.  $\mu < 0$  is excluded in particular scenarios like minimal SUGRA, in which the sign of  $A_t$  is fixed and  $\mu < 0$  does not allow for satisfying the  $\bar{B} \rightarrow X_s\gamma$  constraint [26], but cannot be excluded in general.

We will analyze (6.44) numerically in detail in section 7.3.

## 6.4 Unitarity Triangle

The rate of the  $B_d^0 \rightarrow \mu^+ \mu^-$  decay depends on the element  $V_{td}^{\text{eff}}$  of the low energy CKM matrix. The value of  $V_{td}^{\text{eff}}$  cannot be extracted by using exclusively tree level dominated processes and requires an analysis of the combination of data on  $|V_{ub}^{\text{eff}}/V_{cb}^{\text{eff}}|$ ,  $\sin 2\beta_{\text{ut}}$  from the CP asymmetry  $a_{\psi K_S}$ ,  $\varepsilon_K$ ,  $\Delta M_d$  and  $\Delta M_s$  (the so-called UT analysis). While in the scenario of the MSSM we are considering the extraction of the first two quantities from the data is not affected by the new particles,  $\varepsilon_K$ ,  $\Delta M_d$  and  $\Delta M_s$  receive additional contributions which can modify the extracted value of  $V_{td}^{\text{eff}}$ . The unitarity triangle in the MSSM with large  $\tan \beta$  has been discussed in refs. [23, 7]. Here we recall this discussion briefly and outline the procedure we use in sec. 7.3 in order to consistently determine  $V_{td}^{\text{eff}}$  for a given set of the MSSM parameters.

Let us first recall that the contribution of the new particles enter  $\varepsilon_K$ ,  $\Delta M_d$  and  $\Delta M_s$  through the factors

$$F_{tt}^\varepsilon = S_0(x_t)[1 + f_\varepsilon], \quad F_{tt}^d = S_0(x_t)[1 + f_d], \quad F_{tt}^s = S_0(x_t)[1 + f_s] \quad (6.45)$$

respectively where  $S_0(x_t)$  is the universal contribution of the SM particles.  $F_{tt}^s$  is explicitly given in eq. (6.7). The hierarchy of the new contributions to the parameters  $f_i$  is then as follows:

- The contributions to  $f_\varepsilon$  at large  $\tan \beta$  generated by the diagrams similar to the ones shown in figure 14 are fully negligible being strongly suppressed by  $\overline{m}_s \overline{m}_d$ ,  $\overline{m}_s^2$  and higher order terms in  $\overline{m}_{d,s}$ . Also the charged Higgs and chargino box diagram contributions are known to be negligible for  $\tan \beta \gg 1$ . Consequently  $f_\varepsilon$  can be set to zero and the constraint on the UT stemming from  $\varepsilon_K$  is the same as in the SM.
- The double penguin and charged Higgs boson contributions to  $\Delta M_d$  are proportional to  $\overline{m}_d \overline{m}_b \tan^4 \beta$  and  $\overline{m}_d \overline{m}_b \tan^2 \beta$ , respectively [23, 27]. Detailed calculation shows that  $|f_d|$  is at least one order of magnitude smaller than  $|f_s|$ . The latter, in the most likely scenario with  $0 < 1 + f_s < 1$ , is in turn bounded by  $(\Delta M_s)_{\text{exp}}$  to be smaller than 0.5 [23]. Consequently  $|f_d| \lesssim 0.05$  and can be safely neglected in view of the uncertainties in  $F_{B_d} \sqrt{\hat{B}_{B_d}}$ . In the unlikely scenario in which  $1 + f_s < 0$  and  $|f_s| > 1.5$ ,  $|f_d|$  could reach 0.2 and having negative sign would suppress  $\Delta M_d$  relative to the SM prediction. For fixed  $F_{B_d} \sqrt{\hat{B}_{B_d}}$  and  $(\Delta M_d)_{\text{exp}}$ , this would imply a larger  $|V_{td}^{\text{eff}}|$ .
- The new contributions to  $f_s$  can be substantial [23, 29]. They will be investigated numerically in detail in section 7 using the approach developed in sec. 2 which takes into account the resummation of leading higher order terms pointed out in [27]. In our

scenario  $f_s$  is always negative and suppresses  $\Delta M_s$  with respect to the expectations based on the SM.

In order to determine the impact of  $f_s \neq 0$  on the determination of  $|V_{td}^{\text{eff}}|$  let us recall that

$$\Delta M_d \propto F_{B_d}^2 \hat{B}_{B_d} |V_{td}^{\text{eff}}|^2 S_0(x_t) \quad (6.46)$$

$$\Delta M_s \propto F_{B_s}^2 \hat{B}_{B_s} |V_{ts}^{\text{eff}}|^2 S_0(x_t) |1 + f_s| \quad (6.47)$$

and

$$|V_{td}^{\text{eff}}| \propto \xi \sqrt{\frac{\Delta M_d}{\Delta M_s}} \sqrt{|1 + f_s|}, \quad \text{where} \quad \xi = \frac{F_{B_s} \sqrt{\hat{B}_{B_s}}}{F_{B_d} \sqrt{\hat{B}_{B_d}}} \quad (6.48)$$

Exact expressions can be found in [23, 37].

If the value of  $F_{B_d}^2 \hat{B}_{B_d}$  was known precisely  $|V_{td}^{\text{eff}}|$  could be determined directly from eq. (6.46) and the value of  $f_s$  would not have any impact on it. In our scenario  $|V_{td}^{\text{eff}}|$  would then assume the same value as in the SM. Since  $|V_{ts}^{\text{eff}}|$  is almost fixed by the unitarity of CKM matrix the eq. (6.47) would then only provide a constraint on the MSSM parameters space, the more stringent, the smaller was the uncertainty in  $F_{B_s}^2 \hat{B}_{B_s}$  [23]. In other words, a precise value of  $F_{B_s}^2 \hat{B}_{B_s}$  combined with a precise measurement of  $\Delta M_s$  could directly probe by means of the formula (6.47) the value of  $|1 + f_s|$ .

At present, however,  $F_{B_d}^2 \hat{B}_{B_d}$  (and also  $F_{B_s}^2 \hat{B}_{B_s}$ ) is poorly known and a more precise value of  $|V_{td}^{\text{eff}}|$  is obtained by using the relation (6.48) in which  $\xi$ , calculated by QCD sum rules or lattice methods that are insensitive to new short distance contributions, is known with much better accuracy than are  $F_{B_d}^2 \hat{B}_{B_d}$  and  $F_{B_s}^2 \hat{B}_{B_s}$  separately. This means that  $F_{B_d}^2 \hat{B}_{B_d}$  and  $F_{B_s}^2 \hat{B}_{B_s}$  are positively correlated and cannot simultaneously assume values from the opposite extremes of their respective allowed ranges. Therefore, as seen in (6.48)  $0 < 1 + f_s < 1$  leads to a smaller value of  $|V_{td}^{\text{eff}}|$  and smaller angle  $\gamma$  than does  $f_s = 0$ . For example, if the value of  $\Delta M_s$  is close to its present experimental bound,  $|1 + f_s| \approx 0.6$  gives  $|V_{td}^{\text{eff}}| \approx 7 \times 10^{-3}$ . This can be also viewed as follows: for a given experimental value of  $\Delta M_s$ , the factor  $F_{B_s}^2 \hat{B}_{B_s}$  must be larger if  $0 < |1 + f_s| < 1$  than if  $f_s = 0$ . With  $\xi$  fixed, this means that also  $F_{B_d}^2 \hat{B}_{B_d}$  must be larger implying a smaller value of  $|V_{td}^{\text{eff}}|$  and of the angle  $\gamma$ . Similarly,  $1 + f_s < 0$  leads to bigger  $|V_{td}^{\text{eff}}|$  and bigger  $\gamma$  provided  $|1 + f_s| > 1$ . For example if  $1 + f_s \approx -1.3$  one has  $|V_{td}^{\text{eff}}| \approx 1 \times 10^{-2}$  [7].

In our global scans in sec. 7 we proceed as in [29, 7]: For a given set of the MSSM parameters we scan over the Wolfenstein parameters  $\lambda$ ,  $A$ ,  $\bar{\rho}$  and  $\bar{\eta}$  which parametrize  $V^{\text{eff}}$  (see e.g.[37]) as well as over the non-perturbative parameters  $F_{B_d}^2 \hat{B}_{B_d}$  and  $F_{B_s}^2 \hat{B}_{B_s}$  in their respective ranges specified in ref. [44] and compute the quantities of interest only for those  $\lambda$ ,  $A$ ,  $\bar{\rho}$  and  $\bar{\eta}$  for which  $\varepsilon_K$ ,  $\Delta M_d$ ,  $a_{\psi K_S} = \sin 2\beta_{\text{ut}}$ ,  $|V_{ub}^{\text{eff}}/V_{cb}^{\text{eff}}|$  and  $\xi$  assume

acceptable values. This allows to take into account in  $BR(B_d^0 \rightarrow \mu^+ \mu^-)$  also the small effects related to the dependence of  $|V_{td}^{\text{eff}}|$  on the supersymmetric parameters.

## 6.5 $\bar{B} \rightarrow X_s \gamma$

Finally we recall certain aspects of the  $BR(\bar{B} \rightarrow X_s \gamma)$  calculation referring frequently to the formulae present in the literature. We would like to present for completeness simple recipes allowing to use the corrections  $\epsilon^{HL}$  etc. introduced in sec. 2 in the existing formulae for the relevant Wilson coefficients. We also show how to include the recently found correction depending on the neutral Higgs boson masses [28] and on the couplings  $[X_{LR}]^{JI}$  in these formulae.

As far as the SM part of the computation is concerned, we closely follow the approach of ref. [45]. The two loop contribution of  $H^+$  is taken from ref. [46] (see also [47]). As in ref. [25], for our scenario with heavy sparticles we include only one loop contribution of the supersymmetric particles as given in refs. [48, 33].

### 6.5.1 Charged Goldstone and $H^+$ Contributions

In order to see how to include our corrections in the calculation of the  $\bar{B} \rightarrow X_s \gamma$  rate let us recall that at large  $\tan \beta$  the one-loop contributions of  $G^+(H^+)$  to the Wilson coefficients  $C_{7(8)}^{(0)}$  are proportional to the product of the  $\bar{t}_L G^+(H^+) b_R$  vertex and the Hermitian conjugate of the  $\bar{t}_R G^+(H^+) s_L$  vertex. Neglecting the contributions originating in the chiral flip on the external  $b$  quark line and not including yet the large  $\tan \beta$  enhanced corrections one has

$$C_{7(8)}^{(G^\pm)} = -F_{7(8)}^{(2)}(x_t), \quad C_{7(8)}^{(H^\pm)} = F_{7(8)}^{(2)}(y_t). \quad (6.49)$$

Here  $x_t = \bar{m}_t^2/M_W^2$ ,  $y_t = \bar{m}_t^2/M_{H^+}^2$ . Combining the  $G^+$  and  $W^+$  contributions results in replacing  $-F_{7(8)}^{(2)}(x_t)$  by  $F_{7(8)}^{(1)}(x_t)$ . The explicit expressions for  $F_{7(8)}^{(1)}(x_t)$  and  $F_{7(8)}^{(2)}(x_t)$  can be found in [25].

Let us consider the  $G^+$  contribution first. As we have demonstrated in sec. 3, in the  $SU(2) \times U(1)$  symmetry limit  $\epsilon_{JI}^{GL} = \epsilon_{JI}^{GR} = 0$  and the couplings of  $G^+$  have the same form (3.38) as in the SM. This means that in the  $SU(2) \times U(1)$  symmetry limit this contribution is correctly accounted for in the SM contribution to  $C_{7(8)}^{(0)}$ . Small departures of  $\epsilon_{JI}^{GR}$  and  $\epsilon_{JI}^{GL}$  from zero which arise beyond this approximation can be also included but our numerical studies of sec. 5 show that they are too small to have any impact on the  $\bar{B} \rightarrow X_s \gamma$  rate. Nevertheless, we can include them by noting that the full contribution  $G^+$  to the Wilson coefficients is

$$C_{7(8)}^{(G^+)} = -(1 + \epsilon_{ts}^{GL})(1 + \epsilon_{tb}^{GR})F_{7(8)}^{(2)}(x_t). \quad (6.50)$$

As for  $\epsilon_{ts}^{GL} = \epsilon_{tb}^{GR} = 0$  this contribution is taken already into account in the SM contribution, one has only to modify  $C_{7(8)}^{(G^+)}$  by

$$\delta^{G^+} C_{7(8)}^{(0)} = -(\epsilon_{tb}^{GR} + \epsilon_{ts}^{GL} + \epsilon_{tb}^{GR} \epsilon_{ts}^{GL}) F_{7(8)}^{(2)}(x_t) \approx -(\epsilon_{tb}^{GR} + \epsilon_{ts}^{GL}) F_{7(8)}^{(2)}(x_t) \quad (6.51)$$

where we have neglected the higher order term. The prescription (6.51) replaces in our approach the recipe given in eq. (18) of ref. [25]. It formally agrees with the latter if one drops  $\epsilon_{ts}^{GL}$  not considered in [25] and identifies  $V_{ts}$  in the  $\bar{t}_R G^+ s_L$  vertex used in [25] with  $V_{ts}^{\text{eff}}$  (see our discussion in section 4) and recalls that  $V_{tb} = V_{tb}^{\text{eff}}$ . Using then the substitution rule (4.4) in the opposite direction one finds

$$-\epsilon_{tb}^{GR} \rightarrow 1 - \frac{1 + \epsilon'_b(t) \tan \beta}{1 + \epsilon_b \tan \beta} = \frac{[\epsilon_b - \epsilon'_b(t)] \tan \beta}{1 + \epsilon_b \tan \beta} \quad (6.52)$$

as in eq. (18) of [25]. We have stressed however, that one has to be careful in evaluating the corrections  $\epsilon_{tb}^{GR}$  and  $\epsilon_{ts}^{GL}$ , because uncontrolled approximation can result in overestimating their impact on the  $\bar{B} \rightarrow X_s \gamma$  rate.

In the case of  $H^+$  contribution, the formula analogous to (6.50) reads

$$C_{7(8)}^{(H^+)} = (1 - \epsilon_{ts}^{HL}) (1 - \epsilon_{tb}^{HR}) F_{7(8)}^{(2)}(y_t). \quad (6.53)$$

In the approximation of section 3, using eqs. (3.43) and (3.47), we have:

$$(1 - \epsilon_{ts}^{HL}) (1 - \epsilon_{tb}^{HR}) = \frac{1}{1 + \tilde{\epsilon}_3 \tan \beta} \left[ 1 - \epsilon'_0 \tan \beta + y_b^2 y_t^2 \frac{\epsilon_Y \epsilon'_Y \tan^2 \beta}{1 + \epsilon_0 \tan \beta} \right] \quad (6.54)$$

in agreement with the factor multiplying  $F_{7(8)}^{(2)}(y_t)$  in the formula (87) of [28]. However as shown in section 5, the approximation (3.44) is not numerically very accurate and better approximation is obtained by using for  $\epsilon_{ts}^{HL}$  eq. (5.8) with  $J = 3$ ,  $I = 2$  and  $\epsilon_{tb}^{HR} = \tilde{\epsilon}_3 \tan \beta / (1 + \tan \beta)$  obtained from (3.59) with  $\tilde{\epsilon}_3$  calculated by means of (5.1). Thus, the effect of corrections to the charged Higgs boson vertices results in the following modification of the Wilson coefficients  $C_{7(8)}^{(0)}$ :

$$\delta^{H^+} C_{7(8)}^{(0)} = (-\epsilon_{ts}^{HL} - \epsilon_{tb}^{HR} + \epsilon_{ts}^{HL} \epsilon_{tb}^{HR}) F_{7(8)}^{(2)}(y_t). \quad (6.55)$$

Sticking to the naive approximation of sec. 3 with the  $\Delta_{JI}$  term in (3.43) neglected, i.e. inserting in (6.55)

$$\epsilon_{ts}^{HL} = \epsilon'_t(s) \tan \beta, \quad \epsilon_{tb}^{HR} = \frac{\epsilon_b \tan \beta}{1 + \epsilon_b \tan \beta} \quad (6.56)$$

one recovers the rule (19) of ref. [25] if, in agreement with our discussion of sec. 4, one identifies  $V_{ts}$  with  $V_{ts}^{\text{eff}}$  in the  $\bar{t}_R H^+ s_L$  vertex of [25].

### 6.5.2 Chargino Contributions

The inclusion of the  $\tan\beta$  enhanced corrections in the chargino contributions to Wilson coefficients of higher dimensional operators involving down quark fields of arbitrary flavour is achieved by means of the rules (2.53) and (2.54) or (3.48). For the couplings  $\tilde{t}^\dagger c_L^i s_L$  (2.53) amounts simply to the replacements

$$m_t \rightarrow \overline{m}_t, \quad V_{ts} \rightarrow V_{ts}^{\text{eff}}. \quad (6.57)$$

For the couplings  $\tilde{t}^\dagger c_R^i b_R$  the rule (2.54) or (3.48) applies implying

$$V_{tb} m_b \rightarrow V_{tb}^{\text{eff}} \frac{\overline{m}_b}{1 + \tilde{\epsilon}_3 \tan\beta}. \quad (6.58)$$

where following the refinements of sec. 5  $\tilde{\epsilon}_3 \equiv \epsilon_0^{(3)} + y_t^2 \epsilon_Y^{(33)}$ . This is accidentally equivalent to expressing in the tree level formulae simply  $V_{tb}$  and  $m_b$  through  $V_{tb}^{\text{eff}}$  and  $\overline{m}_b$ , respectively. The formula (30) of ref. [25] with  $\epsilon_b = \epsilon_{d_3} \equiv \epsilon_0^{(3)} + y_t^2 \epsilon_Y^{(33)}$  is consistent with this rule provided  $V_{ts}$  and  $V_{tb}$  in this formula are identified with the effective CKM elements.

On the other hand for the Wilson coefficient of the  $m_s/m_b$  suppressed operator  $m_s \bar{s}_R \sigma^{\mu\nu} b_L$  the situation is more involved as our rules imply

$$m_t \rightarrow \overline{m}_t, \quad V_{tb} \rightarrow V_{tb}^{\text{eff}} \quad (6.59)$$

for the vertex involving the  $b_L$  quark and

$$V_{ts} m_s \rightarrow V_{ts}^{\text{eff}} \frac{\overline{m}_s}{1 + \tilde{\epsilon}_3 \tan\beta}, \quad (6.60)$$

for the vertex involving the  $s_R$  quark. If the flavour dependent effects are important  $1/(1 + \tilde{\epsilon}_3 \tan\beta)$  in (6.60) should be replaced by the square bracket of the formula (3.61) with  $I = 2$ . Note that expressing in the tree level formulae simply  $V_{ts}$  and  $m_s$  through  $V_{ts}^{\text{eff}}$  and  $\overline{m}_s$ , respectively would give wrong  $\tan\beta$  dependence.

### 6.5.3 Neutral Higgs boson contribution

For completeness we include the neutral Higgs contribution to the Wilson coefficients found in ref. [28]. It is the natural consequence of the flavour changing neutral Higgs coupling  $[X_{LR}]^{23}$  which, through the diagram shown in figure 17, leads to the contribution [28]

$$\begin{aligned} \delta^{H^0} C_{7(8)}^{(0)} &= \frac{1}{18} \frac{M_W^2}{g_2^2} \sum_{S=A^0, H^0, h^0} [X_{LR}^S]^{23} [X^S]^{33} \frac{\overline{m}_b^2}{M_S^2} \\ &\approx -\frac{1}{36} \frac{\epsilon_Y y_t^2 \tan^3 \beta}{(1 + \epsilon_0 \tan\beta)(1 + \tilde{\epsilon}_3 \tan\beta)^2} \frac{\overline{m}_b^2}{M_A^2} \end{aligned} \quad (6.61)$$

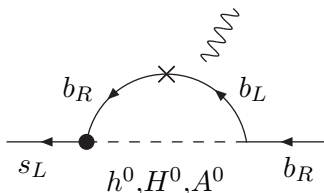


Figure 17: Additional diagram contributing to  $b \rightarrow s\gamma$  or  $b \rightarrow sg$  transition. The dot and the cross denote the flavour changing coupling  $[X_{LR}]^{sb}$  and the helicity flip, respectively.

where  $[X^S]^{33}$  and  $[X_{LR}^S]^{23}$  are given in eqs. (3.22) and (3.27), respectively.

The last comment concerns the dependence of the  $\bar{B} \rightarrow X_s\gamma$  amplitude on the CKM matrix elements. In our scans presented in sec. 7 for a given set of the MSSM parameters we use the value of  $|V_{ts}^{\text{eff}*}V_{tb}^{\text{eff}}|$  determined consistently from the UT analysis as described in the preceding subsection. We do not need therefore to implement the recipe of ref. [33] for correcting the  $\bar{B} \rightarrow X_s\gamma$  amplitude for new physics effects in  $V_{ts}^{\text{eff}}$ .

## 7 Numerical Analysis

In this section we present numerical analysis of the dependence of  $\Delta M_{d,s}$  and  $B_{s,d}^0 \rightarrow \mu^+\mu^-$  on the parameters of the MSSM. We will also present the global analysis of these quantities taking into account available experimental constraints, in particular the one from the measured rate of the  $B \rightarrow X_s\gamma$  decay. We present the results based on our complete approach of section 2 which includes automatically the  $SU(2) \times U(1)$  breaking corrections as well as the dependence of the flavour changing couplings on the electroweak gauge couplings. On some plots we compare these results with the one obtained by using the approximation of sec. 3 based on  $SU(2) \times U(1)$  limit and dominance of  $\alpha_s$  and the top and bottom Yukawa couplings. The latter describe qualitatively the main features of the MSSM effects but are not very accurate.

### 7.1 The Size of $f_s$ and $f_d$

The parameters  $f_s$  and  $f_d$  introduced in eq. (6.3) and directly related to the ratio  $\Delta M_{s,d}/(\Delta M_{s,d})^{\text{SM}}$ :

$$\Delta M_{s,d}/(\Delta M_{s,d})^{\text{SM}} \equiv |1 + f_{s,d}|$$

receive contributions from double penguins, charged Higgs boson box diagrams and chargino box diagrams. As we have already said in sec. 6.1.4, for sparticles heavier than 500 GeV

the latter contributions can be safely neglected. We have also shown in sec. 6.1.3 that for large  $\tan\beta$  the contribution of the  $H^\pm$  box diagrams to  $f_s$  is negative and can give up to  $\delta^H f_s \approx -0.1$  for  $\mu > 0$  and up to  $\delta^H f_s \approx -0.2$  for  $\mu < 0$ . Except for very small values of the  $A_t$  parameter, for which the double penguin diagram contribution is small, the charged Higgs boson box diagram contributions are much smaller than the latter one and do not play any role in the correlation between  $\Delta M_s$  and  $BR(B_{s,d}^0 \rightarrow \mu^+ \mu^-)$ . The contribution of the charged Higgs boson box diagrams to  $f_d$  is negligible  $-0.02 < \delta^H f_d < 0$  whereas the contribution of the double penguin diagrams to  $f_d$  can be of either sign and for very special values of the parameters can reach  $|\delta^{\text{DP}} f_d| \approx 0.2$ .

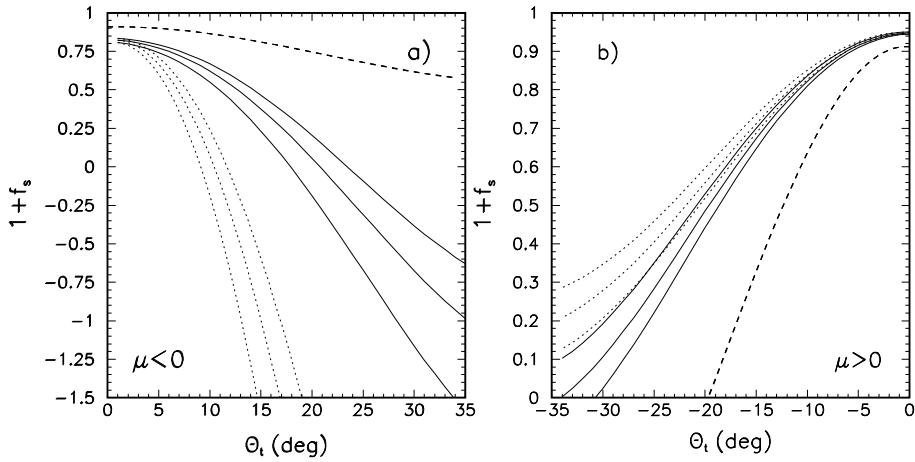


Figure 18:  $(1 + f_s)$  in the MSSM for  $\tan\beta = 50$ ,  $M_{H^\pm} = 200$  GeV,  $m_{\tilde{g}} = 3M_2$ ,  $M_{\tilde{b}_R} = 800$  GeV and the lighter chargino mass 600 GeV as a function of the stop mixing angle  $\theta_t$ . In panel a)  $\mu < 0$  and  $M_{\tilde{t}_1} = 600$  GeV,  $M_{\tilde{t}_2} = 750$  GeV. In panel b)  $\mu > 0$  and  $M_{\tilde{t}_1} = 500$  GeV,  $M_{\tilde{t}_2} = 850$  GeV. Solid lines correspond to the complete calculation. Dotted ones - to the approximation based on the formulae of sec. 6.1.2 and the dashed lines to the calculation without the resummation of the  $\tan\beta$  enhanced terms. Consecutive solid and dotted lines correspond to  $M_2/|\mu| = 3/4, 1$  and  $5/4$  counting from left to right (in both panels). The results without the resummation do not depend in a visible way on  $M_2/|\mu|$ .

In figs. 18 and 19 we show the factor  $(1 + f_s)$  as a function of the parameters to which its value is most sensitive, that is  $M_{H^\pm}$ ,  $\tan\beta$  and the mixing angle of the top squarks  $\theta_t$ . The sign of the latter is always such that  $\mu A_t$  is positive, allowing for the cancellation of the charged Higgs boson and chargino contributions to the amplitude of the  $\bar{B} \rightarrow X_s \gamma$  decay.

Strong dependence of the double penguin contribution to  $f_s$  on the left-right mixing



of the top squarks is clearly visible in fig. 18 where we show  $1 + f_s$  as a function of the stop mixing angle  $\theta_t$ . As expected from our considerations of sec. 5, for  $\mu < 0$  ( $\mu > 0$ ) the resummation of the  $\tan\beta$  enhanced terms leads to dramatic increase (decrease [27]) of  $|f_s|$  due to the appearance of the factors  $(1 + \tilde{\epsilon}_3 \tan\beta)(1 + \epsilon_0 \tan\beta)$  in the denominators in eqs. (6.20), (6.21) as compared to the formulae (4.11) of ref. [23]. Curves for different values of the ratio  $M_2/|\mu|$  in fig. 18 illustrate the impact of the heavier chargino. Indeed, for shown values of  $M_2/|\mu|$  the lighter chargino is always almost higgsino-like and to an accuracy of few GeV,  $m_{C_1} \approx |\mu|$ . (Without the resummation, the lines corresponding to different values of  $M_2/|\mu|$  are indistinguishable on the plot.)

Dotted lines in fig. 18 have been obtained by using the formulae (6.20)-(6.22) and correspond to the approximation of sec. 3.3. We observe that for  $\mu > 0$  (which is favoured by models like minimal SUGRA) when the resummation suppresses the effects of the double penguin diagrams as compared to the calculation of [23], the approximation of sec. 3.3 works well for  $|\theta_t| \lesssim 20^\circ$  but in general gives too strong a suppression. However, for  $\mu < 0$ , the approximation of sec. 3.3 grossly overestimates the impact of the double penguin diagrams on  $\Delta M_s$  already for  $\theta_t \lesssim 5^\circ$  and should not be used for realistic applications.

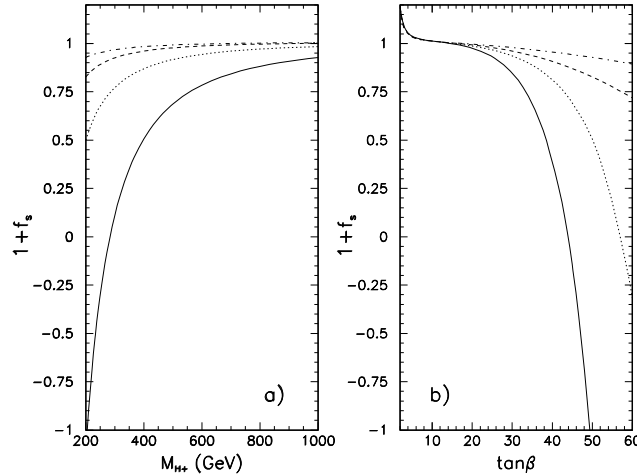


Figure 19:  $(1 + f_s)$  in the MSSM for the lighter chargino mass 750 GeV,  $|r| \equiv M_2/|\mu| = 1$ ,  $m_{\tilde{g}} = 3M_2$  and  $M_{\tilde{b}_R} = 800$  GeV as a function of  $M_{H^+}$  for  $\tan\beta = 50$  (panel a) and as a function of  $\tan\beta$  for  $M_{H^+} = 200$  GeV (panel b). Solid and dashed (dotted and dot-dashed) lines correspond to  $M_{\tilde{t}_1} = 500$  GeV,  $M_{\tilde{t}_2} = 850$  GeV (600 and 750 GeV). Solid and dotted lines, correspond to  $\mu < 0$  whereas the dashed and dot-dashed lines to  $\mu > 0$ . The stop mixing angle  $\theta_t = +(-)10^\circ$  for  $\mu < 0$  ( $\mu > 0$ ).

For the same value of the mixing angle  $\theta_t$ , larger effects are obtained for bigger stop

mass splitting because in this case the parameter  $|A_t|$  has to be larger. This is clearly seen in fig. 19. It should be also stressed that the double penguin contribution does not vanish when the mass scale of the sparticles is increased (i.e. when all mass parameters are scaled uniformly). Thus, large effects decreasing  $1 + f_s$  below unity can be present in the MSSM also for the heavy sparticles provided the mass scale of the MSSM Higgs sector remains low and  $\tan\beta$  is large as illustrated in fig. 19. Positive contribution to  $1 + f_s$  seen in fig. 19b for  $\tan\beta < 2.5$  and  $M_{H^+} = 200$  GeV is due to the ordinary charged Higgs boson box diagrams which contribute to the universal part of  $f_s$ ,  $f_d$  and  $f_\varepsilon$  through the Wilson coefficient of the standard  $Q_1^{\text{VLL}}$  operator. For lighter  $H^+$  and light charginos  $1 + f_s$  can reach values  $\sim 2$  [4]. Such high values of  $1 + f_s$  will be definitely excluded if the measured  $\Delta M_s$  is below 40/ps.

The lines corresponding to  $M_{\tilde{t}_1} = 500$  GeV,  $M_{\tilde{t}_2} = 850$  GeV in fig. 19 can be directly compared with their counterparts in fig. 13 of ref. [23]. As can be read off, for  $\mu = -750$  GeV ( $\mu = 750$  GeV) the resummation of the  $\tan\beta$  enhanced terms increases (decreases)  $f_s$  roughly by a factor of 1.5 (2.4).

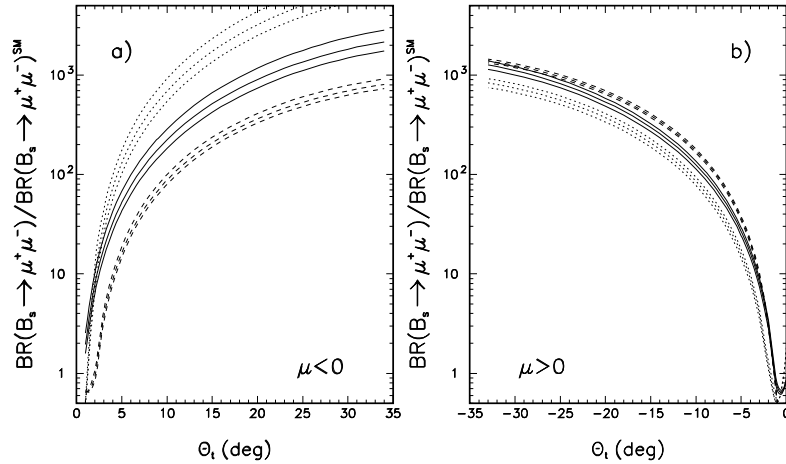


Figure 20: The ratio  $BR(B_s^0 \rightarrow \mu^+\mu^-)/BR(B_s^0 \rightarrow \mu^+\mu^-)^{\text{SM}}$  in the MSSM for  $\tan\beta = 50$ ,  $M_{H^+} = 200$ ,  $m_{\tilde{g}} = 3M_2$ ,  $M_{\tilde{b}_R} = 800$  GeV and the lighter chargino mass 600 GeV as a function of the stop mixing angle  $\theta_t$ . In panel a)  $\mu < 0$  and  $M_{\tilde{t}_1} = 600$  GeV,  $M_{\tilde{t}_2} = 750$  GeV. In panel b)  $\mu > 0$  and  $M_{\tilde{t}_1} = 500$  GeV,  $M_{\tilde{t}_2} = 850$  GeV. Solid lines correspond to the complete calculation. Dotted ones - to the approximation of based on the formulae of sec. 6.2 and the dashed lines to the calculation without the resummation of the  $\tan\beta$  enhanced terms. Consecutive lines of each type correspond to  $M_2/|\mu| = 3/4, 1$  and  $5/4$  counting from left to right (in both panels).

## 7.2 Predictions for $B_{s,d}^0 \rightarrow \mu^+ \mu^-$

In [6] and [22] the branching ratios  $B_{s,d}^0 \rightarrow \mu^+ \mu^-$  have been calculated diagrammatically with one loop accuracy. The resummation of large  $\tan\beta$  effects have not been done in these papers. The latter effects have been included in the  $SU(2) \times U(1)$  limit first in [20] and their importance has been subsequently emphasized in [27]. Here we present for the first time results for  $B_{s,d}^0 \rightarrow \mu^+ \mu^-$  in the approach that combines the full one loop diagrammatic calculation of refs. [6] and [22] with the resummation of large  $\tan\beta$  enhanced terms. This includes both,  $SU(2) \times U(1)$  breaking corrections to the calculations of refs. [20, 27] and the effects of the electroweak gauge couplings. We will assess the importance of these improvements with respect to the approaches of refs. [20, 27].

In figure 20 we show the ratio of the branching ratios  $BR(B_s^0 \rightarrow \mu^+ \mu^-)$  predicted in the SM and in the MSSM with  $\tan\beta = 50$  and  $M_{H^+} = 200$  GeV as a function of the mixing angle of the top squark. Strong dependence on the latter parameter is evident. As in figure 18, curves of a given type corresponding to smaller values of  $M_2/|\mu|$  illustrate the effects of lowering the mass of the heavier chargino ( $m_{C_1} \approx |\mu|$ ,  $m_{C_2} \approx M_2$  for all these curves) and of the increasing deviation of the lighter chargino from pure higgsino. Dotted lines in figure 20 have been obtained by using the formulae (6.35) and (6.36) of sec. 6.2 which correspond to the approach of ref. [27] that is, to the one of sec. 3 with  $\epsilon_0$  and  $\epsilon_Y$  computed from the formulae (5.2) and (5.5), respectively. Dashed lines show the prediction of the MSSM without the resummation of the  $\tan\beta$  enhanced terms.  $SU(2) \times U(1)$  symmetry limit (secs. 3.2-3.4) of ref. [27].

As it could be expected, for  $\mu > 0$  ( $\mu < 0$ ) the resummation decreases (increases) the branching ratio predicted in the MSSM. Similarly as in the case of  $f_s$ , for  $\mu > 0$  the approximation of sec. 3 gives the branching ratio smaller than the complete calculation, while for  $\mu < 0$  it overestimates this rate significantly. For example, for  $\mu > 0$ ,  $M_2/|\mu| = 1$  and  $\theta_t = -15^\circ$  and other parameters as in fig. 20,  $BR(B_s^0 \rightarrow \mu^+ \mu^-)$  obtained in the approximation of sec. 6.2 is smaller than the one obtained using the complete approach by a factor of 1.5, while it is bigger by a factor of 2 if no resummation of  $\tan\beta$  enhanced terms is performed. For  $\mu < 0$  and  $\theta_t = 15^\circ$ , instead, the formulae of sec. 6.2 give  $BR(B_s^0 \rightarrow \mu^+ \mu^-)$  approximately 3 times bigger than the complete calculation, while neglecting the resummation results in the branching ratio that is smaller by a factor of 1.3 than obtained in the full approach.

In figures 21a and 21b we show the dependence of the ratio of the branching ratios  $BR(B_s^0 \rightarrow \mu^+ \mu^-)$  predicted in the SM and in the MSSM as a functions of the charged Higgs boson mass and  $\tan\beta$ , respectively for two different choices of the top squark masses and both signs of  $\mu$ . Here we show only the results of our complete calculation based on

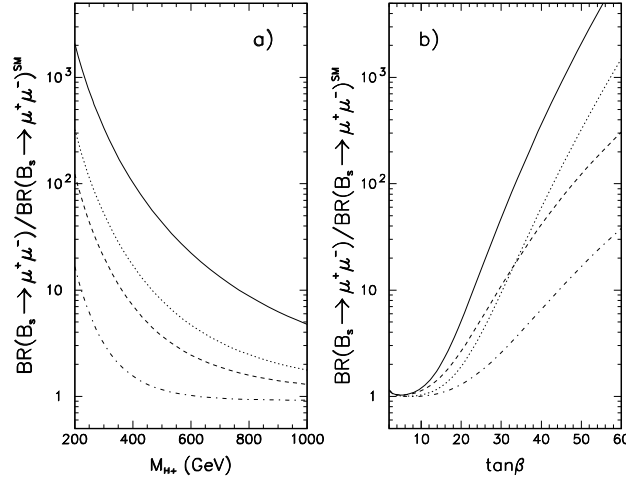


Figure 21: The ratio  $BR(B_s^0 \rightarrow \mu^+\mu^-)/BR(B_s^0 \rightarrow \mu^+\mu^-)^{\text{SM}}$  in the MSSM for the lighter chargino mass 750 GeV,  $|r| \equiv M_2/|\mu| = 1$ ,  $m_{\tilde{g}} = 3M_2$  and  $M_{\tilde{b}_R} = 800$  GeV as a function of  $M_{H^+}$  for  $\tan\beta = 50$  (panel a) and as a function of  $\tan\beta$  for  $M_{H^+} = 200$  GeV (panel b). Solid and dashed (dotted and dot-dashed) lines correspond to  $M_{\tilde{t}_1} = 500$  GeV,  $M_{\tilde{t}_2} = 850$  GeV (600 and 750 GeV). Solid and dotted lines, correspond to  $\mu < 0$  whereas the dashed and dot-dashed lines to  $\mu > 0$ . The stop mixing angle  $\theta_t = +(-)10^\circ$  for  $\mu < 0$  ( $\mu > 0$ ).

the approach of sec. 2.

The values of the ratio  $BR(B_s^0 \rightarrow \mu^+\mu^-)/BR(B_s^0 \rightarrow \mu^+\mu^-)^{\text{SM}}$  shown in figures 20 and 21 are also representative for the ratio  $BR(B_d^0 \rightarrow \mu^+\mu^-)/BR(B_d^0 \rightarrow \mu^+\mu^-)^{\text{SM}}$  if one neglects the small variation of  $|(V_{td}^{\text{eff}})^{\text{MSSM}}/(V_{td}^{\text{eff}})^{\text{SM}}|^2$  with the supersymmetric parameters which we have discussed in sec. 6.4.

Finally, in figure 22 we show the scatter plot of the ratio of the  $B_s^0 \rightarrow \mu^+\mu^-$  rates computed by using the formulae (6.35) and (6.36) of sec. 6.2 and computed using our complete approach of sec. 2 for the charged Higgs boson mass equal 300 and 400 GeV. Large, up to 50%, deviations of the approximate method with respect to the full calculation are typical for most of the points. We observe that the  $\bar{B} \rightarrow X_s\gamma$  constraint allow the approximate predictions of the branching ratio to be both, smaller and bigger than the one based on the complete calculation. Approximate predictions overestimating the exact ones correspond to very big negative contributions to  $\Delta M_s$  ( $1 + f_s < 0$ ) but, as found in [29], are not excluded by the lower experimental limit  $\Delta M_s > 15/\text{ps}$  provided  $1 + f_s \lesssim -0.5$ . However, for  $M_{H^+} = 200$  GeV such points give  $BR(B_s^0 \rightarrow \mu^+\mu^-)$  above the CDF bound (6.2).

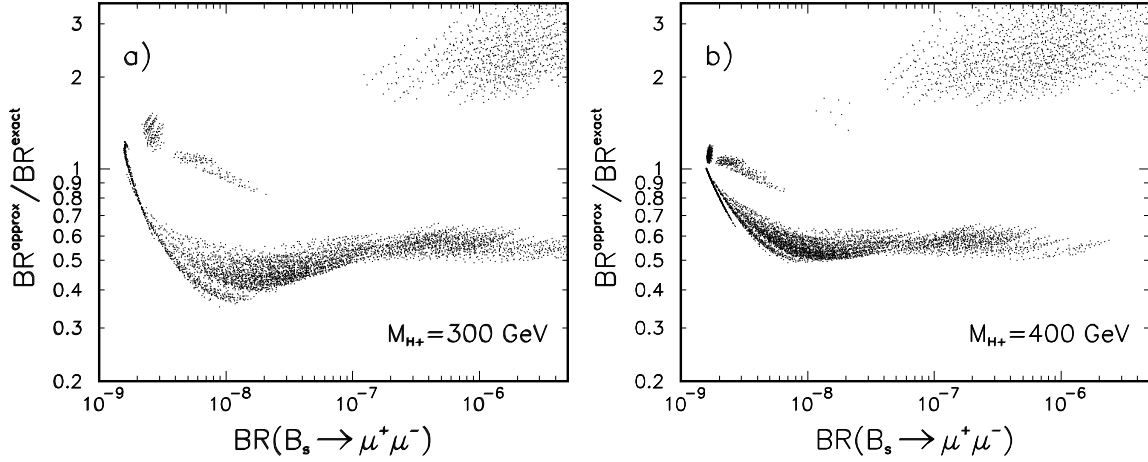


Figure 22: The ratio  $BR(B_s^0 \rightarrow \mu^+\mu^-)^{\text{approx}}/BR(B_s^0 \rightarrow \mu^+\mu^-)^{\text{exact}}$  in the MSSM for  $\tan\beta = 50$  and  $M_{H^+} = 300$  GeV (panel a) and 400 GeV (panel b). Points corresponding to unacceptable  $\bar{B} \rightarrow X_s\gamma$  rate have been rejected.

### 7.3 Correlation between $\Delta M_s$ and $B_{s,d}^0 \rightarrow \mu^+\mu^-$

As seen from eq. (6.44), important in the study of the correlation in question is the ratio  $(\Delta M_s)^{\text{exp}}/(\Delta M_s)^{\text{SM}}$  [29]. In order to find  $(\Delta M_s)^{\text{exp}}/(\Delta M_s)^{\text{SM}}$  one has to deal with the non-perturbative uncertainties contained in the evaluation of  $(\Delta M_s)^{\text{SM}}$ . The allowed range for  $(\Delta M_s)^{\text{exp}}/(\Delta M_s)^{\text{SM}}$  can be obtained by varying all relevant SM parameters like  $\bar{m}_t$ ,  $V_{ts}^{\text{eff}}$  and  $F_{B_s}\sqrt{\hat{B}_{B_s}}$ . A conservative scanning of these parameters performed in [23] resulted in

$$a \left[ \frac{(\Delta M_s)^{\text{exp}}}{15/ps} \right] \leq \frac{(\Delta M_s)^{\text{exp}}}{(\Delta M_s)^{\text{SM}}} \leq b \left[ \frac{(\Delta M_s)^{\text{exp}}}{15/ps} \right] \quad (7.62)$$

with  $a = 0.52$  and  $b = 1.29$ . It is however clear that the numerical values of the parameters  $a$  and  $b$  depend on the error analysis and the difference  $b - a$  should become smaller as the uncertainties in the parameters  $\bar{m}_t$ ,  $V_{ts}^{\text{eff}}$  and in particular in  $F_{B_s}\sqrt{\hat{B}_{B_s}}$  are reduced with time. For example, the very recent analysis which uses the Bayesian approach gives  $a = 0.71$  and  $b = 1.0$  [44] that correspond to the 95% probability range  $15.1/ps \leq (\Delta M_s)^{\text{SM}} \leq 21.0/ps$ .

We illustrate the correlations between  $\Delta M_s$  and  $BR(B_{s,d}^0 \rightarrow \mu^+\mu^-)$  in fig. 23 where we plot  $BR(B_{s,d}^0 \rightarrow \mu^+\mu^-)$  as functions of  $(\Delta M_s)^{\text{exp}}/(\Delta M_s)^{\text{SM}}$  for  $\tan\beta = 50$  and  $M_A = 300$  and 400 GeV by scanning the other MSSM parameters with the restriction that sparticles are heavier than 500 GeV and the  $\bar{B} \rightarrow X_s\gamma$  constraint is satisfied. For each point in the MSSM parameter space we satisfy the experimental constraints on  $\epsilon_K$ ,  $V_{ub}/V_{cb}$ ,  $a_{\psi K_S}$

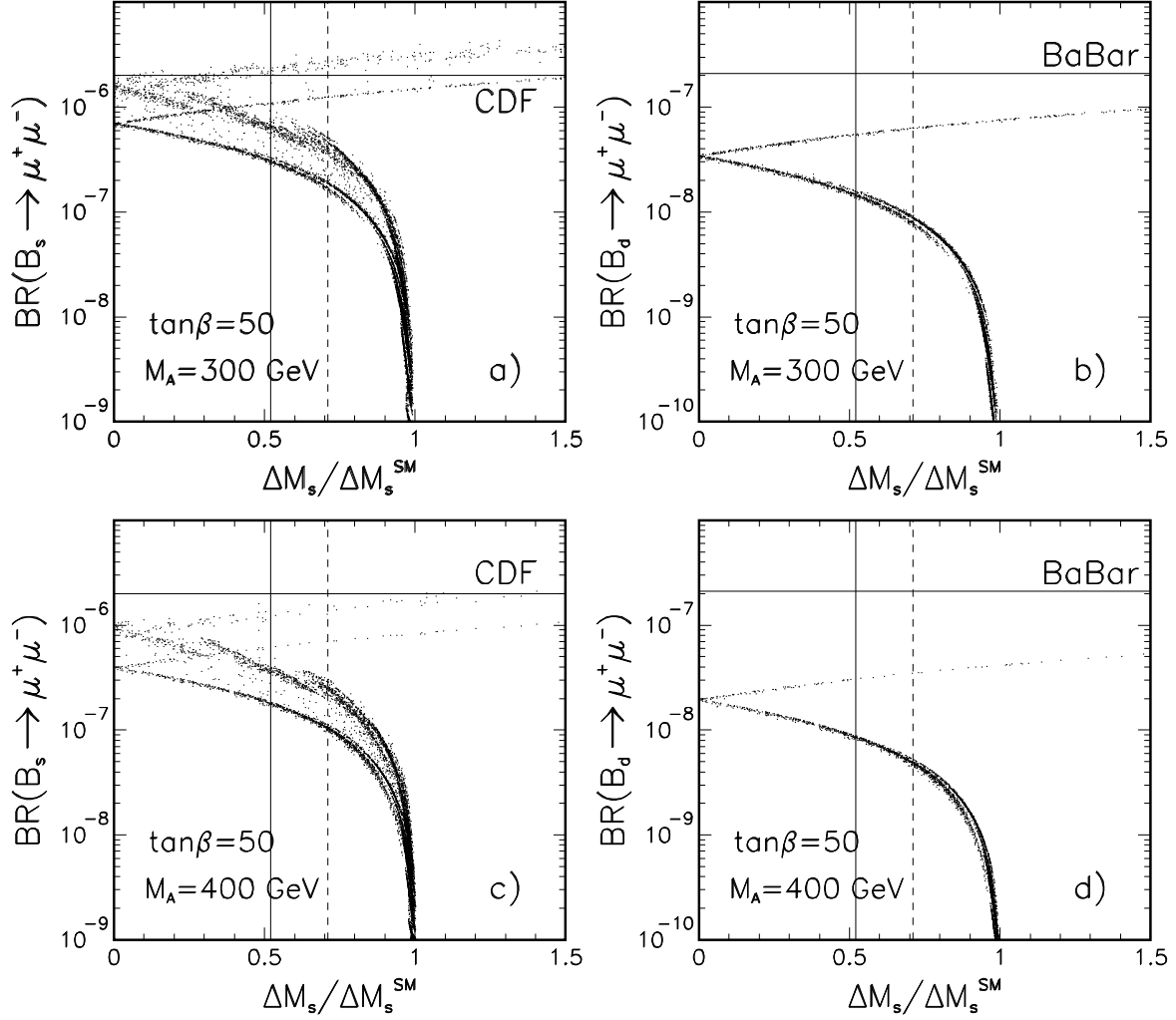


Figure 23: Correlation between  $\Delta M_s/(\Delta M_s)^{\text{SM}}$  and  $B_{s,d}^0 \rightarrow \mu^+\mu^-$  in the MSSM with flavour violation ruled by the CKM matrix. Lower (upper) branches of points correspond to  $0 < 1 + f_s < 1$  ( $1 + f_s < 0$ ). Current experimental bounds:  $BR(B_s^0 \rightarrow \mu^+\mu^-) < 2 \cdot 10^{-6}$  (CDF) [35] and  $BR(B_d^0 \rightarrow \mu^+\mu^-) < 2.1 \cdot 10^{-7}$  (BaBar) [34] are shown by the horizontal solid lines. Solid (dashed) vertical lines show the lower limit on  $\Delta M_s/(\Delta M_s)^{\text{SM}}$  following from eq. (7.62) with  $a = 0.52$  as in ref. [23] ( $a = 0.71$  as in [44]).

and  $\Delta M_d$  by appropriately adjusting the Wolfenstein and nonperturbative  $\hat{B}_K$ ,  $F_{B_d}$  and  $\xi$  parameters, that is, performing the unitarity triangle analysis [23, 7, 44] described in sec. 6.4 (points for which these constraints cannot be satisfied are rejected).  $(\Delta M_d)^{\text{exp}}$  and the parameter  $\varepsilon_K$  do not constrain our scan significantly as the corresponding quantities  $f_d$  and  $f_\varepsilon$  are small in most of the parameter space. Since the element  $V_{td}^{\text{eff}}$  is well constrained by  $\varepsilon_K$ ,  $V_{ub}/V_{cb}$ ,  $a_{\psi K_S}$ , fitting the experimental value of  $\Delta M_d$  practically fixes  $F_{B_d}$ . For this reason, the correlation of  $BR(B_d^0 \rightarrow \mu^+ \mu^-)$  with  $\Delta M_s/\Delta M_s^{\text{exp}}$  clearly seen in figures 23b and 23d is much tighter than the analogous correlation of  $BR(B_s^0 \rightarrow \mu^+ \mu^-)$  (figures 23a,c) where the  $F_{B_s} \approx \xi F_{B_d}$  can still be varied independently (some structure in the density of points visible in figs. 23a,c is an artifact of the scanning method used to produce the figure, preferring the points concentrated around the minimal or the maximal allowed value for  $BR(B_s^0 \rightarrow \mu^+ \mu^-)$ ). Vertical lines shown in figures 23 correspond to the lower limit on  $(\Delta M_s)^{\text{exp}}/(\Delta M_s)^{\text{SM}}$  following from (7.62) with  $a$  taken from ref. [23] (solid) and [44] (dashed).

For  $M_A = 200$  GeV and  $\tan \beta = 50$  shown in the plots of [29] all points corresponding to the rather unlikely scenario with  $1 + f_s < 0$  were eliminated by the combination of the lower limit (7.62) and the CDF upper bound  $BR(B_s^0 \rightarrow \mu^+ \mu^-) < 2 \times 10^{-6}$  [35]. This is not the case for heavier  $A^0$  and/or smaller  $\tan \beta$  values.

Therefore for such points we can only use (6.41) to find

$$BR(B_d^0 \rightarrow \mu^+ \mu^-) < 3.6 (3.1) \cdot 10^{-8} \left[ \frac{1.15}{F_{B_s}/F_{B_d}} \right]^2 \left[ \frac{BR(B_s^0 \rightarrow \mu^+ \mu^-)^{\text{exp}}}{10^{-6}} \right] \quad (7.63)$$

with the numerical factor corresponding to the analyses in [23] and [44], respectively. With the current CDF bound one has the upper bound  $BR(B_d^0 \rightarrow \mu^+ \mu^-) < 8 (7) \cdot 10^{-8}$  which is still lower than the current BaBar bound [34].

For a more likely situation of  $0 < 1 + f_s < 1$  and  $(\Delta M_s)^{\text{exp}}$  satisfying (7.62) we get upper bounds on both branching ratios:

$$\begin{aligned} BR(B_s^0 \rightarrow \mu^+ \mu^-) &\lesssim 1.2 \cdot 10^{-6} (8 \cdot 10^{-7}) \quad \text{for } a = 0.52 \text{ (0.71),} \\ BR(B_d^0 \rightarrow \mu^+ \mu^-) &\lesssim 3 \cdot 10^{-8} (2 \cdot 10^{-8}) \quad \text{for } a = 0.52 \text{ (0.71).} \end{aligned} \quad (7.64)$$

where the two values for the parameter  $a$  correspond to the analyses in [23] and [44], respectively. This should be compared with the SM values that are in the ballpark of  $3 \cdot 10^{-9}$  and  $1 \cdot 10^{-10}$ , respectively. On the basis of our discussion of the contribution  $(\Delta M_s)^{x^\pm}$  in sec. 6, we would like to emphasize that the upper limits on  $BR(B_{s,d}^0 \rightarrow \mu^+ \mu^-)$  obtained here for heavy sparticle spectrum cannot be significantly altered by lowering the sparticle masses.

The upper bounds (7.64) and (7.63) are very important because, as has been pointed out in ref. [7] and recently confirmed in [8], they do not apply in the MSSM in which flavour violation originates from the squark mass matrices. The reason is that in this case leading supersymmetric corrections to  $\Delta M_s$  and to  $BR(B_d^0 \rightarrow \mu^+ \mu^-)$  are governed by different off diagonal elements of the squark mass matrices and the correlation between these two quantities does not hold. One concludes therefore, that within the supersymmetric framework, observation of the  $B_d^0 \rightarrow \mu^+ \mu^-$  decay at the level higher than  $\approx 3 \times 10^{-8}$ , apart from implying that the scale of the Higgs boson sector is not far from the electroweak scale, would be also a very strong evidence for non-minimal flavour violation in the quark sector.

In principle, if the measured values of  $BR(B_{s,d}^0 \rightarrow \mu^+ \mu^-)$  turn out to be significantly bigger than predicted by the SM but do not respect the correlation with the measured value of  $\Delta M_s$ , this could also be a sign of nonminimal flavour violation. In practice, however, usefulness of this test is limited by the precision with which the nonperturbative parameters  $F_{B_s}$ ,  $B_{B_s}$  etc. are known.

## 8 Summary and Conclusions

In this paper we have presented an effective Lagrangian formalism for the calculation of flavour changing neutral and charged currents that is suited for theories containing a sector of heavy fields. While our approach is rather general, we have discussed it explicitly in the context of the MSSM with the CKM matrix as the only source of flavour violation, heavy supersymmetric particles and neutral and charged Higgs masses below 500 GeV.

Recently a number of analyses of large  $\tan \beta$  effects in weak decays appeared in the literature. The present analysis is the first one that includes simultaneously

- Resummed large  $\tan \beta$  effects,
- $SU(2) \times U(1)$  gauge symmetry breaking effects,
- The contributions of electroweak couplings  $g_1$  and  $g_2$  to the effective parameters in the low energy Lagrangian.

Our approach is therefore equivalent to the full diagrammatic one loop calculation supplemented by the resummation of the  $\tan \beta$  enhanced terms. We have analyzed the importance of these effects demonstrating that for reliable quantitative predictions all of them have to be taken into account. Thus, we have generalized previous analyses where either the resummed large  $\tan \beta$  effects have been calculated in the  $SU(2) \times U(1)$  symmetry



limit [20, 27, 28] or the complete one loop calculations have been performed leaving out, however, the resummation of large  $\tan\beta$  effects [6, 22, 21].

To compare our approach with the one of [27, 28] we have also derived analytic formulae for the neutral and charged Higgs boson couplings to quarks in the  $SU(2)\times U(1)$  symmetry limit resumming large  $\tan\beta$  terms. Our results agree here with those presented in [27, 28]. These transparent formulae, which make all large  $\tan\beta$  effects explicit, depend only on four universal flavour independent parameters  $\epsilon_0$ ,  $\epsilon_Y$ ,  $\epsilon'_0$  and  $\epsilon'_Y$ . However, the comparison of the results obtained in this approximation with the ones following from the complete calculation shows clearly that the former can only be used for a semi-quantitative analysis. We have also shown that the accuracy of the approximation can be greatly improved while maintaining the transparency of the resulting expressions. This is achieved by introducing flavour dependence into the parameters  $\epsilon_0$ ,  $\epsilon_Y$ ,  $\epsilon'_0$  and  $\epsilon'_Y$  by extracting them directly from the complete (but relatively simple to compute) correction to the down quark mass matrix. In this manner we have obtained analytic formulae for the neutral and charged Higgs couplings to quarks that still make the large  $\tan\beta$  effects explicit but include automatically the effects of electroweak couplings  $g_1$ ,  $g_2$  and of the, slightly less important,  $SU(2)\times U(1)$  symmetry breaking effects. Our analytic formulae reproduce within 5–10% the results of the full approach to be compared with only 20–40% accuracy of the formulae obtained in the approach of refs. [27, 28].

The main message of our analysis is that the simple approach adopted in [20, 27, 28] overestimates the effects of the resummation of large  $\tan\beta$  contributions. This is clearly seen in figs. 18, 20.

The most spectacular effects in weak decays predicted by the MSSM with large  $\tan\beta$  are the huge increase of the branching ratios  $BR(B_{s,d}^0 \rightarrow \mu^+\mu^-)$  and a significant suppression of  $\Delta M_s$ . As pointed out in [29] these effects are tightly correlated so that for most probable ranges of supersymmetric parameters the experimental lower bound on  $\Delta M_s$  implies an upper bound on  $BR(B_{s,d}^0 \rightarrow \mu^+\mu^-)$ . In [29] and in the present paper both these quantities, as well as their correlation have been calculated including for the first time all the effects listed above. Simultaneously we have clarified some points in the calculation of large  $\tan\beta$  effects in the  $B \rightarrow X_s\gamma$  rate that we have used to constrain the allowed range of supersymmetric parameters.

For the same set of parameters our results for  $BR(B_{s,d}^0 \rightarrow \mu^+\mu^-)$  without the inclusion of the  $\Delta M_s$  constraint are typically between the values presented in [27, 28] and in [6, 21, 22]. We also find that the impact of the resummed large  $\tan\beta$  corrections on our analysis of  $\Delta M_s$  in [23] is smaller than obtained in [27, 28]. Moreover we have shown that large  $\tan\beta$  effects in  $\Delta M_s$  are dominated by double neutral Higgs penguin diagrams and receive significant contributions from box diagrams with charged Higgs exchanges.

For the near future of particular interest are the upper bounds on  $BR(B_{s,d}^0 \rightarrow \mu^+ \mu^-)$  as functions of the ratio  $(\Delta M_s)^{\text{exp}}/(\Delta M_s)^{\text{SM}}$  that we have already presented in [29]. In the most likely scenario with  $0 < (1 + f_s) < 1$  these bounds are becoming very strong when this ratio approaches unity. This is illustrated in fig. 23. For  $(\Delta M_s)^{\text{exp}} \geq (\Delta M_s)^{\text{SM}}$  substantial enhancements of  $BR(B_{s,d}^0 \rightarrow \mu^+ \mu^-)$  with respect to the values obtained in the SM are not possible within the MSSM scenario considered here. Violation of our bounds would either rule out this version of MSSM and/or signal new sources of flavour violation [7].

As the upper bounds on  $BR(B_{s,d}^0 \rightarrow \mu^+ \mu^-)$  discussed here are sensitive functions of the ratio  $(\Delta M_s)^{\text{exp}}/(\Delta M_s)^{\text{SM}}$ , their quantitative usefulness will depend on the value of  $(\Delta M_s)^{\text{exp}}$  and on the accuracy with which  $(\Delta M_s)^{\text{SM}}$  can be calculated. In this respect the present efforts of experimentalists to measure  $BR(B_{s,d}^0 \rightarrow \mu^+ \mu^-)$  and  $\Delta M_s$  and of theorists to calculate  $F_{B_{d,s}}$  and the parameters  $B_{d,s}$  are very important.

*Note added:* Very recently a new analysis of resummed large  $\tan \beta$  effects in FCNC transitions has been presented in [49]. It goes beyond the framework of minimal flavour and CP violation and discusses the ratio  $\varepsilon'/\varepsilon$  and CP asymmetries not considered in our paper as the new physics effects in these quantities in our scenario are tiny. However these authors, similarly to [27, 28], work in the  $SU(2) \times U(1)$  limit and do not take into account the refinements discussed in section 5 nor they included the constraint from  $B \rightarrow X_s \gamma$  decay on the supersymmetric parameters. On the other hand they stress that the inclusion of light quark contributions in the formalism of [27, 28] could have an impact for certain very special values of supersymmetric parameters for which  $\tilde{\epsilon}_3$  approaches  $-1$ . We would like to emphasize that in our full approach of section 2 and in the improved approximation presented in section 5 the contributions of light quarks are automatically included. Moreover when the experimental constraints from  $B \rightarrow X_s \gamma$  decay,  $\Delta M_{s,d}$  and  $B \rightarrow \mu^+ \mu^-$  are taken into account and the Higgs masses are kept below 500 GeV,  $\tilde{\epsilon}_3$  never approaches  $-1$  and the light quarks except for assuring the GIM mechanism are unimportant in the resummed large  $\tan \beta$  corrections.

## Acknowledgements

A.J.B. would like to thank A. Dedes, G. Isidori, F. Krüger and J. Urban for their interest and discussions. P.H.Ch. would like to thank G. Isidori for the discussions and the CERN Theory group for hospitality during the completion of this paper. The work of A.J.B. and J.R. has been supported in part by the German Bundesministerium für Bildung und Forschung under the contract 05HT1WOA3 and the DFG Project Bu. 706/1-1. J.R. and

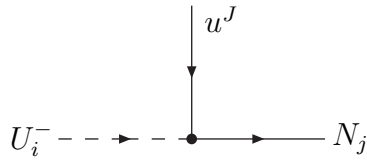
L.S. have been supported by the Polish State Committee for Scientific Research grant 2 P03B 040 24 for 2003-2005. The work of P.H.Ch. has been partly supported by the Polish State Committee for Scientific Research grant 2 P03B 129 24 for 2003-2004 and by the EC Contract HPRN-CT-2000-00148 for years 2000-2004.

# Appendix Feynman rules and Green's functions

For completeness we collect here some of the the Feynman rules given in [30] and formulae for the 2-, 3- and 4-point Green's functions used in the paper.

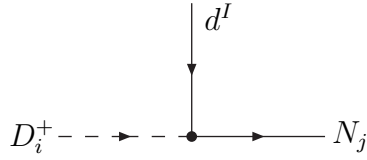
## A.1 Feynman rules

We write the fermion-fermion-scalar vertices as  $i(V_L P_L + V_R P_R)$ . The couplings  $V_L, V_R$  are listed below:



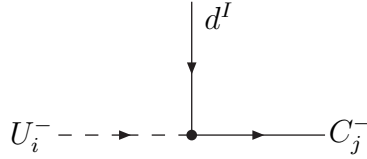
$$V_{uUN}^{LJij} = \frac{-1}{\sqrt{2}} Z_U^{Ji^*} \left( \frac{g_1}{3} Z_N^{1j} + g_2 Z_N^{2j} \right) - y_{u_j} Z_U^{(J+3)i^*} Z_N^{4j}$$

$$V_{uUN}^{RJij} = \frac{2\sqrt{2}}{3} g_1 Z_U^{(J+3)i^*} Z_N^{1j^*} - y_{u_j} Z_U^{Ji^*} Z_N^{4j^*}$$



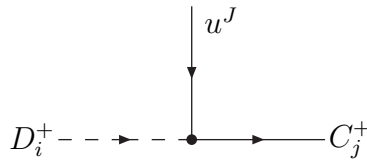
$$V_{dDN}^{LIij} = \frac{-1}{\sqrt{2}} Z_D^{Ii} \left( \frac{g_1}{3} Z_N^{1j} - g_2 Z_N^{2j} \right) + y_{d_I} Z_D^{(I+3)i} Z_N^{3j}$$

$$V_{dDN}^{RIij} = \frac{-\sqrt{2}}{3} g_1 Z_D^{(I+3)i} Z_N^{1j^*} + y_{d_I} Z_D^{Ii} Z_N^{3j^*}$$



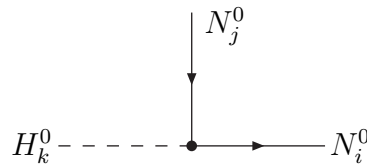
$$V_{dUC}^{LIij} = (-g_2 Z_U^{Ji^*} Z_+^{1j} + y_{u_j} Z_U^{(J+3)i^*} Z_+^{2j}) V^{JI}$$

$$V_{dUC}^{RIij} = -y_{d_I} Z_U^{Ji^*} Z_-^{2j^*} V^{JI}$$

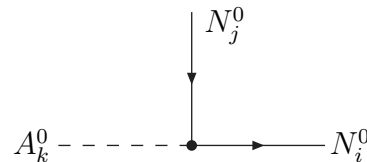


$$V_{uDC}^{LJij} = -(g_2 Z_D^{Ii} Z_-^{1j} + y_{d_I} Z_D^{(I+3)i} Z_-^{2j}) V^{JI^*}$$

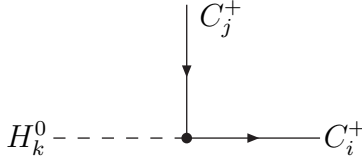
$$V_{uDC}^{RJij} = y_{u_j} Z_D^{Ii} Z_+^{2j^*} V^{JI^*}$$



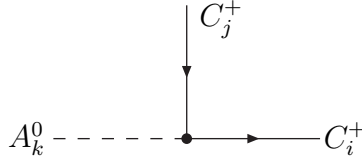
$$V_{NNS}^{Lijk} = V_{NNS}^{Rijk^*} = \frac{1}{2} \left[ (Z_R^{1k} Z_N^{3j} - Z_R^{2k} Z_N^{4j}) \times (g_1 Z_N^{1i} - g_2 Z_N^{2i}) + (j \leftrightarrow i) \right]$$



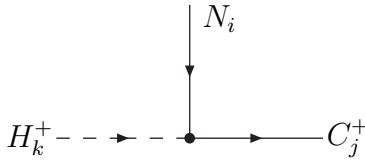
$$V_{NNP}^{Lijk} = -V_{NNP}^{Rjik^*} = \frac{-i}{2} \left[ (Z_H^{1k} Z_N^{3j} - Z_H^{2k} Z_N^{4j}) \times (g_1 Z_N^{1i} - g_2 Z_N^{2i}) + (j \leftrightarrow i) \right]$$



$$V_{CCS}^{Lijk} = V_{CCS}^{Rjik^*} = -\frac{g_2}{\sqrt{2}}(Z_R^{1k} Z_-^{2i} Z_+^{1j} + Z_R^{2k} Z_-^{1i} Z_+^{2j})$$



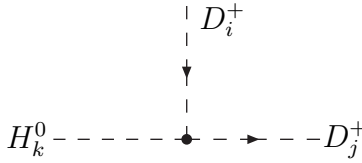
$$V_{CCP}^{Lijk} = -V_{CCP}^{Rjik^*} = \frac{ig_2}{\sqrt{2}}(Z_H^{1k} Z_-^{2i} Z_+^{1j} + Z_H^{2k} Z_-^{1i} Z_+^{2j})$$



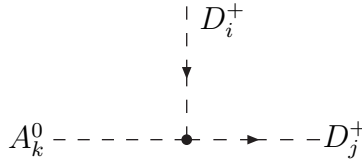
$$V_{NCH}^{Lijk} = Z_H^{1k} \left( \frac{1}{\sqrt{2}} Z_-^{2j} (g_1 Z_N^{1i} + g_2 Z_N^{2i}) - Z_-^{1j} Z_N^{3i} g_2 \right)$$

$$V_{NCH}^{Rijk} = -Z_H^{2k} \left( \frac{1}{\sqrt{2}} Z_+^{2j^*} (g_1 Z_N^{1i^*} + g_2 Z_N^{2i^*}) + Z_+^{1j^*} Z_N^{4i^*} g_2 \right)$$

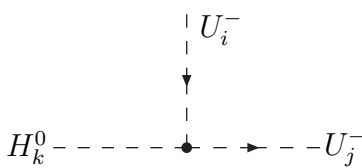
The three-scalar vertices are defined as  $iV$ , with  $V$  given by:



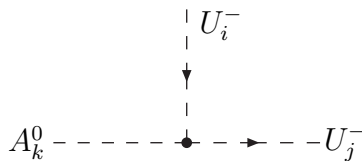
$$V_{DDS}^{ijk} = \left( \frac{g_1^2}{6} B_R^k \left( \delta^{ji} + \frac{3 - 4s_W^2}{4s_W^2} Z_D^{Ij^*} Z_D^{Ii} \right) \right. \\ \left. - v_d y_{d_I}^2 Z_R^{1k} (Z_D^{Ij^*} Z_D^{Ii} + Z_D^{(I+3)j^*} Z_D^{(I+3)i}) \right. \\ \left. - \frac{1}{\sqrt{2}} Z_R^{1k} (A_d^{IJ^*} Z_D^{Ii} Z_D^{(J+3)j^*} + A_d^{IJ} Z_D^{Ij^*} Z_D^{(J+3)i}) \right. \\ \left. - \frac{1}{\sqrt{2}} y_{d_I} Z_R^{2k} (\mu^* Z_D^{Ij^*} Z_D^{(I+3)i} + \mu Z_D^{Ii} Z_D^{(I+3)j^*}) \right)$$



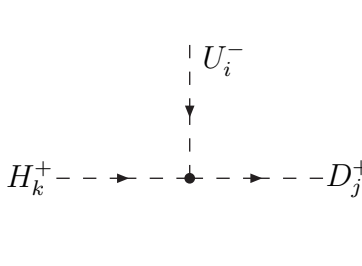
$$V_{DDP}^{ijk} = \frac{i}{\sqrt{2}} \left( y_{d_I} (\mu^* Z_D^{Ij^*} Z_D^{(I+3)i} - \mu Z_D^{Ii} Z_D^{(I+3)j^*}) Z_H^{2k} \right. \\ \left. + (A_d^{IJ^*} Z_D^{Ii} Z_D^{(J+3)j^*} - A_d^{IJ} Z_D^{Ij^*} Z_D^{(J+3)i}) Z_H^{1k} \right)$$



$$V_{UUS}^{ijk} = \left( -\frac{g_1^2}{3} B_R^k \left( \delta^{ij} + \frac{3 - 8s_W^2}{4s_W^2} Z_U^{Ii^*} Z_U^{Ij} \right) \right. \\ \left. - v_u y_{u_I}^2 Z_R^{2k} (Z_U^{Ii^*} Z_U^{Ij} + Z_U^{(I+3)i^*} Z_U^{(I+3)j}) \right. \\ \left. + \frac{1}{\sqrt{2}} Z_R^{2k} (A_u^{IJ^*} Z_U^{Ii^*} Z_U^{(J+3)j} + A_u^{IJ} Z_U^{Ij} Z_U^{(J+3)i^*}) \right. \\ \left. + \frac{1}{\sqrt{2}} y_{u_I} Z_R^{1k} (\mu^* Z_U^{Ij} Z_U^{(I+3)i^*} + \mu Z_U^{Ii^*} Z_U^{(I+3)j}) \right)$$



$$V_{UUP}^{ijk} = \frac{i}{\sqrt{2}} \left( y_{u_I} (\mu Z_U^{Ii^*} Z_U^{(I+3)j} - \mu^* Z_U^{Ij} Z_U^{(I+3)i^*}) Z_H^{1k} \right. \\ \left. + (A_u^{IJ} Z_U^{Ij} Z_U^{(J+3)i^*} - A_u^{IJ^*} Z_U^{Ii^*} Z_U^{(J+3)j}) Z_H^{2k} \right)$$



$$\begin{aligned}
V_{UDH}^{ijk} = & \left[ -\frac{\sqrt{2}M_W}{g_2} y_{u_j} y_{d_I} V^{JI} Z_D^{(I+3)j^*} Z_U^{(J+3)i^*} \delta^{1k} \right. \\
& + \frac{1}{\sqrt{2}} \left( \frac{-g_2^2}{2} v_l Z_H^{lk} + v_d y_{d_I}^2 Z_H^{1k} + v_u y_{u_j}^2 Z_H^{2k} \right) V^{JI} Z_D^{Ij^*} Z_U^{Ji^*} \\
& + (Z_H^{1k} \mu^* y_{u_j} V^{JI} - Z_H^{2k} A_u^{KJ} V^{KI}) Z_U^{(J+3)i^*} Z_D^{Ij^*} \\
& \left. + (Z_H^{1k} A_d^{KI^*} V^{JK} - Z_H^{2k} \mu y_{d_I} V^{JI}) Z_U^{Ji^*} Z_D^{(I+3)j^*} \right]
\end{aligned}$$

As explained in sec. 2, the CKM matrix  $V$  in the above rules is related to the “measured” CKM matrix  $V_{\text{eff}}$  as in (2.21) or, in the approximation of sec. 3, as in (3.25). The Yukawa couplings are related to the physical quark masses as:

$$y_{d_I} = -\frac{\sqrt{2}}{v_d} \frac{\bar{m}_{d_I}}{(1 + \tilde{\epsilon}_I \tan \beta)}, \quad y_{u_j} = \frac{\sqrt{2}}{v_u} \bar{m}_{u_j} \quad (\text{A.1})$$

Definitions of the mixing matrices  $Z_U$ ,  $Z_{\bar{U}}$ ,  $Z_{\pm}$  and  $Z_N$  can be found in [30]. Note that it is  $V$ , not  $V_{\text{eff}}$  that enters the squark mass squared matrices. It should be also remembered that computing Wilson coefficients of the higher dimension operators generated by charginos one should modify their vertices according to the rules formulated in secs. 2.6 and 3.5.

## A.2 Quark self-energies

Definitions of the formfactors are given in fig. 1. Also,  $(\Sigma_{mR}^q)^{IJ} = (\Sigma_{mL}^q)^{JI^*}$

$$\begin{aligned}
(4\pi)^2 \left( \Sigma_{VL}^d \right)^{JI} &= \frac{32\pi\alpha_s}{3} \sum_{k=1}^6 Z_D^{Jk^*} Z_D^{Ik} B_1(s, m_{\tilde{g}}^2, m_{D_k}^2) \\
&+ \sum_{k=1}^6 \sum_{l=1}^4 V_{dDN}^{LJkl^*} V_{dDN}^{LIkl} B_1(s, m_{N_l}^2, m_{D_k}^2) + \sum_{k=1}^6 \sum_{l=1}^2 V_{dUC}^{LJkl^*} V_{dUC}^{LIkl} B_1(s, m_{C_l}^2, m_{U_k}^2) \\
(4\pi)^2 \left( \Sigma_{VR}^d \right)^{JI} &= \frac{32\pi\alpha_s}{3} \sum_{k=1}^6 Z_D^{(J+3)k^*} Z_D^{(I+3)k} B_1(s, m_{\tilde{g}}^2, m_{D_k}^2) \\
&+ \sum_{k=1}^6 \sum_{l=1}^4 V_{dDN}^{RJkl^*} V_{dDN}^{RIkl} B_1(s, m_{N_l}^2, m_{D_k}^2) + \sum_{k=1}^6 \sum_{l=1}^2 V_{dUC}^{RJkl^*} V_{dUC}^{RIkl} B_1(s, m_{C_l}^2, m_{U_k}^2) \\
(4\pi)^2 \left( \Sigma_{mL}^d \right)^{JI} &= -\frac{32\pi\alpha_s}{3} m_{\tilde{g}} \sum_{k=1}^6 Z_D^{(J+3)k^*} Z_D^{Ik} B_0(s, m_{\tilde{g}}^2, m_{D_k}^2) \\
&+ \sum_{k=1}^6 \sum_{l=1}^4 V_{dDN}^{RJkl^*} V_{dDN}^{LIkl} m_{N_l} B_0(s, m_{N_l}^2, m_{D_k}^2) \\
&+ \sum_{k=1}^6 \sum_{l=1}^2 V_{dUC}^{RJkl^*} V_{dUC}^{LIkl} m_{C_l} B_0(s, m_{C_l}^2, m_{U_k}^2) \quad (\text{A.2})
\end{aligned}$$

$$\begin{aligned}
(4\pi)^2 (\Sigma_{VL}^u)^{JI} &= \frac{32\pi\alpha_s}{3} \sum_{k=1}^6 Z_U^{Jk} Z_U^{Ik*} B_1(s, m_{\tilde{g}}^2, m_{U_k}^2) \\
&+ \sum_{k=1}^6 \sum_{l=1}^4 V_{uUN}^{LJkl*} V_{uUN}^{LIkl} B_1(s, m_{N_l}^2, m_{U_k}^2) + \sum_{k=1}^6 \sum_{l=1}^2 V_{uDC}^{LJkl*} V_{uDC}^{LIkl} B_1(s, m_{C_l}^2, m_{D_k}^2) \\
(4\pi)^2 (\Sigma_{VR}^u)^{JI} &= \frac{32\pi\alpha_s}{3} \sum_{k=1}^6 Z_U^{(J+3)k} Z_U^{(I+3)k*} B_1(s, m_{\tilde{g}}^2, m_{U_k}^2) \\
&+ \sum_{k=1}^6 \sum_{l=1}^4 V_{uUN}^{RJkl*} V_{uUN}^{RIkl} B_1(s, m_{N_l}^2, m_{U_k}^2) + \sum_{k=1}^6 \sum_{l=1}^2 V_{uDC}^{RJkl*} V_{uDC}^{RIkl} B_1(s, m_{C_l}^2, m_{D_k}^2) \\
(4\pi)^2 (\Sigma_{mL}^u)^{JI} &= -\frac{32\pi\alpha_s}{3} m_{\tilde{g}} \sum_{k=1}^6 Z_U^{(J+3)k} Z_U^{Ik*} B_0(s, m_{\tilde{g}}^2, m_{U_k}^2) \\
&+ \sum_{k=1}^6 \sum_{l=1}^4 V_{uUN}^{RJkl*} V_{uUN}^{LIkl} m_{N_l} B_0(s, m_{N_l}^2, m_{U_k}^2) \\
&+ \sum_{k=1}^6 \sum_{l=1}^2 V_{uDC}^{RJkl*} V_{uDC}^{LIkl} m_{C_l} B_0(s, m_{C_l}^2, m_{D_k}^2) \tag{A.3}
\end{aligned}$$

### A.3 Higgs-fermion effective couplings

The effective Higgs-fermion vertex is defined in fig. 3. The formulae given below are completely general and are valid also in the MSSM with flavour violation originating in the sfermion mass matrices.

i) **CP-even neutral Higgs boson vertex**  $H_k^0 \bar{d}_j d_l$ . Using the general notation of eq. (2.24) with  $S = H_k^0$  ( $H_1^0 = H^0, H_2^0 = h^0$ ) we find:

$$\begin{aligned}
(4\pi)^2 \left( \Delta F_L^{dH_k^0} \right)^{JI} &= \frac{32\pi\alpha_s}{3} m_{\tilde{g}} \sum_{l,m=1}^6 V_{DDS}^{lmk} Z_D^{(J+3)l*} Z_D^{Im} C_0(m_{\tilde{g}}^2, m_{D_l}^2, m_{D_m}^2) \\
&- \sum_{l,m=1}^6 \sum_{n=1}^4 V_{DDS}^{lmk} V_{dDN}^{RJln*} V_{dDN}^{LIln} m_{N_n} C_0(m_{N_n}^2, m_{D_l}^2, m_{D_m}^2) \\
&- \sum_{l,m=1}^4 \sum_{n=1}^6 V_{dDN}^{RJln*} V_{dDN}^{LIln} \left[ V_{NNS}^{Rlmk} C_2(m_{D_n}^2, m_{N_l}^2, m_{N_m}^2) \right. \\
&\quad \left. + V_{NNS}^{Llmk} m_{N_l} m_{N_m} C_0(m_{D_n}^2, m_{N_l}^2, m_{N_m}^2) \right] \\
&- \sum_{l,m=1}^6 \sum_{n=1}^2 V_{UUS}^{lmk} V_{dUC}^{RJln*} V_{dUC}^{LIln} m_{C_n} C_0(m_{C_n}^2, m_{U_l}^2, m_{U_m}^2) \\
&- \sum_{l,m=1}^2 \sum_{n=1}^6 V_{dUC}^{RJln*} V_{dUC}^{LIln} \left[ V_{CCS}^{Rlmk} C_2(m_{U_n}^2, m_{C_l}^2, m_{C_m}^2) \right. \\
&\quad \left. + V_{CCS}^{Llmk} m_{C_l} m_{C_m} C_0(m_{U_n}^2, m_{C_l}^2, m_{C_m}^2) \right] \tag{A.4}
\end{aligned}$$

$$\begin{aligned}
(4\pi)^2 \left( \Delta F_R^{dH_k^0} \right)^{JI} &= \frac{32\pi\alpha_s}{3} m_{\tilde{g}} \sum_{l,m=1}^6 V_{DDS}^{lmk} Z_D^{Jl*} Z_D^{(I+3)m} C_0(m_{\tilde{g}}^2, m_{D_l}^2, m_{D_m}^2) \\
&- \sum_{l,m=1}^6 \sum_{n=1}^4 V_{DDS}^{lmk} V_{dDN}^{LJln*} V_{dDN}^{RI mn} m_{N_n} C_0(m_{N_n}^2, m_{D_l}^2, m_{D_m}^2) \\
&- \sum_{l,m=1}^4 \sum_{n=1}^6 V_{dDN}^{LJnl*} V_{dDN}^{RI nm} \left[ V_{NNS}^{Lmk} C_2(m_{D_n}^2, m_{N_l}^2, m_{N_m}^2) \right. \\
&\quad \left. + V_{NNS}^{Rmk} m_{N_l} m_{N_m} C_0(m_{D_n}^2, m_{N_l}^2, m_{N_m}^2) \right] \\
&- \sum_{l,m=1}^6 \sum_{n=1}^2 V_{UUS}^{lmk} V_{dUC}^{LJln*} V_{dUC}^{RI mn} m_{C_n} C_0(m_{C_n}^2, m_{U_l}^2, m_{U_m}^2) \\
&- \sum_{l,m=1}^2 \sum_{n=1}^6 V_{dUC}^{LJnl*} V_{dUC}^{RI nm} \left[ V_{CCS}^{Lmk} C_2(m_{U_n}^2, m_{C_l}^2, m_{C_m}^2) \right. \\
&\quad \left. + V_{CCS}^{Rmk} m_{C_l} m_{C_m} C_0(m_{U_n}^2, m_{C_l}^2, m_{C_m}^2) \right] \quad (A.5)
\end{aligned}$$

ii) **CP-odd neutral Higgs boson vertex**  $A_k^0 \bar{d}_J d_I$ . In this case  $S = A_k^0$  ( $A_1^0 = A^0$ ,  $A_2^0 = G^0$ ) and

$$\begin{aligned}
(4\pi)^2 \left( \Delta F_L^{dA_k^0} \right)^{JI} &= \frac{32\pi\alpha_s}{3} m_{\tilde{g}} \sum_{l,m=1}^6 V_{DDP}^{lmk} Z_D^{(J+3)l*} Z_D^{Im} C_0(m_{\tilde{g}}^2, m_{D_l}^2, m_{D_m}^2) \\
&- \sum_{l,m=1}^6 \sum_{n=1}^4 V_{DDP}^{lmk} V_{dDN}^{RJln*} V_{dDN}^{LI mn} m_{N_n} C_0(m_{N_n}^2, m_{D_l}^2, m_{D_m}^2) \\
&- \sum_{l,m=1}^4 \sum_{n=1}^6 V_{dDN}^{RJnl*} V_{dDN}^{LI nm} \left[ V_{NNS}^{Rmk} C_2(m_{D_n}^2, m_{N_l}^2, m_{N_m}^2) \right. \\
&\quad \left. + V_{NNS}^{Lmk} m_{N_l} m_{N_m} C_0(m_{D_n}^2, m_{N_l}^2, m_{N_m}^2) \right] \\
&- \sum_{l,m=1}^6 \sum_{n=1}^2 V_{UUP}^{lmk} V_{dUC}^{RJln*} V_{dUC}^{LI mn} m_{C_n} C_0(m_{C_n}^2, m_{U_l}^2, m_{U_m}^2) \\
&- \sum_{l,m=1}^2 \sum_{n=1}^6 V_{dUC}^{RJnl*} V_{dUC}^{LI nm} \left[ V_{CCP}^{Rmk} C_2(m_{U_n}^2, m_{C_l}^2, m_{C_m}^2) \right. \\
&\quad \left. + V_{CCP}^{Lmk} m_{C_l} m_{C_m} C_0(m_{U_n}^2, m_{C_l}^2, m_{C_m}^2) \right] \quad (A.6)
\end{aligned}$$

$$(4\pi)^2 \left( \Delta F_R^{dA_k^0} \right)^{JI} = \frac{32\pi\alpha_s}{3} m_{\tilde{g}} \sum_{l,m=1}^6 V_{DDP}^{lmk} Z_D^{Jl*} Z_D^{(I+3)m} C_0(m_{\tilde{g}}^2, m_{D_l}^2, m_{D_m}^2)$$



$$\begin{aligned}
& - \sum_{l,m=1}^6 \sum_{n=1}^4 V_{DDP}^{lmk} V_{dDN}^{LJln\star} V_{dDN}^{RI mn} m_{N_n} C_0(m_{N_n}^2, m_{D_l}^2, m_{D_m}^2) \\
& - i \sum_{l,m=1}^4 \sum_{n=1}^6 V_{dDN}^{LJnl\star} V_{dDN}^{RI nm} \left[ V_{NNP}^{Lmk} C_2(m_{D_n}^2, m_{N_l}^2, m_{N_m}^2) \right. \\
& \quad \left. + V_{NNP}^{Rmk} m_{N_l} m_{N_m} C_0(m_{D_n}^2, m_{N_l}^2, m_{N_m}^2) \right] \\
& - \sum_{l,m=1}^6 \sum_{n=1}^2 V_{UUP}^{lmk} V_{dUC}^{LJln\star} V_{dUC}^{RI mn} m_{C_n} C_0(m_{C_n}^2, m_{U_l}^2, m_{U_m}^2) \\
& - \sum_{l,m=1}^2 \sum_{n=1}^6 V_{dUC}^{LJnl\star} V_{dUC}^{RI nm} \left[ V_{CCP}^{Lmk} C_2(m_{U_n}^2, m_{C_l}^2, m_{C_m}^2) \right. \\
& \quad \left. + V_{CCP}^{Rmk} m_{C_l} m_{C_m} C_0(m_{U_n}^2, m_{C_l}^2, m_{C_m}^2) \right] \quad (A.7)
\end{aligned}$$

iii) Charged Higgs boson vertex  $H_k^+ \bar{u}_j d_l$  where  $H^{+1} = H^+$  and  $H_2^+ = G^+$  (see fig 4).

$$\begin{aligned}
(4\pi)^2 (\Delta F_L^k)^{JI} & = -\frac{32\pi\alpha_s}{3} m_{\bar{g}} \sum_{l,m=1}^6 V_{UDH}^{mlk} Z_U^{(J+3)m} Z_D^{ll} C_0(m_{\bar{g}}^2, m_{U_m}^2, m_{D_l}^2) \\
& + \sum_{l,m=1}^6 \sum_{n=1}^4 V_{UDH}^{mlk} V_{uUN}^{RJmn\star} V_{dDN}^{Lln} m_{N_n} C_0(m_{N_n}^2, m_{U_m}^2, m_{D_l}^2) \\
& + \sum_{l=1}^4 \sum_{m=1}^2 \sum_{n=1}^6 V_{uDC}^{RJnm\star} V_{dDN}^{Llnl} \left[ V_{NCH}^{Rmk} C_2(m_{D_n}^2, m_{C_m}^2, m_{N_l}^2) \right. \\
& \quad \left. + V_{NCH}^{Lmk} m_{C_m} m_{N_l} C_0(m_{D_n}^2, m_{C_m}^2, m_{N_l}^2) \right] \\
& + \sum_{l=1}^4 \sum_{m=1}^2 \sum_{n=1}^6 V_{uUN}^{RJnl\star} V_{dUC}^{LI nm} \left[ V_{NCH}^{Rmk} C_2(m_{U_n}^2, m_{N_l}^2, m_{C_m}^2) \right. \\
& \quad \left. + V_{NCH}^{Lmk} m_{N_l} m_{C_m} C_0(m_{U_n}^2, m_{N_l}^2, m_{C_m}^2) \right] \quad (A.8)
\end{aligned}$$

$$\begin{aligned}
(4\pi)^2 (\Delta F_R^k)^{JI} & = -\frac{32\pi\alpha_s}{3} m_{\bar{g}} \sum_{l,m=1}^6 V_{UDH}^{mlk} Z_U^{Jm} Z_D^{(I+3)l} C_0(m_{\bar{g}}^2, m_{U_m}^2, m_{D_l}^2) \\
& + \sum_{l,m=1}^6 \sum_{n=1}^4 V_{UDH}^{mlk} V_{uUN}^{LJmn\star} V_{dDN}^{RI ln} m_{N_n} C_0(m_{N_n}^2, m_{U_m}^2, m_{D_l}^2) \\
& + \sum_{l=1}^4 \sum_{m=1}^2 \sum_{n=1}^6 V_{uDC}^{LJnm\star} V_{dDN}^{RI nl} \left[ V_{NCH}^{Lmk} C_2(m_{D_n}^2, m_{C_m}^2, m_{N_l}^2) \right. \\
& \quad \left. + V_{NCH}^{Rmk} m_{C_m} m_{N_l} C_0(m_{D_n}^2, m_{C_m}^2, m_{N_l}^2) \right] \\
& + \sum_{l=1}^4 \sum_{m=1}^2 \sum_{n=1}^6 V_{uUN}^{LJnl\star} V_{dUC}^{RI nm} \left[ V_{NCH}^{Lmk} C_2(m_{U_n}^2, m_{N_l}^2, m_{C_m}^2) \right. \\
& \quad \left. + V_{NCH}^{Rmk} m_{N_l} m_{C_m} C_0(m_{U_n}^2, m_{N_l}^2, m_{C_m}^2) \right]
\end{aligned}$$

$$+ V_{NCH}^{Rlmk} m_{N_i} m_{C_m} C_0(m_{U_n}^2, m_{N_i}^2, m_{C_m}^2)] \quad (\text{A.9})$$

## A.4 Box diagram contributions

Box contributions to  $\Delta F = 2$  processes as given below are related to the Wilson coefficients  $C_i$  defined in eq. (6.4) through

$$B_i = G_F^2 M_W^2 (V_{\text{eff}}^{tb*} V_{\text{eff}}^{ts})^2 C_i(M_{SU5Y}) \quad (\text{A.10})$$

**i) Charged Higgs contributions** (including the mixed  $H^\pm W^\mp$  diagram). In order to simplify the notation, we denote  $P_{LR}^{JI1} \equiv [P_{LR}^H]^{JI}$ ,  $P_{LR}^{JI2} \equiv [P_{LR}^G]^{JI}$  and similarly for the  $RL$  couplings ( $[P^H], [P^G]$  are defined in eqs. (2.39), (2.40)). If not written down explicitly, the arguments of the loop integrals  $D_0$  and  $D_2$  are  $(m_{H_k^+}^2, m_{H_l^+}^2, \bar{m}_{u_M}^2, \bar{m}_{u_N}^2)$ .

$$\begin{aligned} (B^{\text{VLL}})_{hg} &= -\frac{g_2^2}{2} \sum_{M,N=1}^3 V_{\text{eff}}^{MJ*} V_{\text{eff}}^{NI} P_{RL}^{NJ1*} P_{RL}^{MI1} \bar{m}_{u_M} \bar{m}_{u_N} D_0(M_W^2, m_{H_1^+}^2, \bar{m}_{u_M}^2, \bar{m}_{u_N}^2) \\ &+ \frac{1}{8} \sum_{M,N=1}^3 P_{RL}^{MJ1*} P_{RL}^{NJ1*} P_{RL}^{MI1} P_{RL}^{NI1} D_2(m_{H_1^+}^2, m_{H_1^+}^2, \bar{m}_{u_M}^2, \bar{m}_{u_N}^2) \\ &+ \frac{1}{4} \sum_{M,N=1}^3 P_{RL}^{MJ2*} P_{RL}^{NJ1*} P_{RL}^{MI1} P_{RL}^{NI2} D_2(M_W^2, m_{H_1^+}^2, \bar{m}_{u_M}^2, \bar{m}_{u_N}^2) \\ (B^{\text{VRR}})_{hg} &= \frac{1}{8} \sum_{k,l=1}^2 \sum_{M,N=1}^3 P_{LR}^{NJk*} P_{LR}^{MJl*} P_{LR}^{MIk} P_{LR}^{NIl} D_2 \\ (B_1^{\text{SLL}})_{hg} &= \frac{1}{2} \sum_{k,l=1}^2 \sum_{M,N=1}^3 P_{LR}^{MJl*} P_{LR}^{NJk*} P_{LR}^{MIk} P_{LR}^{NIl} \bar{m}_{u_M} \bar{m}_{u_N} D_0 \\ (B_2^{\text{SLL}})_{hg} &= 0 \\ (B_1^{\text{SRR}})_{hg} &= \frac{1}{2} \sum_{k,l=1}^2 \sum_{M,N=1}^3 P_{LR}^{MJl*} P_{LR}^{NJk*} P_{LR}^{MIk} P_{LR}^{NIl} \bar{m}_{u_M} \bar{m}_{u_N} D_0 \\ (B_2^{\text{SRR}})_{hg} &= 0 \\ (B_1^{\text{LR}})_{hg} &= \frac{1}{4} \sum_{k,l=1}^2 \sum_{M,N=1}^3 P_{LR}^{MJl*} P_{LR}^{NJk*} P_{LR}^{MIk} P_{LR}^{NIl} D_2 \\ (B_2^{\text{LR}})_{hg} &= -\frac{g_2^2}{2} \sum_{k=1}^2 \sum_{M,N=1}^3 V_{\text{eff}}^{MJ*} V_{\text{eff}}^{NI} P_{LR}^{NJk*} P_{LR}^{MIk} D_2(M_W^2, m_{H_k^+}^2, \bar{m}_{u_M}^2, \bar{m}_{u_N}^2) \\ &+ \sum_{k,l=1}^2 \sum_{M,N=1}^3 P_{LR}^{MJl*} P_{LR}^{NJk*} P_{LR}^{MIk} P_{LR}^{NIl} \bar{m}_{u_M} \bar{m}_{u_N} D_0 \end{aligned} \quad (\text{A.11})$$

**Chargino contributions.** Arguments of the loop integrals are  $(m_{C_m}^2, m_{C_n}^2, m_{U_k}^2, m_{U_l}^2)$ .

$$\begin{aligned}
(B^{\text{VLL}})_C &= \frac{1}{8} \sum_{k,l=1}^6 \sum_{m,n=1}^2 V_{dUC}^{LJkn^*} V_{dUC}^{LJlm^*} V_{dUC}^{LIkm} V_{dUC}^{LIln} D_2 \\
(B^{\text{VRR}})_C &= \frac{1}{8} \sum_{k,l=1}^6 \sum_{m,n=1}^2 V_{dUC}^{RJkn^*} V_{dUC}^{RJlm^*} V_{dUC}^{RIkm} V_{dUC}^{RIln} D_2 \\
(B_1^{\text{SLL}})_C &= -\frac{1}{4} \sum_{k,l=1}^6 \sum_{m,n=1}^2 V_{dUC}^{RJkn^*} V_{dUC}^{RJlm^*} V_{dUC}^{LIkm} V_{dUC}^{LIln} m_{C_m} m_{C_n} D_0 \\
(B_2^{\text{SLL}})_C &= \frac{1}{16} \sum_{k,l=1}^6 \sum_{m,n=1}^2 V_{dUC}^{RJkn^*} V_{dUC}^{RJlm^*} V_{dUC}^{LIkm} V_{dUC}^{LIln} m_{C_m} m_{C_n} D_0 \\
(B_1^{\text{SRR}})_C &= -\frac{1}{4} \sum_{k,l=1}^6 \sum_{m,n=1}^2 V_{dUC}^{LJkn^*} V_{dUC}^{LJlm^*} V_{dUC}^{RIkm} V_{dUC}^{RIln} m_{C_m} m_{C_n} D_0 \\
(B_2^{\text{SRR}})_C &= \frac{1}{16} \sum_{k,l=1}^6 \sum_{m,n=1}^2 V_{dUC}^{LJkn^*} V_{dUC}^{LJlm^*} V_{dUC}^{RIkm} V_{dUC}^{RIln} m_{C_m} m_{C_n} D_0 \\
(B_1^{\text{LR}})_C &= -\frac{1}{2} \sum_{k,l=1}^6 \sum_{m,n=1}^2 V_{dUC}^{LJkn^*} V_{dUC}^{RJlm^*} V_{dUC}^{LIkm} V_{dUC}^{RIln} m_{C_m} m_{C_n} D_0 \\
(B_2^{\text{LR}})_C &= -\frac{1}{2} \sum_{k,l=1}^6 \sum_{m,n=1}^2 V_{dUC}^{LJlm^*} V_{dUC}^{RJkn^*} V_{dUC}^{LIkm} V_{dUC}^{RIln} D_2
\end{aligned} \tag{A.12}$$

## A.5 Loop integrals

We define three- and four-point loop integrals at vanishing external momenta as:

$$\frac{1}{(4\pi)^2} C_{2n}(m_1^2, m_2^2, m_3^2) = \int \frac{d^d k}{(2\pi)^d} \frac{i k^{2n}}{(k^2 - m_1^2)(k^2 - m_2^2)(k^2 - m_3^2)}, \tag{A.13}$$

$$\frac{1}{(4\pi)^2} D_{2n}(m_1^2, m_2^2, m_3^2, m_4^2) = \int \frac{d^d k}{(2\pi)^d} \frac{i k^{2n}}{(k^2 - m_1^2)(k^2 - m_2^2)(k^2 - m_3^2)(k^2 - m_4^2)}. \tag{A.14}$$

Explicit formulae for the  $C_0$ ,  $C_2$ ,  $D_0$  and  $D_2$  functions are as follows

$$C_0(x, y, z) = \frac{y}{(x-y)(z-y)} \log \frac{y}{x} + \frac{z}{(x-z)(y-z)} \log \frac{z}{x}, \tag{A.15}$$

$$C_2(x, y, z) = \Delta + \log \frac{x}{\mu^2} + \frac{y^2}{(x-y)(z-y)} \log \frac{y}{x} + \frac{z^2}{(x-z)(y-z)} \log \frac{z}{x}. \tag{A.16}$$

where  $\Delta = \frac{2}{d-4} + \log 4\pi\gamma_E - 1$  and  $\mu$  is the renormalization scale. In the flavour changing penguin diagrams  $\Delta$  and  $\mu$  dependence always cancels out after summation over squark, chargino and neutralino mixing matrices.

$$D_0(x, y, z, t) = \frac{y}{(y-x)(y-z)(y-t)} \log \frac{y}{x} + \frac{z}{(z-x)(z-y)(z-t)} \log \frac{z}{x}$$

$$+ \frac{t}{(t-x)(t-y)(t-z)} \log \frac{t}{x}, \quad (\text{A.17})$$

$$D_2(x, y, z, t) = \frac{y^2}{(y-x)(y-z)(y-t)} \log \frac{y}{x} + \frac{z^2}{(z-x)(z-y)(z-t)} \log \frac{z}{x} \\ + \frac{t^2}{(t-x)(t-y)(t-z)} \log \frac{t}{x}. \quad (\text{A.18})$$

The two-point loop integrals  $B_0$  and  $B_1$  at  $s = 0$  can be expressed as

$$B_0(0, x, y) = \Delta + \frac{x}{x-y} \log \frac{x}{\mu^2} + \frac{y}{y-x} \log \frac{y}{\mu^2} \equiv \Delta + \log \frac{x}{\mu^2} + \frac{y}{x-y} \log \frac{x}{y} \quad (\text{A.19})$$

$$B_1(0, x, y) = \frac{1}{2} B_0(0, x, y) - \frac{1}{4} \frac{x+y}{x-y} + \frac{1}{2} \frac{xy}{(x-y)^2} \log \frac{x}{y} = \frac{1}{4} + \frac{1}{2} C_2(x, y, y) \quad (\text{A.20})$$

The function  $H_2$  of eq. (5.4) is related to  $C_0$  as follows:

$$H_2(x, y) = -m^2 C_0(m^2, xm^2, ym^2) \equiv -C_0(1, x, y). \quad (\text{A.21})$$

## References

- [1] M. Misiak, S. Pokorski and J. Rosiek, in *Heavy Flavours II*, eds. A.J. Buras and M. Lindner, World Scientific, Singapore, 1998, p. 795 (hep-ph/9703442).
- [2] Y. Grossman, Y. Nir and R. Rattazzi, in *Heavy Flavours II*, eds. A.J. Buras and M. Lindner, World Scientific, Singapore, 1998, p. 755 (hep-ph/9701231).
- [3] L. Silvestrini, hep-ph/0210031.
- [4] A.J. Buras, P. Gambino, M. Gorbahn, S. Jäger and L. Silvestrini, *Nucl. Phys.* **B592** (2001) 55.
- [5] F. Gabbiani, E. Gabrielli, A. Masiero and L. Silvestrini, *Nucl. Phys.* **B477** (1996) 321.
- [6] P.H. Chankowski and L. Ślawnianowska, *Phys. Rev.* **D63** (2001) 054012; *Acta Phys. Polon.* **B32** (2001) 1895.
- [7] P.H. Chankowski and J. Rosiek, *Acta Phys. Polon.* **B33** (2002) 2329.
- [8] G. Isidori and A. Retico, *JHEP* **0209** (2001) 063.
- [9] G.C. Branco, A.J. Buras and J.-M. Gérard, *Phys. Lett.* **B155** (1985) 192; *Nucl. Phys.* **B259** (1985) 306.
- [10] M. Olechowski and S. Pokorski, *Phys. Lett.* **B214** (1988) 393.
- [11] L.J. Hall, R. Rattazzi and U. Sarid, *Phys. Rev.* **D50** (1994) 7048; M. Carena, M. Olechowski, S. Pokorski and C.E.M. Wagner, *Nucl. Phys.* **B426** (1994) 269; R. Rattazzi and U. Sarid, *Nucl. Phys.* **B501** (1997) 297; H. Baer, M. Brhlik, D. Castano and X. Tata, *Phys. Rev.* **D58** (1998) 015007; T. Blažek and S. Raby, *Phys. Rev.* **D59** (1999) 095002.
- [12] J.A. Coarasa and J. Solà, *Phys. Lett.* **B389** (1996) 53; J.A. Coarasa, D. Garcia, J. Guasch, R.A. Jiménez and J. Solà, *Eur. Phys. J.* **C2** (1998) 373; J.A. Coarasa, R.A. Jiménez and J. Solà, *Phys. Lett.* **B406** (1997) 337.
- [13] K.S. Babu and C. Kolda, *Phys. Lett.* **B451** (1999) 77.
- [14] J. Guasch, W.F.L. Hollik and S. Penaranda, *Phys. Lett.* **B515** (2001) 367.
- [15] H.E. Haber et al., *Phys. Rev.* **D63** (2001) 055004; M.J. Herrero, S. Pennaranda and D. Temes, *Phys. Rev.* **D64** (2001) 115003.

- [16] A.M. Curiel, M.J. Herrero, D. Temes and J.F. De Troconiz, **D65** (2002) 075006; A. Dobado, M.J. Herrero, D. Temes, **D65** (2002) 075023; A.M. Curiel, M.J. Herrero and D. Temes, preprint FTUAM-02-21, hep-ph/0210335.
- [17] M. Carena, D. Garcia, U. Nierste and C.E.M. Wagner, *Nucl. Phys.* **B577** (2000) 88.
- [18] C.-S. Huang and Q.-S. Yan, *Phys. Lett.* **B442** (1998) 209; C.-S. Huang, W. Liao and Q.-S. Yan, *Phys. Rev.* **D59** (1999) 011701.
- [19] C. Hamzaoui, M. Pospelov and M. Toharia, *Phys. Rev.* **D59** (1999) 095005.
- [20] K.S. Babu and C. Kolda, *Phys. Rev. Lett.* **84** (2000) 228.
- [21] C.-S. Huang, W. Liao, Q.-S. Yan and S.-H. Zhu, *Phys. Rev.* **D63** (2001) 114021, Erratum: *Phys. Rev.* **D64** (2001) 059902.
- [22] C. Bobeth, T. Ewerth, F. Krüger and J. Urban, *Phys. Rev.* **D64** (2001) 074014 and **D66** (2002) 074021.
- [23] A.J. Buras, P.H. Chankowski, J. Rosiek and L. Ślawniowska, *Nucl. Phys.* **B619** (2001) 434.
- [24] T. Blažek, S. Raby and S. Pokorski, *Phys. Rev.* **D52** (1995) 4151.
- [25] G. Degrassi, P. Gambino and G.-F. Giudice, *JHEP* **0012** (2000) 009.
- [26] M. Carena, D. Garcia, U. Nierste and C.E.M. Wagner, *Phys. Lett.* **B499** (2001) 141.
- [27] G. Isidori and A. Retico, *JHEP* **0111** (2001) 001 and hep-ph/0110121 v3, July 2002.
- [28] G. D'Ambrosio, G.-F. Giudice, G. Isidori and A. Strumia, *Nucl. Phys.* **B645** (2002) 155.
- [29] A.J. Buras, P.H. Chankowski, J. Rosiek and L. Ślawniowska, *Phys. Lett.* **B546** (2002) 96.
- [30] J. Rosiek, *Phys. Rev.* **D41** (1990) 3464, *Erratum* hep-ph/9511250.
- [31] P.H. Chankowski and S. Pokorski in *Perspectives on supersymmetry*, G.L. Kane ed., World Scientific Publishing Co., Singapore 1998 (hep-ph/9707497); M. Carena, U. Nierste and C.E.M. Wagner, *Nucl. Phys.* **B577** (2000) 88.
- [32] P.H. Chankowski, J. Ellis, M. Olechowski and S. Pokorski, *Phys. Lett.* **B214** (1988) 393.

- [33] M. Ciuchini, G. Degrossi, P. Gambino and G.-F. Giudice, *Nucl. Phys.* **B534** (1998) 3.
- [34] B. Aubert et al., BaBar Collaboration, hep-ex/0207083.
- [35] F. Abe et al., The CDF Collaboration, *Phys. Rev.* **D57** (1998) 3811.
- [36] A. Dedes, H.K. Dreiner and U. Nierste, *Phys. Rev. Lett.* **87** (2001) 251804.
- [37] A.J. Buras, hep-ph/0101336, lectures at the International Erice School, August, 2000.
- [38] A.J. Buras, M. Jamin, and P.H. Weisz, *Nucl. Phys.* **B347** (1990) 491.
- [39] M. Ciuchini, E. Franco, V. Lubicz, G. Martinelli, I. Scimemi and L. Silvestrini, *Nucl. Phys.* **B523** (1998) 501; M. Ciuchini, et al., *JHEP* **9810** (1998) 008.
- [40] A.J. Buras, M. Misiak and J. Urban, *Nucl. Phys.* **B586** (2000) 397.
- [41] A.J. Buras, S. Jäger and J. Urban, *Nucl. Phys.* **B605** (2001) 600.
- [42] D. Becirevic, V. Gimenez, G. Martinelli, M. Papinutto and J. Reyes, hep-lat/0110091, hep-lat/0110117.
- [43] C. Bobeth, A.J. Buras, F. Krüger and J. Urban, *Nucl. Phys.* **B630** (2002) 87.
- [44] A.J. Buras, F. Parodi and A. Stocchi, *JHEP* **0209** (2003) 0301.
- [45] P. Gambino and M. Misiak, *Nucl. Phys.* **B611** (2001) 338.
- [46] M. Ciuchini, G. Degrossi, P. Gambino and G.-F. Giudice, *Nucl. Phys.* **B527** (1998) 21.
- [47] P. Ciafaloni, A. Romanino and A. Strumia, *Nucl. Phys.* **B524** (1998) 361; F. Borzumati and C. Greub, *Phys. Rev.* **D58** (1998) 074004.
- [48] R. Barbieri and G.-F. Giudice, *Phys. Lett.* **B309** (1993) 86.
- [49] A. Dedes and A. Pilaftsis, *Phys. Rev.* **D67** (2003) 015012.